

## 7. VALIDATION

### 7.1 VALIDATION ACTIVITIES

The purpose of this report is to document simulations of the TH behavior in Yucca Mountain fractured rock close to emplacement drifts. This includes determining (1) the fluid flow in the vicinity of the drifts for a range of thermal conditions, and (2) the amount of thermal seepage into the emplacement drifts. Therefore, the TH seepage model in this report is a model supporting seepage into emplacement drifts relevant to TSPA component model “Seepage into Emplacement Drifts.” AP-2.27Q, *Planning for Science Activities* (Attachment 3, Table 1), requires Level I validation for models supporting seepage into emplacement drifts (models with less importance on annual dose). However, thermal seepage influences the moisture conditions close to waste packages and drip shields at elevated temperatures. Thus, the TH seepage model also supports the TSPA component model “Waste Package/Drip Shield Moisture and Chemistry,” which requires Level II validation. Therefore, the more stringent Level II validation is considered adequate for the drift-scale TH seepage process model (models with moderate effect on annual dose). The general validation criteria for Level II validation are listed in Attachment 3 of AP-2.27Q, and are further explained in Section 2.2.1.2 of *Technical Work Plan for: Near-Field Environment and Transport: Near-Field Coupled Processes (TH Seepage and THM) Model Report Integration* (BSC 2004 [DIRS 170236]). The choice of Level II validation criteria in this report is different from the model validation plan in the previous technical work plan (TWP) (BSC 2004 [DIRS 167969]), where a Level I validation was considered sufficient.

#### 7.1.1 Confidence Building During Model Development to Establish Scientific Basis and Accuracy for Intended Use

For Level II validation, Section 2.2.1.2 of the current TWP (BSC 2004 [DIRS 170236]) specifies the following steps for *Confidence Building During Model Development*: The development of the model should be documented in accordance with the requirements of Section 5.3.2(b) of AP-SIII.10Q, *Models*. Additional steps are listed in AP-2.27Q, Attachment 3. The development of the TH seepage model has been conducted according to all these criteria, as follows:

1. *Selection of input parameters and/or input data, and a discussion of how the selection process builds confidence in the model. [AP-SIII.10 Q 5.3.2(b) (1) and AP-2.27Q Attachment 3 Level I (a)]*

The inputs to the TH seepage model have all been obtained from controlled sources (see Section 4.1.1, Table 4.1-1), including discussion about selection of input and design parameters. Model assumptions have been described in Section 5. Detailed discussion about model concepts can be found in Section 6.2.1. In short, the input data to the model have been developed from the best available sources for this modeling effort, based on site-specific test information (and often subsequent calibration) acquired mostly in underground niches and alcoves. Most of these tests were designed explicitly for the purpose of developing hydrogeologic model parameters at the scale relevant for seepage and thermal seepage. The model parameters developed from the input data have been applied in a model framework consistent with the scale of the underground tests and the

uncertainty pertaining to some test data. Thus, this requirement can be considered satisfied.

2. *Description of calibration activities, and/or initial boundary condition runs, and/or run convergences, simulation conditions set up to span the range of intended use and avoid inconsistent outputs, and a discussion of how the activity or activities build confidence in the model. Inclusion of a discussion of impacts of any non-convergence runs. [(AP-SIII.10Q 5.3.2(b)(2) and AP-2.27Q Attachment 3 Level I (e)).*

Detailed discussion of initial and boundary conditions for the TH seepage model can be found in Sections 4.1.1.2 and 6.2.1. Sections 6.2.2 through 6.2.4 provide detailed discussion of various model results (i.e., those of convergence runs), including discussion of the range of conditions studied and how this range is appropriate considering the intended use of the model. Discussion about nonconvergence runs is not relevant for this report. In short, most of the upper and lower model boundary conditions as well as the initial conditions have been developed from available input sources reflecting the ambient (nonheated) conditions at Yucca Mountain. These are the boundary conditions that remain essentially unchanged over the heating period because the model boundary is far away from the waste emplacement drifts. Other boundary conditions such as the heat source imposed in the drifts or the percolation flux through the mountain, both important for thermal seepage, have been varied in wide ranges that cover the expected variability and uncertainty related to them. Thus, this requirement can also be considered satisfied.

3. *Discussion of the impacts of uncertainties to the model results including how the model results represent the range of possible outcomes consistent with important uncertainties. [(AP-SIII.10 Q 5.3.2(b)(3) and AP-2.27Q Attachment 3 Level 1 (d) and (f)]*

Discussion of model uncertainties and sensitivity analyses are provided in Section 6.2.4.2. A summary discussion on uncertainties and their impact is given in Section 8.3. In short, uncertainty of model input parameters was adequately addressed with the TH seepage model by conducting sensitivity analyses with respect to the uncertain hydrogeologic properties or the uncertain model boundary conditions. It was shown that the main feeds of this report to TSPA—i.e., the qualitative findings on thermal seepage that form the basis for seepage abstraction—hold true for the range of conditions analyzed. Uncertainty with respect to the conceptual model is adequately accounted for by selecting an abstraction method for thermal seepage (see Section 6.2.4.1 and BSC 2004 [DIRS 169131], Sections 6.5.2 and 6.5.3) that safely covers all uncertainties (in choosing a conservative upper bound for thermal seepage). Thus, this requirement can also be considered satisfied.

4. *Formulation of defensible assumptions and simplifications. [AP-2.27Q Attachment 3 Level I (b)].*

Discussion of assumptions and simplifications is provided in Section 5 and Section 6.2.1 (TH seepage model), and in Section 6.3.1 (THMEFF). These assumptions and simplifications are adequate and defensible. Thus, this requirement can also be considered satisfied.

5. *Consistency with physical principles, such as conservation of mass, energy, and momentum. [AP-2.27Q Attachment 3 Level I (c)]*

Consistency with physical principles is demonstrated by the conceptual and mathematical formulation in Section 6.2.1.1 and the selection of the thoroughly tested and widely used TOUGH2 Code (LBNL 2003 [DIRS 161491]) in Section 3. Thus, this requirement can also be considered satisfied.

### **7.1.2 Confidence Building After Model Development to Support the Scientific Basis of the Model**

For confidence building after model development, the TWP (BSC 2004 [DIRS 170236], Section 2.2.1.2, “*Confidence Building After Model Development*”) imposes the following requirements for model validation:

1. *AP-SIII.10Q, Section 5.3.2(c), Method 1: Corroboration of model results with data acquired from the Drift Scale Test (DST).*

Comparison of model results with experimental data is the main method of validation for the TH seepage model. The remainder of Section 7 explains the respective validation and modeling activities in great detail, and discusses explicitly how the criteria for this validation method, as defined in Section 2.2.1.4 of the TWP (BSC 2004 [DIRS 170236]), have been met.

2. *AP-SIII.10Q, Section 5.3.2(d), Technical review through publication in a refereed professional journal to demonstrate additional confidence in the model, if publication is used in conjunction with the above validation step.*

The validation criterion is that technical review is conducted through at least one publication in a professional journal (BSC 2004 [DIRS 170236], Section 2.2.1.4). The publication needs to describe the modeling activity for the models in the DST TH Seepage report. Since the following articles on the subject have already been published, this validation criterion has been met:

- “Modeling the Thermal-Hydrologic Processes in a Large-Scale Underground Heater Test in Partially Saturated Fractured Tuff.” *Water Resources Research* (Birkholzer and Tsang 2000 [DIRS 154608]).

This publication describes the modeling approach and model results for the DST TH model, and discusses comparison with measured data from the early heating phase of the DST.

- “Uncertainties in Coupled Thermal–Hydrological Processes Associated with the Drift Scale Test at Yucca Mountain, Nevada.” *Journal of Contaminant Hydrology* (Mukhopadhyay and Tsang 2003 [DIRS 160790]).

This publication describes the modeling approach and model results for the DST TH model, and discusses the issue of heat losses through the bulkhead and how these are accounted for in the model (Section 7.3.4).

- “Understanding the Anomalous Temperature Data from the Large Block Test at Yucca Mountain, Nevada.” *Water Resources Research* (Mukhopadhyay and Tsang 2002 [DIRS 160788]).

This publication provides additional confidence in the TH seepage model because it describes application of a similar TH model to the temperature response measured in the Large Block Test at Yucca Mountain.

- “Predictions and Observations of the Thermal-Hydrological Conditions in the Single Heater Test.” *Journal of Contaminant Hydrology* (Tsang and Birkholzer 1999 [DIRS 137577]).

This publication provides additional confidence in the TH seepage model because it describes application of a similar TH model to the thermal-hydrological response measured in the Single Heater Test at Yucca Mountain.

3. *AP-SIII.10Q, Section 5.3.2(c), Method 2: Corroboration of results with alternative conceptual models*

This method was suggested as an optional requirement in the TWP (BSC 2004 [DIRS 170236]). The validation criterion is that alternative conceptual or mathematical models shall qualitatively support the results of the main model. As pointed out in Section 6.3, this criterion has been met by applying the alternative conceptual model THMEFF and demonstrating that it corroborates the findings of the TH seepage model.

### 7.1.3 Corroboration of Model Results with Experimental Data

Corroboration of model results with experimental data is the preferred method of validation in this report because measured data allow for a direct validation with respect to the relevant processes. In situ heater tests conducted in the unsaturated fracture tuff at Yucca Mountain provide a wealth of valuable data for model validation. Three heater tests have been conducted at Yucca Mountain, all of which are located in one of the repository units, the middle nonlithophysal unit (Tptpmn). Of these three tests, the Drift Scale Test (DST) is the best suited for validation against measured data, in particular because its geometric setup and scale is similar to the proposed design of waste emplacement drifts. Thus measured data from this test are used for validation of the TH seepage model. The other two tests—the Single Heater Test (SHT) and the Large Block Test (LBT)—are of smaller scale and of a geometry different from that of waste emplacement drifts. Comparative analysis of the Single Heater Test and the Large Block Test shall not be presented in this report. However, the coupled TH processes observed in these two tests have been successfully simulated with conceptual approaches similar to the one used here. Documentation of the modeling of the Single Heater Test can be found in *Thermal Tests Thermal-Hydrological Analyses/Model Report* (BSC 2001 [DIRS 157330]) or in the peer-reviewed journal article of Tsang and Birkholzer (1999 [DIRS 137577]). Modeling of the



Large Block Test is found in the *Large Block Test Final Report* (Lin et al. 2001 [DIRS 159069]) and in the peer-reviewed journal article of Mukhopadhyay and Tsang (2002 [DIRS 160788]).

The numerical model used to demonstrate the good agreement of model results with data from the DST is the Drift Scale Test (DST) TH model. The DST TH model uses the same conceptual model as the TH seepage model, and both models are at the same scale (drift scale). Therefore, if the DST TH model is validated by comparison with data, the predictive TH seepage model can also be considered validated with respect to TH behavior of the fractured rock in the vicinity of emplacement drifts. Results from the DST TH model are directly compared to measured data from the DST. The thermal load applied to the DST is designed to induce TH coupled processes such as vaporization, vapor transport, drying, and condensation in the duration of the DST for four years of heating. In the repository, these same processes will also occur, but over a time period of hundreds of years after emplacement. By the agreement of model predictions with measurements, confidence is gained that similar models deploying these same processes and incorporating the repository conditions/time scales can help to address questions important to repository performance. The good agreement between the DST TH model and the measured data is described in the journal article of Birkholzer and Tsang (2000 [DIRS 154608]).

The thermal load in the DST resulted in vigorous boiling and subsequent condensation of water, with rock temperature exceeding 200°C. With such intense TH processes occurring, the DST data provide the base for an excellent model validation with respect to the near-field TH conditions in the rock mass, as described by temperature and saturation changes. With respect to the vaporization barrier, however, the DST data are not sufficient for validation. To this date, no seepage of liquid water has been observed in the Heated Drift of the DST. The vaporization barrier generated by the heater output appears to be totally effective in the DST, because of the intense thermal load. However, heat load designed for the repository is less intense and will be applied over much longer time frames, thus giving rise to maximum temperatures lower than in the DST. This, together with concern over vapor losses through the bulkhead of the Heated Drift (see Section 7.3.4), implies that the DST results should not be used as direct evidence for “no seepage.” The DST results therefore provide demonstration of the potential performance of the repository under a “hot” thermal operating mode, but offer no seepage data (observed seepage rates and seepage fractions) that can be used for thermal-seepage validation purposes. Therefore, validation of the seepage part of the TH seepage model is an indirect one. First, the better the overall TH behavior can be predicted by the DST TH model, the more confidence is gained for the seepage results obtained with the TH seepage model. In other words, a successful validation of the DST TH model with respect to coupled processes (i.e., saturation distribution, temperature signals) adds confidence to the seepage part of the TH seepage model. Second, the conceptual model for thermal seepage calculation is similar to the conceptual model applied in the ambient seepage studies (see Section 6.2.1.1.2), i.e., the seepage model for PA (SMPA). Applying a similar conceptual model and key properties (permeability variability and fracture capillary-strength parameter) that are identical to the SMPA increases confidence in the seepage part of the TH seepage model, since the modeling framework for the capillary barrier treatment can already be considered validated from the validation activities performed for ambient seepage studies (BSC 2004 [DIRS 171764], Section 7; BSC 2004 [DIRS 167652], Section 7). Third, to gain additional confidence, an alternative conceptual model was introduced in Section 6.3, demonstrating that an alternative conceptualization of unsaturated fracture flow confirms the assessment of the vaporization barrier from the TH seepage model.

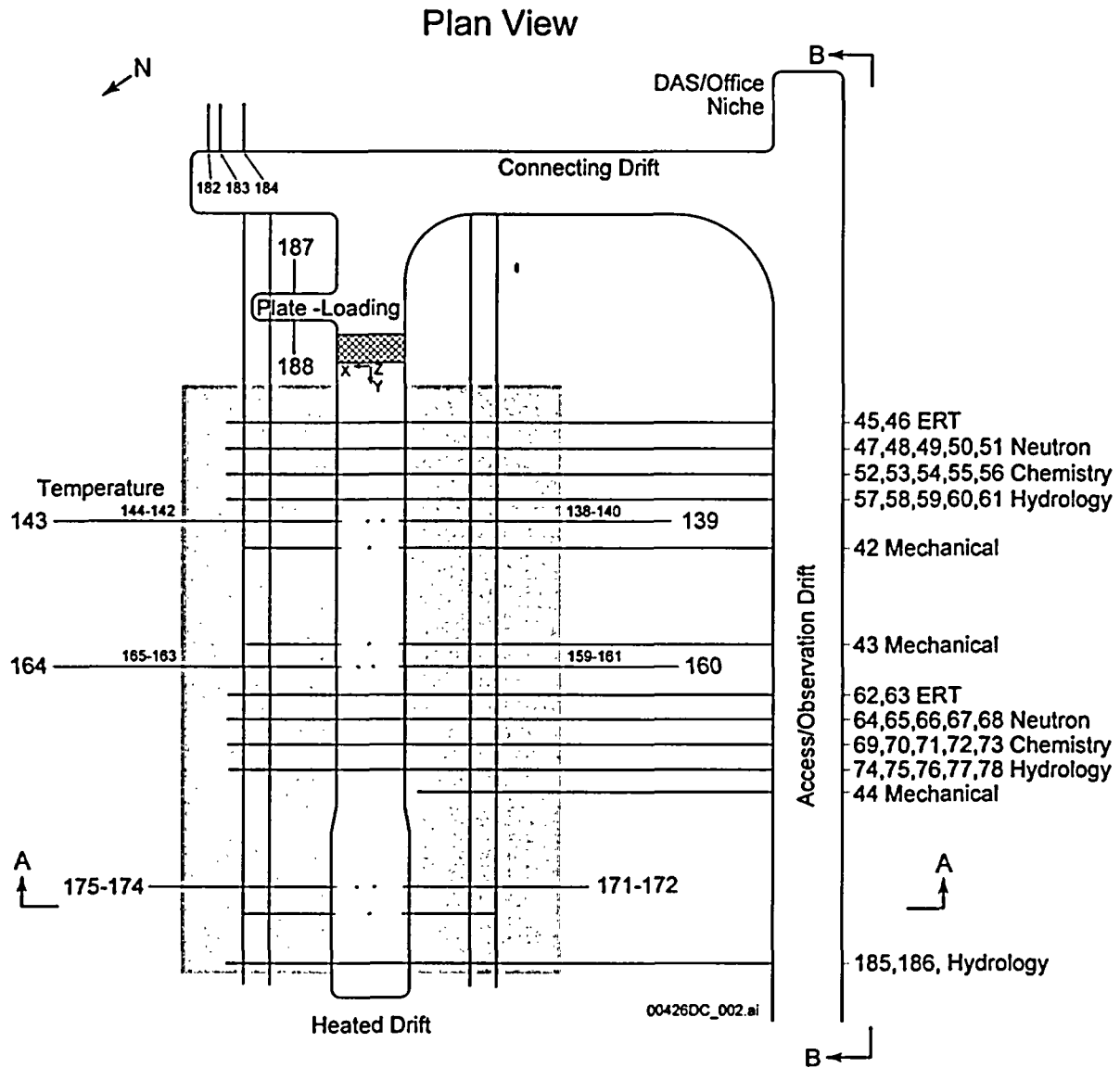
Since there is no thermal test in the lower lithophysal unit at Yucca Mountain, validation of the TH seepage model does not include direct comparison with measured data from the Tptpll. By the agreement of the model predictions with data from the Tptpmn, confidence is gained that the TH processes in response to heating are well captured by the model. This means that application to the Tptpll unit is appropriate because essentially the same TH processes need to be described. Uncertainties regarding the lower lithophysal unit are mostly captured and propagated to the seepage abstraction through the uncertainties in the rock properties and through the choice of an adequate upper-bound abstraction method for thermal seepage (Section 6.2.4.1).

The following sections describe in detail the validation activities performed with the DST TH model. Section 7.2 introduces the DST setup and measurement activities. Section 7.3 briefly describes the DST conceptual model and different phases of model development and refinement. Comparison of model data and measured data is presented in Section 7.4. A summary and discussion of the validation activities using the DST data is given in Section 7.5.

## **7.2 THE DRIFT SCALE TEST**

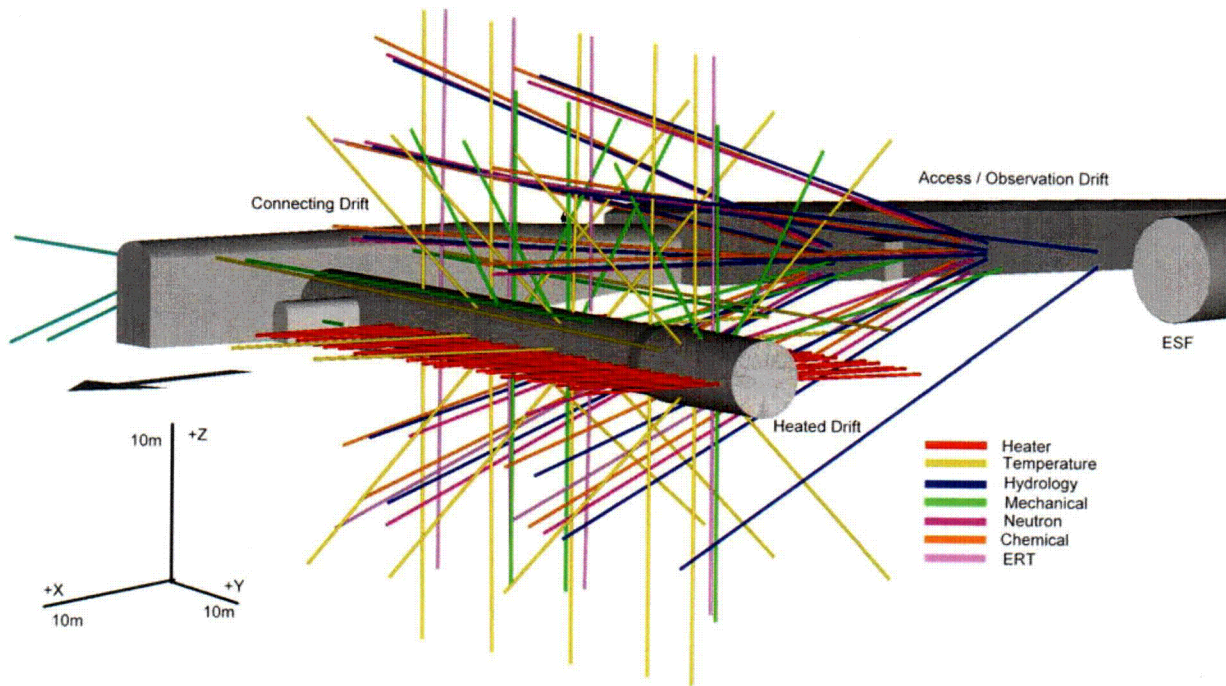
### **7.2.1 Design and Geometry**

The Drift Scale Test (DST) is probably the largest in situ heater test ever performed in a fractured rock environment. The test area is located in one of the side alcoves of the Exploratory Studies Facility (ESF) in the Tptpmn unit. Figure 7.2.1-1 gives a plan view of the test block, and Figure 7.2.1-2 shows a three-dimensional perspective of the DST with heaters and many of the approximately 150 instrumented boreholes for measuring thermal, hydrological, mechanical, and chemical processes. The DST centers around the Heated Drift, having a 47.5 m long heated (hot) section separated from the unheated (cold) section by a thermally insulated bulkhead. Heating is provided by nine canister heaters within the Heated Drift, as well as 50 rod heaters, referred to as "wing heaters," placed into horizontal boreholes emanating from the Heated Drift. Each wing heater is composed of two equal-length segments (4.44 m) separated by a 0.66 m gap. The distance between the Heated Drift wall and the tip of the first heater segments is 1.66 m. The dimensions of the Heated Drift and canister heaters are similar to the current design of waste emplacement drifts. The heaters of the DST were activated on December 3, 1997. The heating phase continued for approximately four years, until January 14, 2002. Currently, the DST is in the midst of a planned four-year period of monitoring the natural cooling process of the rock block.



Source: Birkholzer and Tsang 1997 [DIRS 100597], Figure 3.1-1.

Figure 7.2.1-1. Plan View of DST Area



Source: BSC 2004 [DIRS 169900], Figure 6.3-2.

Figure 7.2.1-2. Three-Dimensional Perspective of the As-Built Borehole Configuration of the DST

### 7.2.2 Measurements to Probe the Coupled Processes

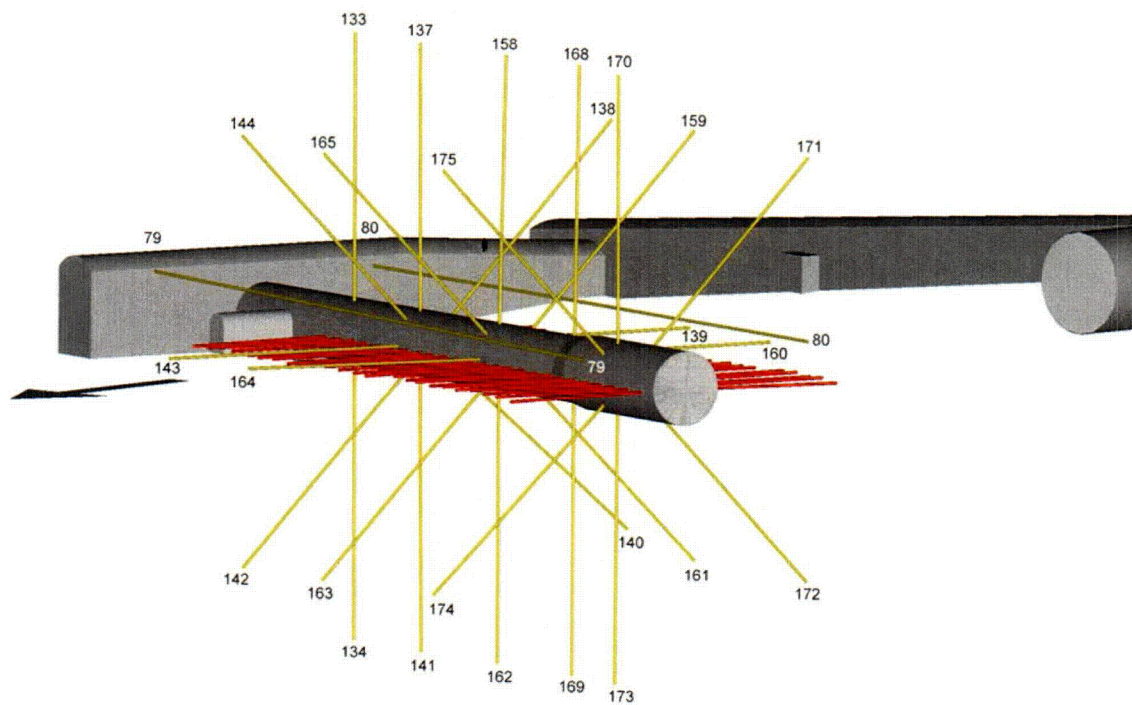
Measurements in the DST include laboratory and field characterization of the thermal test block prior to the activation of heaters; passive monitoring and active testing during the heating and subsequent cooling phase; and planned postcooling laboratory and field characterization activities similar to those conducted prior to activation of heaters. Pretest laboratory characterization included measurements of thermal properties, hydrological properties, mechanical properties, mineral-petrology studies, and pore-water chemical and isotopic analysis from rock cores. Preheat field characterization of the thermal test block involved rock-mass classification, fracture mapping, video logging of the boreholes, geophysical measurements, and air-permeability testing.

Measurements during the heating and cooling phases of the DST are divided into two categories: the continuous passive monitoring data and the active testing data, which are taken periodically. The DST test block has been instrumented with thousands of sensors to monitor the thermal, mechanical, hydrological, and chemical processes on at least an hourly basis. In Figure 7.2.1-2, the instrumented boreholes are color-coded according to their functions. For the purposes of this report, the focus is on boreholes designed to measure thermal (yellow) and hydrological behavior (blue), as extracted in Figures 7.2.2-1 and 7.2.2-2, respectively. Radial arrays of 20 m long boreholes emanating from the Heated Drift monitor the temperature evolution, as do longitudinal

boreholes parallel to and extending over the entire length of the Heated Drift. Temperature sensors are installed at approximately 30 cm intervals. Most boreholes labeled as “hydrological” originate from the Observation Drift. These are clusters of 40 m long boreholes forming vertical fans that bracket the Heated Drift and the wing heaters. Humidity, temperature, and pressure sensors were installed in twelve of the hydrology holes to provide passive monitoring data. These boreholes are also used for periodic active testing of air-permeability changes to track the time evolution and spatial distribution of drying and condensation zones in the test block. Since gas flow occurs predominantly in the fractures, interference air-permeability measurements in selected hydrological boreholes target the spatial variation and time evolution of liquid-saturation changes in the fractures. The hydrology boreholes are also used for collection of water (if present) and gas sampling for chemical and isotopic analysis. Finally, neutron logging, electrical resistivity tomography, and crosshole radar tomography are carried out at appropriate time intervals throughout the heater test to probe the changes in the rock moisture in the matrix pores. Crosshole radar tomography and neutron logging are performed in the boreholes shown in Figure 7.2.2-3.

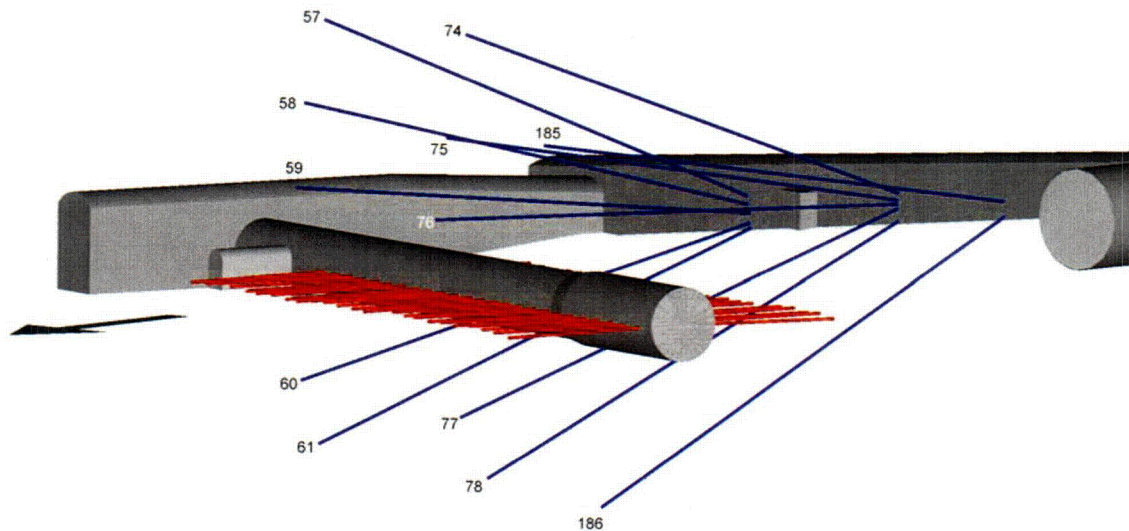
The DST design and geometry are described in the following reports: *Drift Scale Test Design and Forecast Results* (CRWMS M&O 1997 [DIRS 146917]) and *Drift Scale Test As-Built Report* (CRWMS M&O 1998 [DIRS 111115]). The results of preheat characterization of the test block are contained in the report *Ambient Characterization of the Drift Scale Test Block* (CRWMS M&O 1997 [DIRS 101539]). Results of the DST have been presented and discussed in seven thermal tests progress reports, #1 through # 7 (CRWMS M&O 1998 [DIRS 159512]; CRWMS M&O 1999 [DIRS 154585]; CRWMS M&O 1999 [DIRS 159513]; CRWMS M&O 1999 [DIRS 160806]; CRWMS M&O 2000 [DIRS 160807]; Williams 2001 [DIRS 156323]; Williams 2001 [DIRS 160809]), roughly covering the heating phase of the test. A comprehensive documentation of DST measurements for the four-year heating period is given in *Thermal Testing Measurements Report* (BSC 2004 [DIRS 169900]). This report elaborates on the testing methods, gives representative results, and discusses measurement uncertainties. The comparison of simulated and measured DST results below mainly uses data described in this report; some additional temperature data are used to include results for the first several months of natural cooling (see Table 4.1-12).





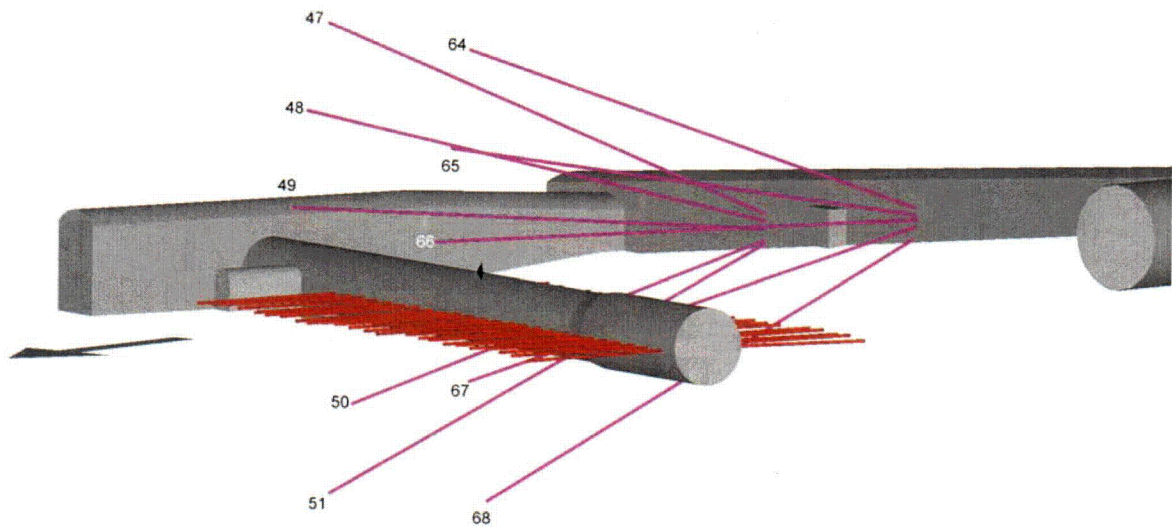
Source: BSC 2004 [DIRS 169900], Figure 6.3-3.

Figure 7.2.2-1. Three-Dimensional Perspective of Wing Heaters and Temperature Boreholes in the DST



Source: BSC 2004 [DIRS 169900], Figure 6.3-4.

Figure 7.2.2-2. Three-Dimensional Perspective of Wing Heaters and Hydrology Boreholes in the DST



Source: BSC 2004 [DIRS 169900], Figure 6.3-6.

Figure 7.2.2-3. Three-Dimensional Perspective of Wing Heaters and Boreholes for Geophysical Measurements (GPR and Neutron Logging) in the DST

### 7.3 DST TH MODEL

#### 7.3.1 Stages of Model Development

In 1997, prior to initiation of the test, a predictive DST TH model was developed accounting for realistic representation of the complex test geometry in three dimensions and using properties based on site-specific pretest characterization (e.g., laboratory measurements of matrix saturation and thermal conductivity, in situ air-injection tests for fracture permeability). The predictive model was used to guide the design of the DST and to predict the outcome of the planned 8-year test period. Different conceptual models, e.g., for fracture-matrix interaction and heat flow within the drift, were analyzed in a sensitivity study. Results of this predictive model were presented in *Pretest Analysis of the Thermal-Hydrological Conditions of the ESF Drift Scale Test* (Birkholzer and Tsang 1997 [DIRS 100597]).

Once the heaters had been activated and the first measurements of temperature, gas pressure, and water saturation became available, early test results from the first six months of heating were used to discriminate between alternative modeling concepts applied in pretest simulations. It became apparent, for example, that the dual-permeability method describes fracture-matrix interaction much better than the effective-continuum model. Temperature data also showed that heat radiation within the Heated Drift is effective, indicating that a uniform temperature distribution at the drift wall can be assumed. In addition to model conceptualization, several model modifications were made to account for test conditions that were different from the assumed conditions of the pretest simulations. These modifications were: (1) adjusting the input heater power to account for the actual heat load of the DST, (2) changing the boundary conditions at the bulkhead to allow for gas exchange between the hot and the cool side of the Heated Drift, (3) adding the concrete invert in the Heated Drift, and (4) including the effects of

ventilation and minor temperature buildup close to the drift walls prior to heater activation. Other than adjusting the conceptual model and better representing the actual test conditions, the predictive model was not changed. In particular, the assumed site-specific rock properties were not adjusted. The rationale for refining the model and comparison of measured and simulated data is given *Drift Scale Test Progress Report Lawrence Berkeley National Laboratory, Version 0.0* (Tsang et al. 1998 [DIRS 144941], Section 2).

At six months of heating, the refined DST TH model was frozen. The frozen model was used to predict the remaining heating and the cooling phase of the DST. With the test ongoing and more and more data becoming available, a continued comparative analysis of predictive simulations and measured data was performed. Based on the generally good agreement between measured and simulated data, only one more model modification became necessary. At 30 months of heating (September 2000), gridblocks representing wing heaters were given a permeability value three orders of magnitude higher than that of the surrounding rock mass, to account for the fact that wing heaters are installed in boreholes that are open conduits for gas flow. All simulation results presented in this report are based on the conceptual model that includes this last modification.

The subsequent re-evaluation of the accuracy of the numerical model is documented in a series of seven informal progress reports intended to communicate the progress of the YMP thermal test program at different test stages (CRWMS M&O 1998 [DIRS 159512]; 1999 [DIRS 154585]; [DIRS 159513]; [DIRS 160806]; 2000 [DIRS 160807]; Williams 2001 [DIRS 156323]; [DIRS 160809]). These reports provide a comprehensive source of information regarding measurements and modeling results, not only for TH behavior, but also for thermally induced mechanical and chemical changes. One specific report, progress report #7 (Williams 2001 [DIRS 160809], Sections 3.2 and 3.3), contains a detailed discussion about the important issue of heat and mass losses through the DST bulkhead. A scientific evaluation of this phenomenon is also provided in the peer-reviewed journal article of Mukhopadhyay and Tsang (2003 [DIRS 160790]). A brief summary is given in Section 7.3.4.

There is only one previous report summarizing results from the DST TH model: *Thermal Tests Thermal-Hydrological Analyses/Model Report* (BSC 2001 [DIRS 157330]). One purpose of this report was to compare model predictions and data using different TH property sets. Comparison was performed for the DST, using data from the first 18 months of the heating, as well as for the SHT and the LBT to analyze in situ tests of varying duration and scale. The first tested property set for the DST was the one based on site-specific characterization as introduced above, referred to as the DKM-TT99 property set; the second utilized results from a mountain-scale calibration effort conducted with ambient hydrological data. While the first properties describe the local test conditions only, the latter properties represent average conditions for the various stratigraphic layers of Yucca Mountain, used for the mountain-scale prediction runs in TSPA. It was concluded that the site-specific property set captured the DST TH behavior slightly better than the mountain-scale property set. However, both property sets were considered to have produced results within acceptable limits of the measured data. This was an important conclusion for performance assessment, because it ensured that the hydrological properties calibrated from the ambient inverse model can also be applied for PA simulations that incorporate the thermal perturbation caused by repository heating. Since the completion of *Thermal Tests Thermal-Hydrological Analyses/Model Report* (BSC 2001 [DIRS 157330]), a new calibrated



property set was developed as described in Section 4, referred to as the DS/AFM-UZ02-Mean property set. As this new property set is applied in Section 6.2 to predict the future repository conditions, the analysis is re-evaluated as a basis for validation of the TH seepage model. Sections 7.4.3 and 7.4.4 of this report present results of this re-evaluation, using measured DST data from 4 years of heating and about 6 months of cooling, while applying the DST TH model with property sets DKM-TT99 and DS/AFM-UZ02-Mean, respectively.

### **7.3.2 Conceptual Model and Mathematical Formulation**

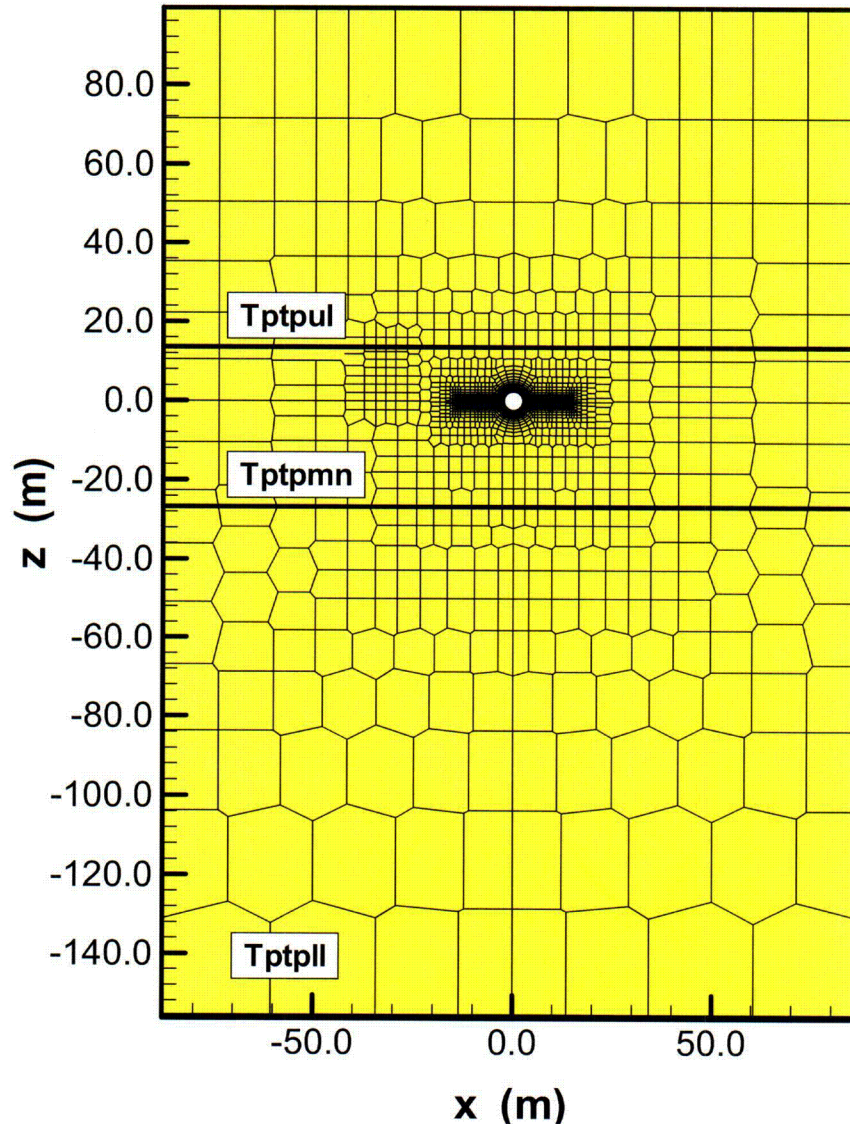
The modeling framework of the DST TH model is similar to that of the TH seepage model (Section 6.2.1.1.1). The mathematical description of the coupled transport of water, water vapor, air, and heat, as described in Section 6.2.1.1.1, is identical. The resulting mass-and energy-balance equations are solved with the integral finite-difference simulator TOUGH2V1.3MEOS4 V1.0 (LBNL 1999 [DIRS 147569]) for simulation presented in Section 7.4.3 and TOUGH2 V1.6 (LBNL 2003 [DIRS 161491]) for simulation presented in Section 7.4. Two DST simulation cases are studied to analyze sensitivity to the conceptual model for fracture-matrix interaction; one uses a standard dual-permeability method (DKM), the other applies the DKM with the active fracture concept (AFM).

### **7.3.3 Model Domain and Numerical Grid**

The numerical grid for the DST TH model was designed to represent the test geometry and dimensions, including the drifts, alcoves, the decline of the observation drift, and the location of boreholes, as realistically as possible. Note that the nominal design dimensions were used for construction of the grid. The differences between nominal and as-built dimensions are small, and do not affect the modeling results. This required development of a three-dimensional model. Significant rock volumes in all directions beyond the immediate DST block are included in the modeled domain to guarantee a proper definition of boundary conditions (that is, to insure that boundaries remain in their ambient, preheat conditions for the duration of the DST).

Figure 7.3.3-1 shows the model domain and discretization of a typical x-z cross section in the three-dimensional model for the DST. The origin of the three-dimensional coordinate system is located on the hot side of the bulkhead, in the center of the drift. The positive x-axis points horizontally, approximately towards the north (transverse to the Heated Drift away from the Observation Drift); the positive y-axis points horizontally along the Heated Drift, approximately towards the west; and the positive z-direction points vertically upward from the origin. Thus, the Heated Drift originates at  $y = 0$  and terminates at  $y = 47.5$  m. Note that the vertical extent of the model region includes the stratigraphic units both above and below that of the middle nonlithophysal unit (Tptpmn) of the test block. (The stratigraphy is extracted from the nearby borehole USW SD-9.) They are respectively the upper (Tptpul) and lower (Tptpll) lithophysal units of the Topopah Spring welded tuff. The grid was designed such that the assumed interfaces between layers are represented by gridblock interfaces (i.e., interfaces are maintained at  $z = +14.0$  m and  $z = -26.68$  m). The discretization in the DST model domain is extremely refined near the sources of heat and is less so away from them. The discretized numerical grid has been developed through trial and experimentation, and is considered adequate for its intended use (as also evidenced by absence of convergence issues with the three-dimensional DST TH model).

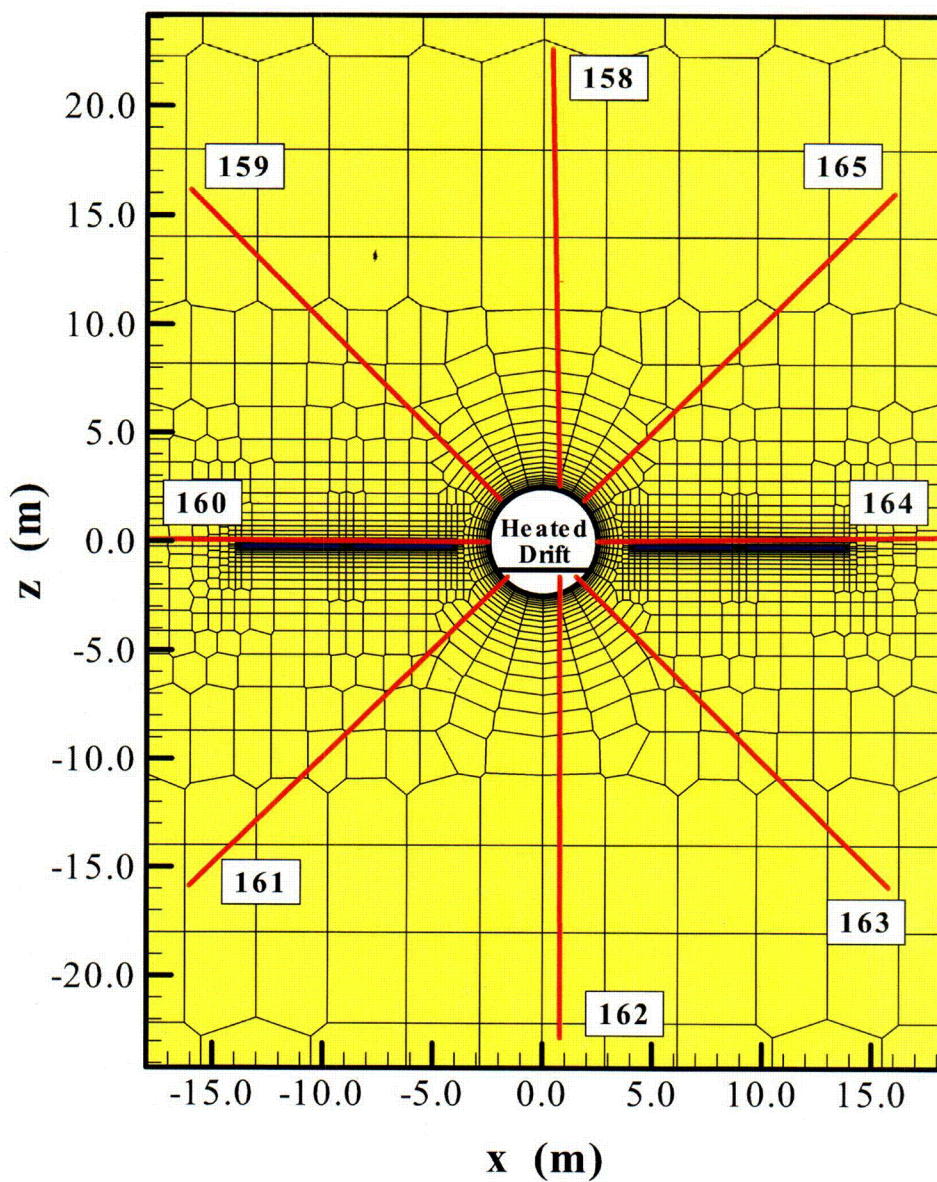
Figure 7.3.3-2 shows the same cross section in a detailed view of the rock areas adjacent to the Heated Drift and the wing heaters. The figure also depicts the configuration of boreholes 158 through 165, which form a cluster oriented radially outward from the Heated Drift. This vertical plane intersects the long axis of the drift at  $y \sim 23$  m. Temperature sensors are grouted in each of these boreholes at approximately 0.3 m spacing. Figure 7.3.3-3 presents a detailed view of another cross section depicting the location of five hydrology boreholes 57 through 61, which are collared on the north wall of the Observation Drift. The solid symbols indicate the location of temperature sensors (DTN: MO0002ABBLSLDS.000 [DIRS 147304]).



Output DTN: NA (See Section 8.5).

Figure 7.3.3-1. Vertical Cross Section of DST Numerical Grid





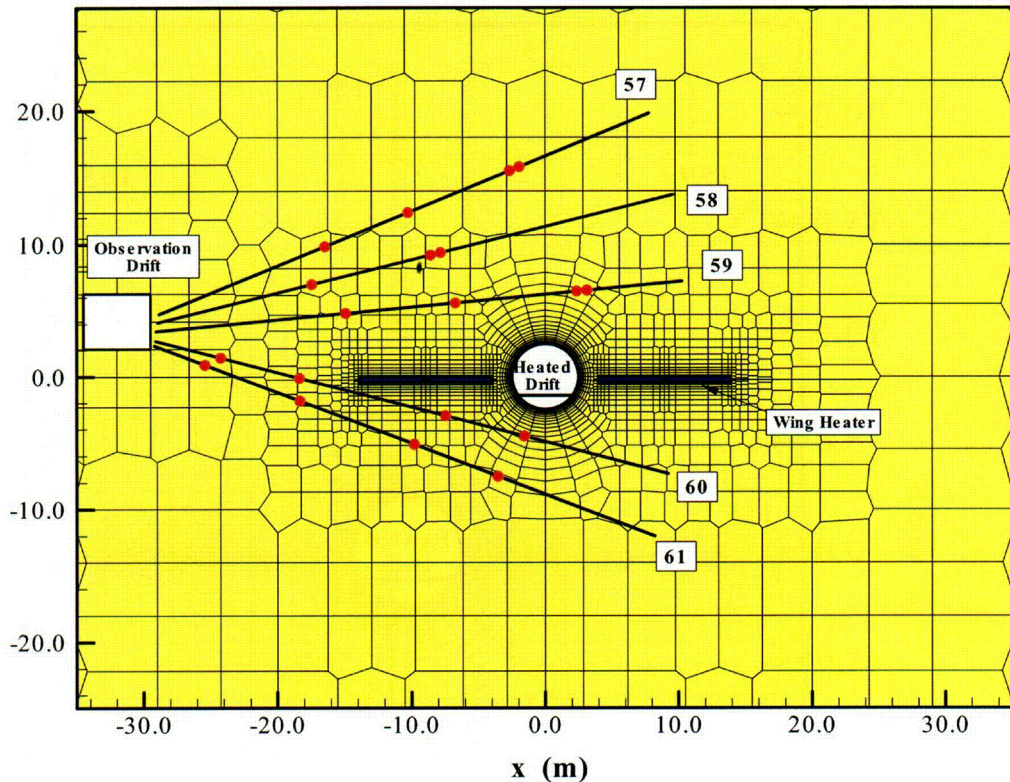
Input DTN (borehole location): MO0002ABBLSLDS.000 [DIRS 147304].

Output DTN: NA (See Section 8.5).

NOTE: Numerous temperature sensors are installed in each borehole with a sensor spacing of about 30 cm.

Figure 7.3.3-2. Detailed View of Vertical Cross Section of DST Numerical Grid through Plane Containing Temperature Boreholes 158 to 165





Input DTN (borehole and sensor location): MO0002ABBLSLDS.000 [DIRS 147304].

Output-DTN: NA (See Section 8.5).

NOTE: Circular symbols indicate location of temperature sensors.

Figure 7.3.3-3. Detailed View of Vertical Cross Section of DST Numerical Grid through Plane Containing Hydrology Boreholes 57 to 61

### 7.3.4 Model Boundary and Initial Conditions

#### Boundary Conditions

The top and bottom boundaries of the DST domain ( $z = +99.39$  m and  $-156.76$  m, respectively) are given constant boundary conditions of pressure, saturation, and temperature (see Section 4.1.2.2). The side boundaries of the domain are located outside of the test influence area and are implemented as no-flow boundaries, i.e., these side boundaries are far away enough not to have an impact on the TH conditions in the DST model domain even if an open boundary was used. The Observation Drift, the Connecting Drift, and the cool section of the Heated Drift are given constant pressure, temperature, and saturation boundary conditions. The nonheated section of the Heated Drift and the walls of the Connecting Drift and Observation Drift near the Heated Drift are insulated, but allow for moisture to escape from the test block in the form of both liquid water and vapor. The Heated Drift is open to advection and conduction of heat and mass as well as vapor diffusion.

## Thermal Bulkhead

Early pressure measurements from the hot and cool sides of the Heated Drift indicated that the insulated bulkhead was acting as an open boundary for gas flow, allowing vapor to escape from the Heated Drift. As a result, the predictive numerical model for the DST was changed in 1998, utilizing a bulkhead boundary condition that conforms to the actual test conditions. A high-permeability connection for gas flow was introduced between the gridblocks, representing the hot side and the cool side of the Heating Drift, so that the simulated bulkhead acts as an open boundary. Model results using this boundary condition show significant amounts of vapor escaping from the Heated Drift. On the other hand, the bulkhead is given small thermal conductivity, preventing heat transfer at the bulkhead by conduction.

The issue of heat and mass loss through the bulkhead has been discussed and evaluated in several thermal workshops. In short, there was concern that the amount of vapor escaping through the bulkhead is not appropriately monitored, and that the thermal response of a closed system might be different from the thermal response of an open system, where the volume of condensed water remaining in the rock is smaller. A detailed evaluation of this issue is presented in the informal thermal test progress report #7 (Williams 2001 [DIRS 160809], Sections 3.2 and 3.3) and in Mukhopadhyay and Tsang (2003 [DIRS 160790], Sections 2 and 3). This issue was further elaborated in Williams (2002 [DIRS 171270]) and it was concluded that the objectives of the DST—acquiring a more in-depth understanding of the coupled TH processes and validating the conceptual models in comparison with data—are being met. The revised model with the open-bulkhead boundary condition was considered appropriate for representing heat losses through the bulkhead, based on a reasonably small difference between measured and simulated temperature. It was concluded that the uncertainty in the fate of thermally mobilized water and uncertainty in understanding the moisture redistribution in the DST is acceptable. However, it was also understood that the measurements in the DST should not be directly used to evaluate the potential of seepage into drifts during the thermal period, because the potential of seepage in the DST might be reduced as a result of the vapor losses.

## Thermal Load

The total heating power applied to the DST TH model reflects average values of the actual heating power. Average values were calculated for each time period that had a different heater output as designed by the Thermal Test Team. This means that the few planned power reductions or increases during the test period are accounted for explicitly, while short-term heater output variations—e.g., as a result of short-term power outages—are averaged out. The periods of identical average heater power output, as applied to the model, are given in Table 7.3.4-1 separately for the floor heaters and the wing heaters. The heaters were turned off on January 14, 2002, after about 49.5 months of heating.

In the DST model, the heat generated from in-drift heaters is applied directly to the drift wall, which is assigned a large thermal conductivity that would equilibrate its temperature. Because the main objective of this report is the quantification of TH processes in the rock mass outside the drift, it is not necessary to capture the rapid radiative heat transfer within the drift in detail. Also, to limit the complexity of the three-dimensional numerical grid, the wing heaters are represented as smeared-out, spatially uniform heat sources. This is appropriate as the rock

between two adjacent wing heaters reaches a uniform temperature rapidly compared to that outside the wing heaters. Only the rock temperatures within one heater spacing of the wing heaters will be misrepresented in the simulation because of this simplified representation, and few temperature sensors are located there.

Table 7.3.4-1. Total Average Heater Power at Various Times of Heating in the DST

Time	Floor Heaters (kW)	Wing Heaters (kW)
12/03/1997-05/31/1999	52.1	132.1
06/01/1999-03/02/2000	50.0	125.1
03/02/2000-05/02/2000	47.9	120.4
05/02/2000-08/15/2000	45.8	114.6
08/15/2000-03/31/2001	43.3	106.4
04/01/2001-05/02/2001	43.4	106.7
05/02/2001-08/22/2001	41.4	101.6
08/22/2001-09/30/2001	39.4	96.3
10/01/2001-01/14/2002	39.4	96.8

Input DTNs: MO9807DSTSET01.000 [DIRS 113644]; MO9810DSTSET02.000 [DIRS 113662]; MO9906DSTSET03.000 [DIRS 113673]; MO0001SEPDSTPC.000 [DIRS 153836]; MO0007SEPDSTPC.001 [DIRS 153707]; MO0012SEPDSTPC.002 [DIRS 153708]; MO0107SEPDSTPC.003 [DIRS 158321]; MO0202SEPDSTTV.001 [DIRS 158320]

### Initial Conditions

The initial values of pressure, temperature, and saturation in the DST model are developed from initialization runs with the three-dimensional grid, using the selected top and bottom boundary conditions. The initialization runs are performed for ten thousand years before turning on the heat, ensuring that an equilibrium condition is achieved. In addition, the impact of elevated temperatures in the drifts (from installation activities in the summer months prior to starting the test), and of rock mass drying within a few meters of drift walls from ventilation of the drifts are accounted for in the numerical model.

### 7.3.5 Model Parameters and Rock Properties

Following a strategy similar to that in the previous *Thermal Tests Thermal-Hydrological Analyses/Model Report* (BSC 2001 [DIRS 157330], Sections 6.2.2 and 6.3.2), the DST TH model employs two different rock-property sets for validation (see Section 4). The first rock-property set utilizes site-specific properties and is identical to the property set used in *Thermal Tests Thermal-Hydrological Analyses/Model Report* (BSC 2001 [DIRS 157330], see Section 4.1, Table 5) (DKM-TT99). The intent of model simulations using this data set is to demonstrate the accuracy of the model, using the best available data for the local conditions in the test block. The second property set is identical to the calibrated property set used in the predictive TH seepage model simulations. This property set, derived from mountain-scale calibration runs for ambient conditions (i.e., DS/AFM-UZ02-Mean), is expected to better represent average properties of the various stratigraphic layers. The intent of model simulations using this data set is to demonstrate that the TH behavior in the DST can be represented with reasonable accuracy using a property set applied in the TH seepage model simulations. Comparison of the model results from the two property sets can help to evaluate the uncertainty

introduced by parameter variability. For example, a reasonable agreement between the simulation results of the two sets would reveal a small uncertainty of model output stemming from parameter variation. Both property sets assume homogeneous rock properties within each geologic layer, so that heterogeneity within the DST test block is not accounted for, and neither data set has been specifically calibrated to the measured DST data to improve the agreement between model and data. This should be considered when assessing the accuracy of the model results.

The active fracture model (AFM) is applied when using the DS/AFM-UZ02-MEAN property set, to be consistent with the TH seepage model. In contrast, simulations performed with the DKM-TT99 property set are performed with a standard dual-permeability method (DKM) to be consistent with the previous DST TH model simulations as presented in *Thermal Tests Thermal-Hydrological Analyses/Model Report* (BSC 2001 [DIRS 157330], Section 6.2.2 and 6.3.2).

## **7.4 DST VALIDATION RESULTS**

### **7.4.1 DST Data Used for Validation and Validation Criteria**

This section introduces the data available from measurements conducted in the DST, gives some information on the data uncertainty introduced by measurement errors or data analysis and reprocessing, provides the rationale for selection of data for model validation, and reiterates on the validation criteria defined in Section 2.2.1.4 of the TWP (BSC 2004 [DIRS 170236]).

The validation criteria for model corroboration with data have been developed based on the model's intended use. The purpose of the TH seepage model is to provide findings on the evolution of thermal seepage to form the basis for thermal seepage abstraction. These findings are (1) that water is prevented from entering drifts as long as the fractured rock near the drift wall is at above-boiling temperature and (2) that the amount of thermal seepage is bounded by the respective long-term ambient seepage rate. Based on these findings, two alternative abstraction methodologies for thermal seepage are developed in *Abstraction of Drift Seepage* (BSC 2004 [DIRS 169131], Sections 6.5.2 and 6.5.3) for further use in the total system performance assessment (TSPA). The selected abstraction methods use upper-bound estimates of thermal seepage to account for various sources of model uncertainty. The first one of the abstraction methods sets thermal seepage equal to ambient seepage, which means that uncertainty is accounted for by not using the potential benefit of a vaporization barrier in the TSPA-LA. Quantitative model results are not needed for this upper-bound method. The second method suggests to set thermal seepage to zero during the period of above-boiling temperatures at the drift wall, which requires prediction of the duration of the boiling period. This quantitative information is provided to TSPA by another model, the multiscale thermohydrologic model (BSC 2004 [DIRS 169565]). In the second method, uncertainty is accounted for by choosing a threshold temperature for the duration of the boiling period that is a few degrees higher than the nominal boiling period (BSC 2004 [169131], Section 6.5.2.2). This ensures that the boiling isotherm is at some distance from the drift (and there is a small completely dry zone around the wall) when the zero seepage is switched back to ambient seepage in the abstraction. Also, the abstraction model does not incorporate the delayed seepage initiation caused by the slow saturation buildup in the near-field rock. In other words, while the predictive results show that



seepage can only occur after a few hundred to thousand years of resaturation because of the capillary barrier at the wall, the seepage abstraction allows for seepage as soon as the fractured rock close to the drifts starts to have non-zero saturation values. Thus both abstraction methods account for a wide uncertainty margin in the TH Seepage Results.

Following the above discussion, for the TH seepage model and its validation, it is most important that the TH processes of moisture redistribution are qualitatively captured so that the basis for the thermal seepage abstraction is valid. Thus for the purpose of providing thermal seepage estimates for seepage abstraction, the model needs to predict reasonably well the disturbance of the fracture and matrix flows induced by heating of the fractured rock, because potential for thermal seepage is mostly affected by the flux perturbation. Considering the selected upper-bound abstraction method with its wide uncertainty margin, the criterion for model validation defined in Section 2.2.1.4 of the TWP (BSC 2004 [DIRS 170236]) is that the simulated locations of dryout and condensation should qualitatively be corroborated by these deduced from temperature, geophysical and air permeability measurements.

The specific data from the DST used for validation of the drift-scale TH model are those data related to TH measurements as follows:

- Temperatures measured at approximately 1750 sensor locations.
- Changes in matrix saturation estimated from geophysical measurements conducted at periodic intervals (approximately once in three months) through the duration of the DST.
- Changes in fracture saturation estimated from air-permeability measurements conducted at periodic intervals (approximately once in three months) through the duration of the DST.

About 1,750 temperature sensors installed in 26 boreholes are available for comparison of temperature data. Qualitative comparison can be performed using temperature profiles at a particular time along temperature boreholes or plotting the temperature history of selected sensors. A quantitative evaluation can be performed using statistical measures such as the mean difference between modeled and measured results. (Definition of these statistical measures is given in Section 7.4.2.) While the temperature rise in the test block is dominated by heat conduction, evidence of TH coupling is manifested in heat-pipe signatures in the temperature data, indicating two-phase conditions with presence of both water and vapor. The location of heat-pipe signatures provides an estimate for the location of the boiling front and indicates the magnitude of heat-induced two-phase circulation processes of water and air. A validation criterion is that the location and duration characteristics of these two-phase heat-pipe signatures in the predictions should also be observed in the measurements (BSC 2004 [DIRS 170236], Section 2.2.1.4). As for temperature statistics, a mean difference of less than 10°C is considered acceptable (BSC 2004 [DIRS 170236], Section 2.2.1.4). A mean difference of 10°C is about 4 percent of the maximum rock temperature at the end of heating. As pointed out above, the TH seepage model does not provide quantitative estimates of temperature to TSPA. Thus, the temperature predictions have to be accurate enough to allow for a reasonable prediction of the heat-induced flux perturbations, but do not require a close quantitative match at all times and



locations. The 10°C temperature criterion ensures that the temperature predictions form a reasonably good basis for the prediction of TH processes.

The measurement uncertainty related to different types of experimental data is described in *Thermal Testing Measurements Report* (BSC 2004 [DIRS 169900]), which points out that the measurement error of temperature devices (either thermocouples or resistance temperature devices) is on the order of 1°C, small compared to the uncertainty related to the simulated temperature.

The main phenomenon of TH coupling is the redistribution of moisture via condensed vapor in the rock mass. As mentioned earlier, zones of increased or decreased water saturation in fractures and matrix (compared to preheat baseline data) are monitored in the DST by periodic geophysical methods and air-permeability measurements. The geophysical measurements provide data related to changes in water saturation of the rock matrix. These data can be used to validate the drift-scale TH seepage process models in the following manner. Simulated matrix liquid saturation contours at different phases of heating are generated in the appropriate planes of geophysical measurements. Measured zones of drying and wetting are compared to the simulated contours of liquid saturation at specific times of measurement.

Periodic air injection tests provide information on the wetting and drying in the fractures. Wetting of fractures means increased resistance to air flow during air-injection tests, leading to a decrease in air permeability from its preheat value in certain boreholes. As heating progresses and the drying front expands, certain borehole sections that were previously zones of increased liquid saturation would become zones of decreased liquid saturation, corresponding to a return of air permeability back toward their preheat levels. These measured permeability data can be used to validate the process model in the following manner. The simulated fracture liquid saturations can be used to estimate the related (simulated) changes in air permeability. These changes in air permeability, as simulated by the numerical model, can then be compared to those observed in the measurements.

All the above methods for estimating moisture redistribution processes are useful for evaluating qualitative changes, but do not give direct and reliable measured values of the absolute liquid saturation. Geophysical measurements such as electrical resistivity tomography (ERT) and ground-penetrating radar (GPR) involve tomographic measurements of electrical resistivity and electromagnetic velocity performed in horizontal or vertical planes between boreholes, with ERT larger in measurement scale than the GPR. In both methods, the measured values must be converted into volumetric water-content changes by means of inverse algorithms, introducing further uncertainty into the processed values. Neutron-logging data are considered more reliable because they stem from point measurements; however, the rock volume covered by the measurement is much smaller than that covered by ERT or GPR (i.e., a radius of 10 to 15 cm from the borehole). It was concluded in *Thermal Tests Thermal-Hydrological Analyses/Model Report* (BSC 2001 [DIRS 157330], Section 7) that results from the three geophysical measurement techniques are comparable and reasonable. Therefore, in this report, the GPR data are used for qualitative comparison of matrix saturation changes with the model results. While air-injection tests provide reliable estimates of fracture permeability, converting the measured changes of air permeability into fracture saturation changes involves selection of an appropriate gas relative-permeability model and increases model uncertainty.

It is evident from the discussion above that measurements for monitoring moisture redistribution in the DST are by nature indirect and qualitative. Accordingly, employment of statistical measures is not appropriate for saturation results. Hence, the criterion for model validation defined in Section 2.2.1.4 of the TWP (BSC 2004 [DIRS 170236]) is that locations of dryout and condensation indicated by the simulated time evolution of the liquid-saturation changes in the matrix and fractures should in general be corroborated by these deduced from geophysical and air permeability measurements.

The many geochemical measurements of the DST (e.g., water and gas chemistry, mineralogic and petrographic analyses) are also valuable for validation of the DST TH model. The simulation model for analyzing THC processes in the DST is fundamentally dependent on a thorough understanding of the water and gas flow processes. Thus, a good agreement between measured chemical data and results from the DST THC model provides additional confidence in the DST TH model, because both models share similar concepts and rock properties. Validation of the DST THC model is described in *Drift-Scale Coupled Processes (DST and THC Seepage) Models* (BSC 2004 [DIRS 169856], Section 7).

#### 7.4.2 Statistical Measures for Temperature Evaluation

Statistical methods have been introduced and applied in *Thermal Tests Thermal-Hydrological Analyses/Model Report* (BSC 2001 [DIRS 157330], Section 6.2.1.2) to derive “single-number” quantitative measures for the goodness of fit between simulated and measured temperature data. They are based on standard statistical tools modified to better adapt to interpretation of measured and simulated behavior in the DST. A brief review of methodology and equations is given below.

The two statistical measures applied in this report are the *mean difference* and the *root mean square difference*. Note that only the first statistical measure is mentioned in the model validation plan as defined in Section 2.2.1 of the TWP (BSC 2004 [DIRS 170236]); the second measure is introduced in this report as an additional evaluation tool. Both statistical measures are a function of simulated ( $T_{sim,i}$ ) and measured ( $T_{meas,i}$ ) temperatures. Simulated temperatures are spatially and temporally interpolated, as needed, to ensure proper correlation to the measured variables. Measured variables are directly taken from sensor readings. The statistical evaluation is conducted for specific times during the DST heating and cooling phase. Usually, all sensors are included in the evaluation; however, investigators can also decide to evaluate subsets of data, e.g., all sensors with temperatures above boiling (greater than 96°C), and all thermal sensors below boiling (less than 96°C).

For a given number of sensors  $N$ , the mean difference (MD) at a specified time is given as:

$$MD = \frac{\sum_{i=1}^N w_i (T_{sim,i} - T_{meas,i})}{\sum_{i=1}^N w_i} \quad (\text{Eq. 7.4-1})$$

In Equation 7.4-1,  $w_i$  is a weighting factor introduced to give equal importance to all temperature subranges in the total range of temperatures observed (see Equation 7.4-3 below). This ensures

that the entire zone affected by heat-induced flux perturbations (which is roughly representative of the volume covered by the instrumented boreholes) is adequately represented. A positive mean difference indicates an overestimate of the measured variable; that is, the simulation predicts more heat in the test block than measured. The opposite applies for a negative mean difference.

The root mean square difference (RMSD) for a specific time is described as:

$$RMSD = \left[ \frac{\sum_{i=1}^N w_i (T_{sim,i} - T_{mea,i})^2}{\sum_{i=1}^N w_i} \right]^{1/2} \quad (\text{Eq. 7.4-2})$$

The smaller the root mean square difference, the better the agreement between simulated and measured data. Thus, the root mean square difference reveals the accuracy of the simulation.

Weighting factors ( $w_i$ ) in Equations 7.4-1 and 7.4-2 are based on a frequency analysis of the temperature measurements, acknowledging that the sensors are not uniformly distributed throughout the test block. The total range of temperature measurements is divided into 20 equally sized temperature subranges, and the number of measurements falling into each subrange was calculated. Then  $w_i$  is defined as the inverse of the number of data in each subrange  $i$  (exception: if this number is zero,  $w_i$  is zero). Basically, this weighing scheme gives equal weighting to (i.e., uses a mean temperature for) each temperature subrange. (Note that a suite of qualified codes is used for data interpolation, extraction, and calculation of the statistical measures. These are codes `mk_3dinter*.f` (LBNL 2000 [DIRS 147550]), `mk_temp3d_all.f` (LBNL 2000 [DIRS 147551]), and `mk_evaluate_*.f` (LBNL 2000 [DIRS 147552]) (see Table 3-1)).

### 7.4.3 Comparative Analysis of Measurements and Results from Simulations with Site-Specific Property Set

In this section, TH data collected from the DST are compared with simulation results from the three-dimensional DST TH model using the site-specific property set DKM-TT99 (see Section 4.1.2.1). As discussed earlier, simulation runs using the DST-TT99 property set are performed with a standard dual-permeability method (DKM). Measured and simulated TH data to be compared are temperature, water redistribution in the matrix, and water redistribution in the fracture. Because of the vast amount of measured data available in the DST, both in space and time, the presentation of validation results can only include selected examples of each data type. Note that the presented examples have been chosen to be representative of the overall TH behavior in the DST.

#### 7.4.3.1 Temperature

The comparison between measured and simulated temperatures is illustrated by showing temperature profiles and temperature history plots for a few selected boreholes. Additionally, statistical measures of the “goodness of fit” are provided as a way to quantitatively compare

simulation and measurements. To start, it should be noted that the simulated temperatures of the fractures are indistinguishable from those of the matrix, implying that, for all practical purposes, the matrix and fractures are in thermal equilibrium. The subsequent discussion of temperature distributions in the DST rock mass does not distinguish between matrix and fracture temperatures.

#### **7.4.3.1.1 Temperature Profile**

Figures 7.4.3.1-1a through 7.4.3.1-1d show a comparison of measured and simulated temperature profiles in boreholes 158 through 160 at 12, 24, 36, and 48 months of heating, respectively. In these figures, temperatures (both measured and simulated) are shown as a function of distance from the borehole collar. The boreholes chosen are arranged in a cluster oriented radially outward from the Heated Drift at a distance of  $y \sim 23$  m to the bulkhead (see Figure 7.2.1-1) and are representative of other temperature borehole clusters. Borehole 158 is oriented vertically up from the Heated Drift wall, borehole 159 makes an angle of  $45^\circ$  with the vertical, and borehole 160 is horizontal and runs slightly above the wing heaters (see Figures 7.2.2-1 and 7.3.3-2).

At 12 months of heating (Figure 7.4.3.1-1a), the drift wall is close to  $160^\circ\text{C}$ . In boreholes 158 and 159, both measured and simulated temperatures decline continually with the increase in distance from the drift wall. A good match exists between the measured and simulated temperatures in these two boreholes. The temperature profile in borehole 160 is different from that in the other two boreholes, because of its proximity with the wing heaters. A gap of about 1.66 m between the wall of the Heated Drift and the start of the inner wing heater accounts for the drop in measured and simulated temperatures near the collar of the borehole. Beyond this gap, temperatures increase with distance because of additional heat emanating from the inner wing heaters. The effect of the gap of 0.66 m between the inner and outer wing heaters is again reflected in the drop in temperatures. Temperatures then rise along the length of the outer wing heaters, before finally declining monotonically with distance beyond the end of the outer wing heaters. In the rock mass further away from the wing heaters, the measured and simulated temperatures in borehole 160 are in good agreement. Along the length of the wing heaters, however, the measured temperatures are higher than the simulated ones. This may be attributed to the fact that the wing heaters in the DST TH model are represented as smeared-out, spatially uniform planar heat sources (see Section 7.3.4), while in reality wing heaters are line sources with a spacing of about 1.8 m in the  $y$ -direction. Thus, measurements close to the wing heater boreholes are expected to be higher than the simulated temperatures that represent a spatial averaging over a few gridblocks. The fact that the simulated temperatures are slightly higher than the measured temperatures at the wall of the Heated Drift is a result of the modeling approximation in which heat was applied directly at the drift wall. This trend is expected to persist through the heating phase.

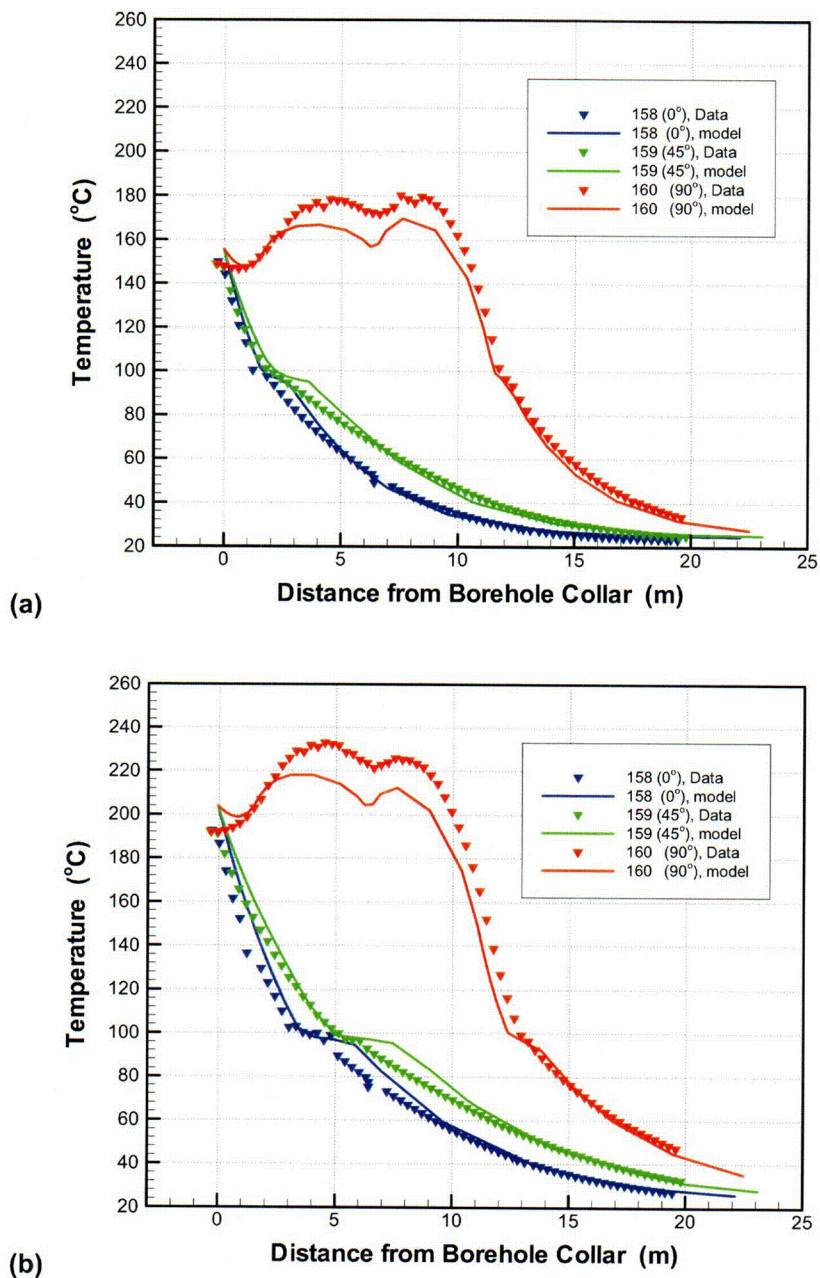
Measured and simulated temperature profiles in these boreholes at 24 months of heating can be seen in Figure 7.4.3.1-1b. The general pattern of the temperature profile in this figure is similar to that of Figure 7.4.3.1-1a, with higher temperatures at 24 months than at 12 months. While there is generally good agreement between measured and simulated temperatures, the simulated temperatures are slightly higher than the measured ones in boreholes 158 and 159, indicating that the model is retaining more heat than the DST test block. This is a likely scenario in an open field test like the DST, where it is difficult to account for all the heat losses in the numerical

model. However, it is later demonstrated that these unaccounted losses have not altered understanding of the TH processes in any significant manner. (This has also been discussed in detail in Mukhopadhyay and Tsang 2003 [DIRS 160790], Sections 2 and 3) The smaller simulated temperatures in borehole 160, on the other hand, result from the smeared-out implementation of the heat sources in the numerical grid, as was explained in the above paragraph. The temperature profiles in Figures 7.4.3.1-1c, for 36 months of heating, and 7.4.3.1-1d, for 48 months of heating, can be similarly explained. Notice that by the end of heating, the difference between measured and simulated temperatures in borehole 160 along the wing heaters has decreased. This confirms that the smeared-out implementation is acceptable, because the averaging of supplied heat evens out over a large-enough time scale. As mentioned above, there are differences between the measured and the simulated temperatures at the wall of the Heated Drift. Most of these differences are an artifact of the modeling approximation in the DST TH model in which the in-drift processes are not considered and the canister heat output is applied directly to the drift walls. Had these processes and boundary conditions been more precisely described rather than the simplifications used for the model analysis, then the agreement between simulated and measured wall temperatures would have improved. In the predictive TH seepage model, these simplifications are not used. Also note that the intended use of the TH seepage model is *not* to provide future temperature results for use in the TSPA, but to demonstrate that the general (qualitative) findings on thermal seepage hold true for a wide range of TH conditions (see discussion in Section 7.4.1). These qualitative findings are used in Section 6.2.4.1 to develop abstraction methods for thermal seepage. Quantitative temperature results are not needed for the first one of the suggested abstraction methods (i.e., thermal seepage equals to ambient seepage). The second method, which conceptualizes setting thermal seepage to zero during the period of above-boiling temperatures at the drift wall, requires prediction of the duration of the boiling period. This information is provided to TSPA by the multiscale thermohydrologic model (BSC 2004 [DIRS 169565]), which simulates the in-drift and near-drift TH processes in great detail. Thus, for the TH seepage model and its validation, it is most important that the TH processes of moisture redistribution are qualitatively captured so that the basis for the qualitative thermal seepage abstraction is valid.

The above analysis of four time snapshots during heating indicates that the model captures the main elements of heat transfer in the DST rock block. Since temperature rise in the rock from heating is predominantly governed by heat conduction, which is a linear process, the coupling between TH processes, which is nonlinear in nature, is evidenced in subtle signals in the temperature data. Typically, effects of TH coupling appear as a zone of flat region in temperature profiles (or temperature evolution plots) at the nominal boiling point of water (heat-pipe signature), indicating two-phase boiling conditions with presence of both liquid water and vapor. (In such conditions, most of the energy supply is used as latent heat of phase change, so that temperature does not change until all water has boiled away.) The general agreement of location, extent, and duration of such temperature signals is an important part of the model validation process, because it indicates that the thermally induced flow processes of vapor and water are accurately represented.

Heat-pipe signals can be seen in both the measured and the simulated data from all time snapshots depicted in Figures 7.4.3.1-1a through 7.4.3.1-1d. At 12 months of heating, boreholes 158 and 159 exhibit small signatures at about 2 to 4 m from the Heated Drift wall, indicating that the boiling front is at that distance from the drift. In borehole 160, a minute heat-pipe signature

exists at around 12 to 13 m, just beyond the end of the wing heaters. As heating progresses, these signals become longer, as more and more water reaches the nominal boiling point, and they move away from the heat source with the location of the boiling front. At 48 months, boiling takes place at about 6 to 10 m from the drift in boreholes 158 and 159, and at around 14 to 15 m in borehole 160. In general, the observed heat-pipe patterns are similar in location and extent for the measured and simulated temperatures. However, there are differences that can be attributed to local heterogeneity in the rock surrounding the DST, which is not accounted for in the DST TH model (but is explicitly accounted for in the predictive TH seepage model, using three realizations of small-scale fracture permeability variations). In borehole 158, for example, the simulated temperature consistently overestimates the measured heat-pipe signature. Borehole 159, on the other hand, exhibits a strong heat-pipe signal in the measured temperatures at 36 and 48 months of heating, a signal longer in extent than with the simulated temperature. In the assessment of the DST model results, heat-pipe signals have been analyzed for all boreholes equipped with temperature sensors. On average, the extent and location of these TH coupling signals is well represented in the temperature profiles, though the measured data show more spatial variability. In short, it can be said that there is good agreement between measured and simulated temperatures, even in the subtle signals that indicate TH coupling. The goodness of agreement between measured and simulated temperature data is defined more quantitatively from the results of a statistical analysis presented in Section 7.4.3.1.3.



Output DTN (for Figures 7.4.3.1-1a through 1d): LB0303DSCPDSTV.001.

Input DTNs (for Figures 7.4.3.1-1a through 1d): MO9807DSTSET01.000 [DIRS 113644], MO9810DSTSET02.000 [DIRS 113662], MO9906DSTSET03.000 [DIRS 113673], MO0001SEPDSTPC.000 [DIRS 153836], MO0007SEPDSTPC.001 [DIRS 153707], MO0012SEPDSTPC.002 [DIRS 153708], MO0107SEPDSTPC.003 [DIRS 158321], MO0202SEPDSTTV.001 [DIRS 158320].

Figure 7.4.3.1-1. Measured and Simulated Temperature Profile in Boreholes 158, 159, and 160 at Different Times of Heating: (a) 12 months, (b) 24 months, (c) 36, and (d) 48 months



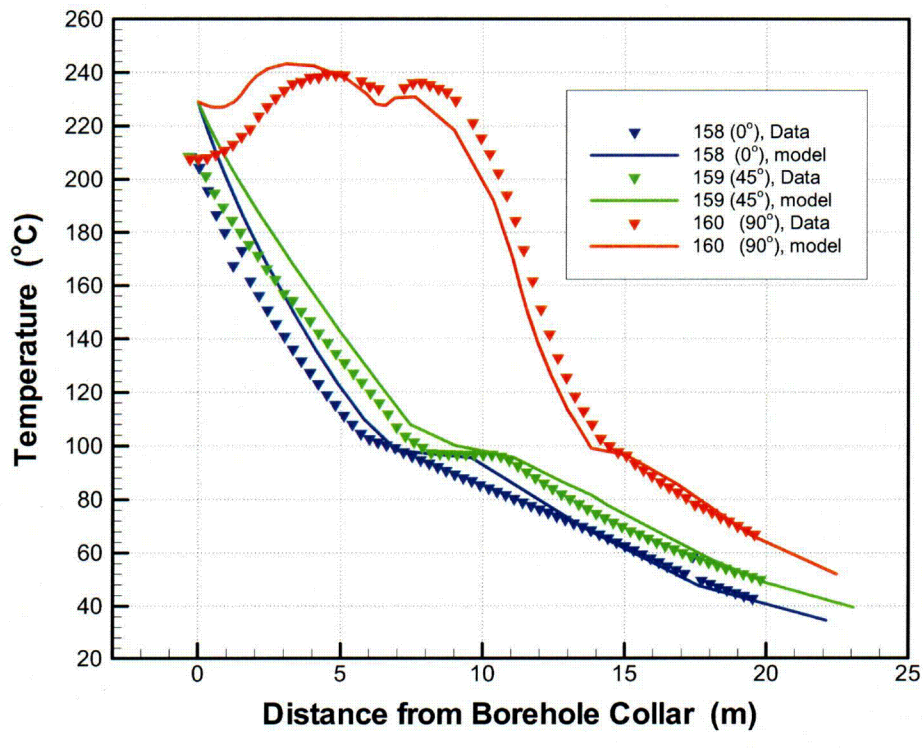
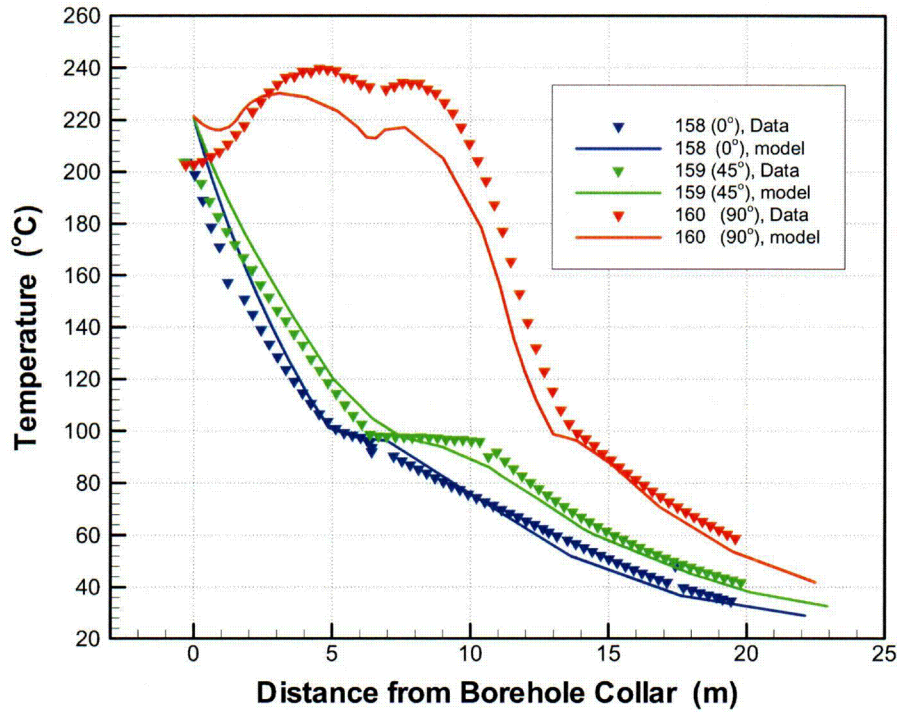
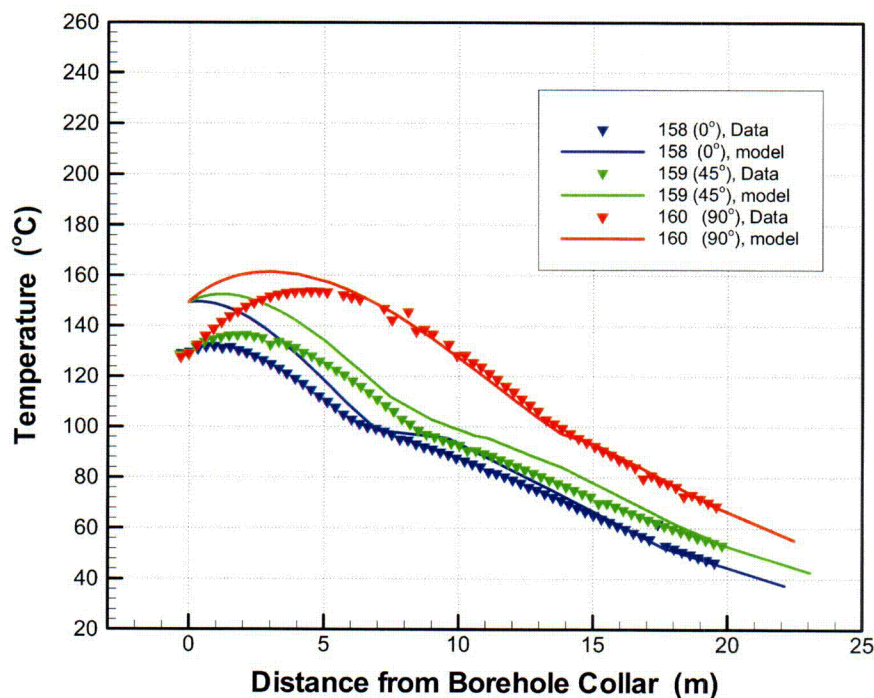


Figure 7.4.3.1-1 (continued).

Measured and Simulated Temperature Profile in Boreholes 158, 159, and 160 at Different Times of Heating: (a) 12 months, (b) 24 months, (c) 36, and (d) 48 months



Figure 7.4.3.1-2 presents simulated and measured temperature profiles at 5 months following heater turn-off in boreholes 158, 159, and 160. (Qualified temperature data are only available through the end of June 2001; i.e., about 5 ½ months of natural cooling in the DST rock block.) Close to the heat sources, the temperatures have significantly dropped. Note that the rock thermal gradients in the drift vicinity are directed towards the drift wall. In horizontal borehole 160, this is mainly a result of the hotter rock region around the wing heaters, where the thermal load was particularly strong during the 4-year heating phase (compare with Figure 7.4.3.1-1d for the temperature profile close to the end of heating). In the other boreholes, the thermal gradient towards the drift wall is a result of the small heat capacity within the drift; much more energy is stored in the rock than in the drift, so that the rock cooling is slower. In general, there is reasonably good agreement between measured and simulated temperatures during cooling. Similar to the heating phase, the simulated temperatures are somewhat higher than the measured temperatures in boreholes 158 and 159. In borehole 160, they are almost identical, particularly far away from the heat sources. The absence of the “humps” in the temperature profile in borehole 160 during cooling is understood because of the absence of heat output from the wing heaters. That the simulated temperatures at the drift wall are higher than the measured temperatures has already been discussed. At the end of heating, the wall of the Heated Drift was at approximately 208°C, whereas the simulated drift-wall temperature was close to 228°C (see Figure 7.4.3.1-1d), i.e., a difference of 20°C. At 5 months of cooling, there is almost an identical difference of 20°C between measured and simulated temperatures. The simulated temperature drop during cooling is very similar to the measured temperature drop.



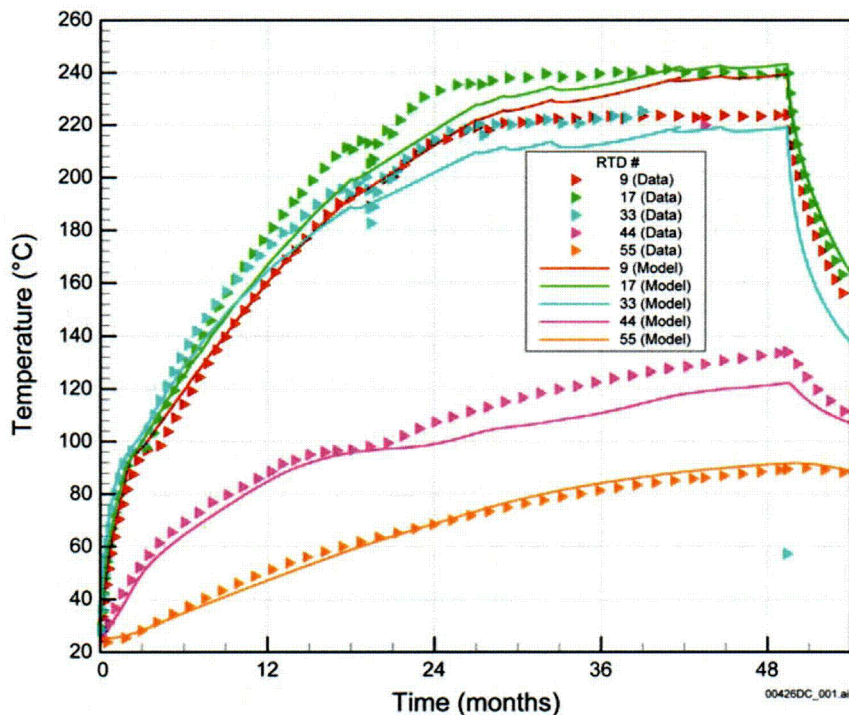
Output DTN: LB0303DSCPDSTV.001.

Input DTN: MO0208SEPDSTTD.001 [DIRS 161767].

Figure 7.4.3.1-2 Measured and Simulated Temperature Profile at 5 Months of Cooling in Boreholes 158, 159, and 160

### 7.4.3.1.2 Temperature History

The temporal evolution of measured and simulated temperatures is shown in Figures 7.4.3.1-3a through 7.4.3.1-3c, for a time period that covers 49.5 months of heating and 5.5 months of cooling. First, the temperature history is analyzed for a few selected sensors in borehole 160. Borehole 160 is the horizontal borehole running slightly above the wing heaters that was already presented in Section 7.4.3.1.1. The sensors selected are 160-9, 160-17, 160-33, 160-44 and 160-55, located at distances of 2.13, 4.54, 9.36, 12.67, and 15.96 m from the borehole collar, respectively. The other boreholes shown are boreholes 59 and 60, two boreholes in the first cluster of hydrology holes (57-61) located about 10 m down the Heated Drift from the bulkhead. In the vertical plane of cluster 57-61, boreholes 59 and 60 are closest to the source of heat, with borehole 59 above and borehole 60 below the Heated Drift (see Figures 7.2.2-2 and 7.3.3-3). Each of these boreholes has four temperature sensors installed in them (59-1 through 59-4 and 60-1 through 60-4), with their locations indicated in Figure 7.3.3-3. All three boreholes chosen for the temperature analysis experience large changes, both in terms of temperature and moisture redistribution (to be discussed later).



(a)

Output DTN (for Figures 7.4.3.1-3a through 3c): LB0303DSCPDSTV.001.

Input DTNs (for Figures 7.4.3.1-3a through 3c): MO9807DSTSET01.000 [DIRS 113644], MO9810DSTSET02.000 [DIRS 113662], MO9906DSTSET03.000 [DIRS 113673], MO0001SEPDSTPC.000 [DIRS 153836], MO0007SEPDSTPC.001 [DIRS 153707], MO0012SEPDSTPC.002 [DIRS 153708], MO0107SEPDSTPC.003 [DIRS 158321], MO0202SEPDSTTV.001 [DIRS 158320], MO0208SEPDSTTD.001 [DIRS 161767]

Figure 7.4.3.1-3. Temporal Evolution of Temperature in Selected Sensors of Boreholes (a) 160, (b) 59, and (c) 60



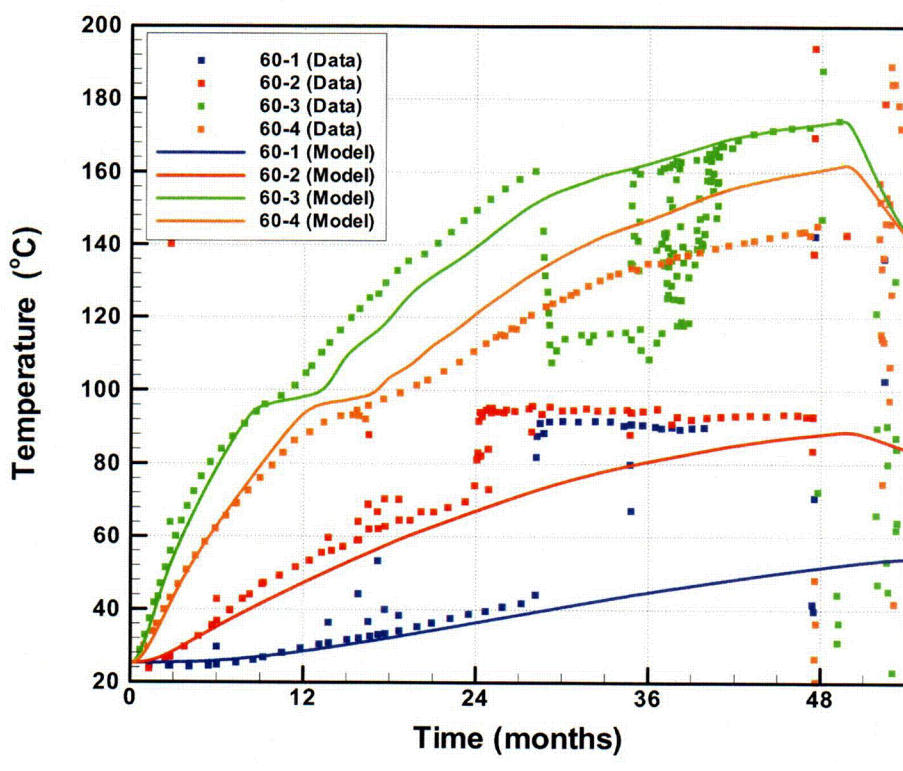
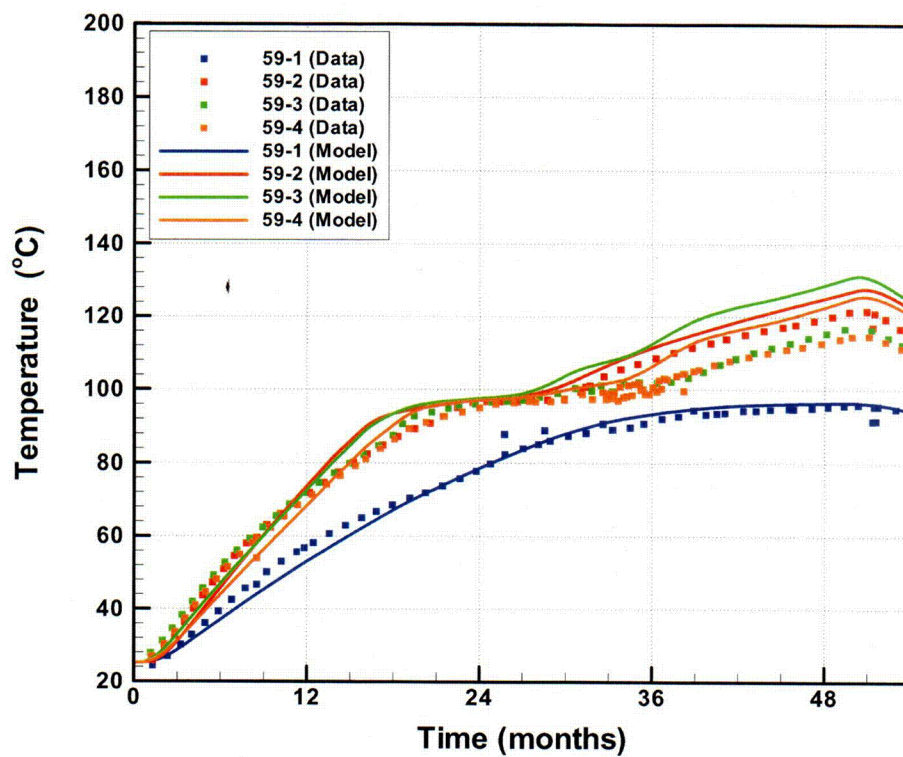


Figure 7.4.3.1-3 (Continued). Temporal Evolution of Temperature in Selected Sensors of Boreholes (a) 160, (b) 59, and (c) 60

The sensors in borehole 160 show a wide variety of temperature responses, depending on their location with respect to the heat sources (Figure 7.4.3.1-3a). The three sensors 160-9, 160-17, and 160-33 are all located directly above wing heater segments, and thus exhibit strong thermal perturbation. Both measured and simulated curves have short heat-pipe signals, indicating that rock water is boiled off within a short time period. At later heating stages, the measured temperatures run slightly higher than the simulated ones, as discussed in the previous section. Sensors with this close proximity to the wing heaters show the effect of the smeared-out heater representation in the model. (Note that Sensor 160-33 stopped functioning at about 37 months of heating.) Sensor 160-44 measures rock temperature close to the tip of the wing heater, a few meters further into the rock. The temperature increase is slower and a heat pipe of significant duration evolves, beginning at about 15 months and lasting for 6 to 9 months. This indicates that the fractured rock at the location of this sensor remained in the two-phase boiling zone during this entire time period, and became dry afterwards as the boiling front eventually moved further away from the heater. While both curves exhibit the same starting point, the simulated temperature results show a slightly longer duration of the heat-pipe signal compared to the measured data. Finally, Sensor 160-55, with the largest distance into the rock, remains below boiling temperature for the entire heating phase. The measured and the simulated results match well for this sensor. Figure 7.4.3.1-3a also shows temperature evolution during the first 5.5 months of cooling. The higher the temperature at the end of heating, the steeper the drop in temperature when the heaters are turned off. For most sensors, the temperature decrease during cooling appears to be slightly more pronounced in the measured data compared to the simulated results. This may indicate that heat capacity is overestimated in the model. However, a longer observation period would be needed to test this hypothesis.

The maximum temperatures in borehole 59 are smaller than those recorded in borehole 160, because of the larger distance from the heat sources (Figure 7.4.3.1-3b). Sensor 59-1, closest to the borehole collar, reaches only about 88°C at the end of heating phase. The other sensors in borehole 59 record higher temperatures, reaching about 115°C towards the end of heating phase. Each of these sensors records a heat-pipe signature of considerable duration, beginning at about 19 months of heating and lasting for close to a year. The long duration of the heat-pipe signal is caused by a significant reflux of water from the condensation zone back to the boiling region, driven by gravitational and capillary forces. Notice that the agreement between measured and simulated temperatures is good in all the four sensors of borehole 59. In particular, the duration of the heat-pipe signal is accurately captured by the numerical model. Good agreement is also seen during the first 5.5 months of cooling.

Compared to borehole 59, borehole 60 is slightly closer to the heat sources, and runs below the Heated Drift instead of above it (Figure 7.4.3.1-3c). Sensors 60-1 and 60-2 record the smallest temperatures, owing to their location several meters sideways from the tip of the wing heaters. They remain below boiling temperatures during the entire test phase, and reasonably good agreement is seen between the measured and simulated curves. The other two sensors, 60-3 and 60-4, record much higher temperatures. Both sensors exhibit heat-pipe signals, though they appear earlier than those in borehole 59 and are of shorter duration. Part of this is caused by the closer proximity of the two sensors to the heat source compared to the sensors in 59. However, the main reason for the shorter duration two-phase conditions in 60 is that the borehole is below the Heated Drift. Here, most of the condensate that accumulates outside the boiling zone will drain downwards with gravity away from the DST rock. While both the measured and simulated

temperatures exhibit short heat-pipe signals compared to borehole 59, the simulation results show more pronounced signals of longer duration. Section 7.4.4 discusses how these subtle differences lead to interesting conclusions regarding the use of the DKM model for fracture-matrix interaction versus the AFM model. Note that the distortions in measured temperature data (sudden rise in 60-1 and 60-2, sudden drop in 60-3) are caused by deflation (failure) of the packers in the borehole. The temperature sensors in boreholes 59 and 60 are not grouted; instead, they are attached to the packer string in the open borehole. Hence, once the packers are deflated, the borehole acts as an open conduit for vapor flow, and temperature in measurement intervals that were originally isolated by packers can easily equilibrate with each other. The packer strings were removed in November 2001, just prior to end of heating. Therefore, no temperature data are available from this borehole during cooling.

In general, the agreement between measured and simulated temperature history is good for all three boreholes, comparing temperature sensors that are representative of locations with fairly different TH behavior. In particular, the temporal evolution of heat-pipe signals has been well represented by the model. For a few sensors, namely 60-3 and 60-4, the predicted heat pipes are of longer duration than the measured heat pipes. Section 7.4.4 demonstrates that these differences can in part be explained by the conceptual model used for fracture-matrix interaction.

#### 7.4.3.1.3 Temperature Statistics

Discussions in Sections 7.4.3.1.1 and 7.4.3.1.2 indicate qualitatively good agreement between measured and simulated temperatures. Results from the statistical analysis of measured and simulated temperatures at the DST are presented for a more quantitative validation. The two statistical measures used are the mean difference and the root mean square difference, the former revealing a systematic bias, the latter giving the overall accuracy of the simulation compared to the measured data (see Section 7.4.2).

Table 7.4.3.1-1. Statistical Comparison of Measured and Simulated Temperatures

Time (months)	Statistical Measure	
	Mean Difference (MD) (°C)	Root Mean Square Difference (RMSD) (°C)
6	0.01	5.63
12	-0.15	7.21
18	0.90	8.72
24	1.06	9.79
30	1.27	10.49
33	1.65	10.61
36	2.01	11.27
42	2.95	12.60
48	3.59	12.80
5 months cooling	4.34	8.12

NOTE: The following DTNs give simulated and measured temperature data that were used to calculate the statistical measures given above, as defined in Section 7.4.2. Simulated Temperature is from Output DTN: LB0303DSCPDTV.001. Measured Temperatures are from Input DTNs: MO9807DSTSET01.000 [DIRS 113644], MO9810DSTSET02.000 [DIRS 113662], MO9906DSTSET03.000 [DIRS 113673], MO0001SEPDSTPC.000 [DIRS 153836], MO0007SEPDSTPC.001 [DIRS 153707], MO0012SEPDSTPC.002 [DIRS 153708], MO0107SEPDSTPC.003 [DIRS 158321], MO0202SEPDSTTV.001 [DIRS 158320], MO0208SEPDSTTD.001 [DIRS 161767]

From Table 7.4.3.1-1, the mean difference is mostly positive and increases slowly through successive months of heating. A positive mean difference implies that overall the temperatures from the DST TH model are higher than the measurements. For example, at 24 months of heating, simulated temperatures are on an average 1.06°C higher than measured temperatures. The difference increases with continuation of heating, reaching 3.59°C at the end of heating and 4.34°C at 5 months of cooling. That the mean difference between the simulated and the measured temperatures is always less than 5°C, i.e., less than 2 percent of the maximum rock temperature at the end of heating and much smaller than the validation criterion of less than 10°C mean difference, is significant considering the complicated nature of the DST and the uncertainties involved in modeling the thermal hydrology in an open field test like the DST.

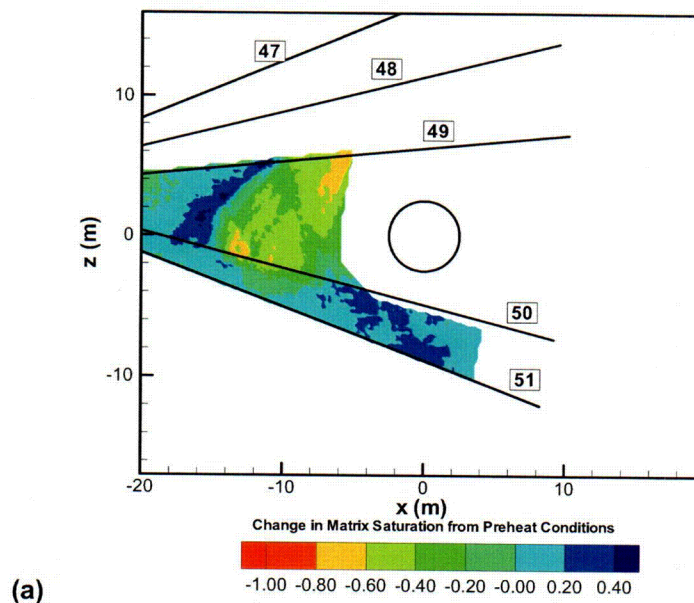
The root mean square difference, though increasing rapidly at the early phases of heating, plateaus during later phases of heating and the first 5 months of cooling. The maximum value of root mean square difference of about 12.8°C, on the order of about 5 percent of the maximum rock temperature, indicates a reasonably good statistical fit between measured and simulated temperatures. In addition, though the RMSD increases with time, it begins to plateau towards the end of the heating period. This trend provides confidence that, even if the test were to be run for a longer period, RMSD would have been within acceptable limits (i.e., there would still be good fit between measured and predicted temperature data). These results, involving more than 1,700 sensors, together with the illustrations of the temperature profiles and the temporal evolution of temperatures shown in Section 7.4.3.1.1 and 7.4.3.1.2, indicate that the TH processes have been accurately captured in the DST TH model.

#### **7.4.3.2 Water Redistribution: Matrix Saturation**

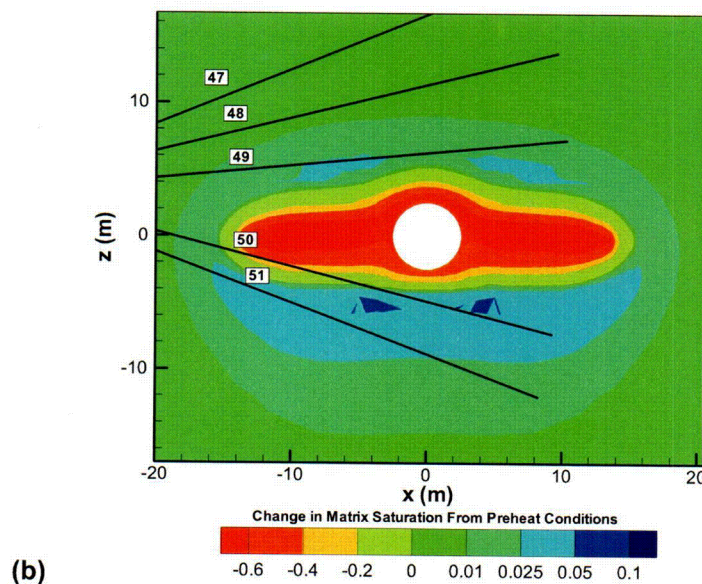
TH processes of water boiling, vapor transport and subsequent condensation, drainage in fractures, and imbibition of water into the matrix result in redistribution of moisture in the DST block. As presented in Section 7.4.1, saturation changes in the rock matrix in the DST are tracked by neutron logging, ERT, and GPR. All three types of measured data show existence of dryout zones in the matrix that expand with time and build-up of condensate outside the dryout regions where matrix saturation increases from the ambient value. To validate the DST TH model, the matrix saturation predicted by the DST TH model is compared against measured geophysical-radar-tomography data. The goal is to demonstrate that the DST TH model captures the essential elements of the coupled TH processes expected to occur in the rock matrix. It needs to be emphasized that, because of the qualitative nature of measured geophysical data, the comparison between measured and simulated matrix saturation is also qualitative. Nevertheless, matching the patterns and time evolution of simulated and measured dryout and condensation zone does provide effective validation for the dominant TH processes. In this report, GPR data are used for comparison with simulated results.

The following sequence of Figures 7.4.3.2-1a through 7.4.3.2-3a show the contours of change in matrix water saturation from preheat ambient conditions as obtained from GPR measurements, at time snapshots of approximately 14 (January 1999), 23 (October 1999), and 49.5 (January 2002) months of heating. (Heating started on 12/03/1997 and lasted until 01/14/2002.) For comparison with the simulated saturation values, the water content data initially derived from the GPR measurements (DTN: LB0210GPRDSTHP.001 [DIRS 160895]) have been divided by the matrix porosity of the Ttpmn rock unit (0.11). The GPR measurements are obtained in a cluster

of boreholes designated for geophysical measurements (boreholes 47 to 51), bracketing the Heated Drift at a distance of about 6 m from the bulkhead (see Figure 7.2.2-3). From this cluster, borehole 49 above the drift and boreholes 50 and 51 below the drift had been selected for cross-borehole GPR testing. Thus, the rock volume covered is bounded between these boreholes. For comparison with the measured results, the simulated saturation changes from the ambient conditions are plotted in Figures 7.4.3.2-1b through Figures 7.4.3.2-3b. The time snapshots selected here are 12, 24, and 48 months of heating, slightly different from the respective GPR collection times, as the full simulation output from the TOUGH2 runs was produced on a 6-month basis.



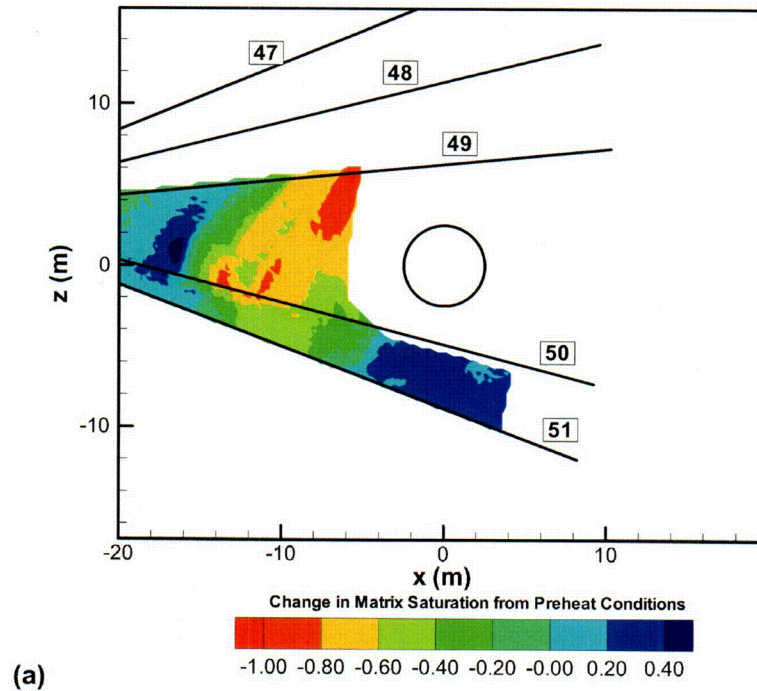
Derived from Input DTN: LB0210GPRDSTHP.001 [DIRS 160895].



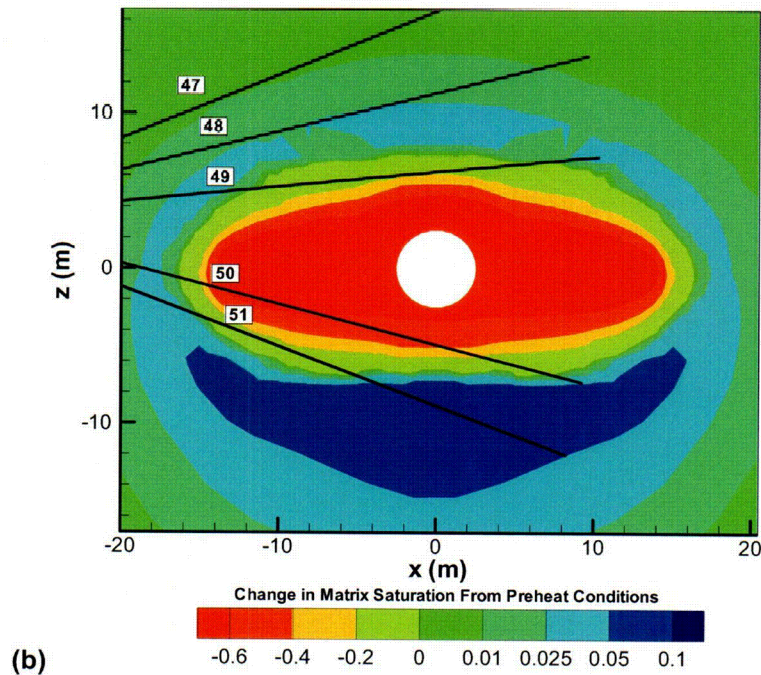
Output DTN: LB0303DSCPDSTV.001.

Figure 7.4.3.2-1 Change in Matrix Saturation from Preheat Saturation (a) Measured GPR Results in Boreholes 49 to 51 in January 1999 (Approximately 14 Months of Heating) and (b) Simulated Results at 12 Months of Heating



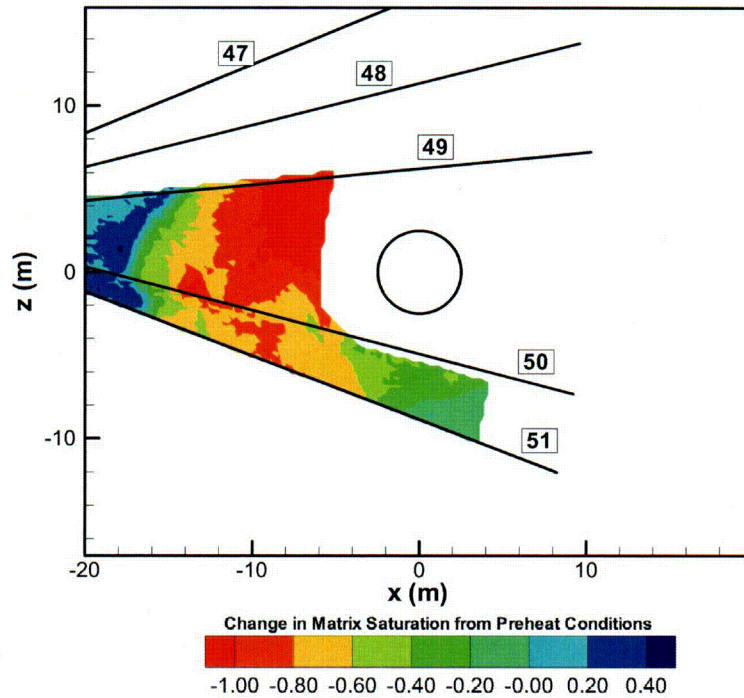


Derived from Input DTN: LB0210GPRDSTHP.001 [DIRS 160895].



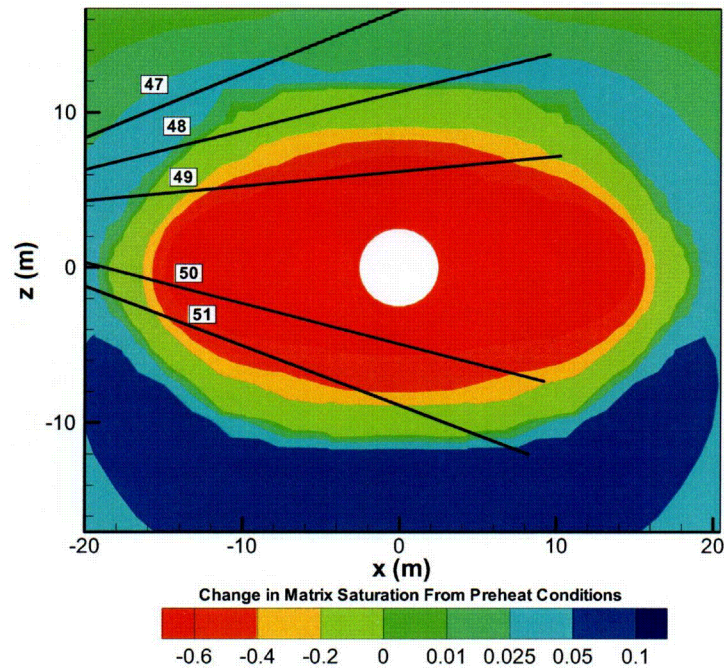
Output DTN: LB0303DSCPDSTV.001.

Figure 7.4.3.2-2. Change in Matrix Saturation from Preheat Saturation (a) Measured GPR Data in Boreholes 49 to 51 in October 1999 (Approximately 23 Months of Heating) and (b) Simulated Results at 24 Months of Heating



(a)

Derived from Input DTN: LB0210GPRDSTHP.001 [DIRS 160895].



(b)

Output DTN: LB0303DSCPDSTV.001.

Figure 7.4.3.2-3. Change in Matrix Saturation from Preheat Saturation (a) Measured GPR Data in Boreholes 49 to 51 in January 2002 (Near the End of Heating) and (b) Simulated Results at End of Heating Phase

Figure 7.4.3.2-1 shows the matrix saturation changes at approximately 1 year of heating. The measured results indicate a significant volume of rock that has saturation less than ambient. The red, yellow, and greenish colors in this figure imply decrease in saturation (or drying), while the blue colors indicate increase in saturation (wetting or condensation). The dryout zone extends mainly between boreholes 49 and 50; however, dryout is also seen at the tip of the wing heater between boreholes 50 and 51. Increase in saturation occurs below the heated area between boreholes 50 and 51, and in the rock just outside of the wing heater tip between boreholes 49 and 50. These observations are now compared with the simulation results. Here, the color map is slightly different. The red, yellow, and light green colors show drying. Increase in saturation corresponds to dark green or blue colors. Comparison indicates that there is remarkable consistency in the location of the dryout and condensation zones between the two plots (i.e., drying between boreholes 49 and 50, and also between 50 and 51 at the tip of the wing heater; condensate buildup between 50 and 51 below the heaters, also at the tip of the wing heater just outside of the heated area). The only difference in saturation pattern is seen above the heaters close to borehole 49, where the measured data indicate that the rock may already be drying.

Similar results can be seen in Figure 7.4.3.2-2, at about 2 years of heating. In both the measured and simulated data, the dryout zone has extended and the saturation decrease in this zone has become more pronounced. Note, for example, that the area between boreholes 50 and 51, close to the tip of the wing heaters, is now fully drying in both plots. Also, signals of condensate buildup are more obvious now in both figures, in particular below the Heated Drift between boreholes 50 and 51. Finally, at the end of heating (Figure 7.4.3.2-3), most of the rock volume bracketed between the GPR boreholes has dried, except for areas outside of the tip of the wing heaters. Again, the agreement between the geophysical measurements and the simulated results is excellent.

Two GPR measurements have been performed during the cooling phase, at approximately 2.5 months of cooling (data collected on 03/25/2002; cooling started 01/14/2002) and at 5 months of cooling (data collected on 06/13/2002). However, the changes in matrix saturation compared to the conditions at the end of heating are very subtle, smaller than the measurement uncertainty related to the GPR method. This is supported by simulation results in which the saturation changes after 6 months of cooling are mostly within  $\pm 0.05$ . Direct comparison of measured and simulated results will be meaningful only for later times when more significant processes of rewetting have occurred; therefore, no results are presented in this report.

### **7.4.3.3 Water Redistribution: Fracture Saturation**

Wetting and drying in fractures (in other words, increase and decrease of liquid saturation) gives rise to changes in air permeability. At the beginning of the heating period, drying first occurs around the Heated Drift and the wing heaters. Just outside of this drying zone, a zone of higher than ambient saturation forms because the produced vapor condenses in cooler areas. Air-injection tests performed in this condensate zone should first exhibit a decrease in air permeability. With continued heating, the drying zone expands, and areas that were initially located in the condensate zone will now be dry. As a result, air permeabilities in these zones should rise because the fracture water content is slightly smaller than at ambient. Thus, by

tracking air-permeability changes, the movement of drying and wetting in the fractures can be tracked.

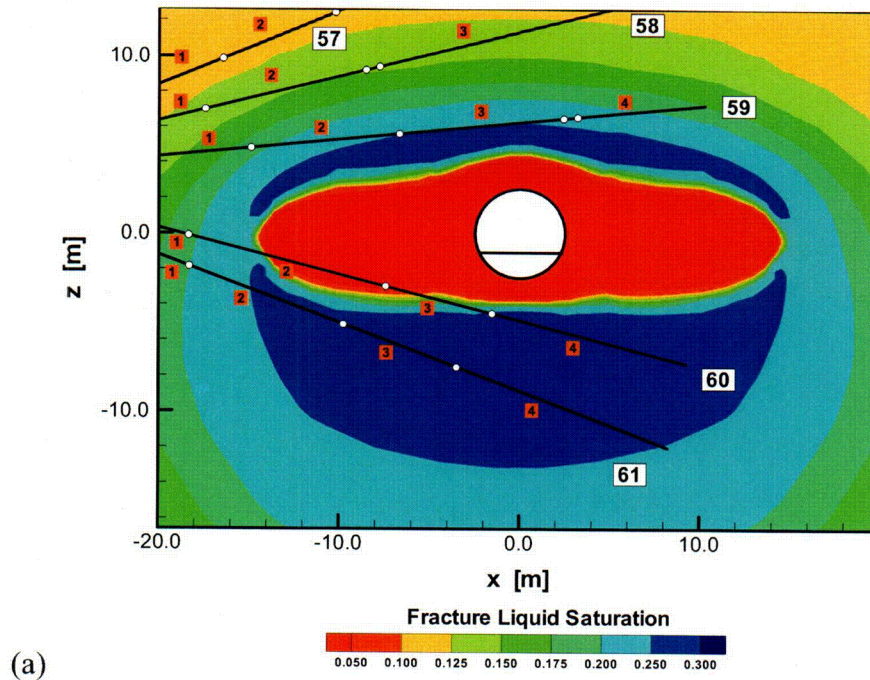
It should be noted that THM effects in response to heating—opening and closure of fractures—also affect air-permeability data. These processes, which are not accounted for in the DST TH model, are explicitly simulated and discussed in *Drift Scale THM Model* (BSC 2004 [DIRS 169864]), documenting a fully coupled THM model. (THC effects on air permeability, e.g., from mineral precipitation/dissolution, are less relevant for DST. The duration of the DST is too short to show significant effects of fracture aperture changes due to THC processes.) For the comparative interpretation of air-permeability data and TH simulation results conducted in this report, the expected effects of THM processes are considered in a qualitative manner. Typically, elevated temperatures lead to closure of fractures in the vicinity of the heat sources (giving rise to a decrease in air permeability) and to fracture opening in cooler regions further away from the heat source (giving rise to an increase in air permeability). The measured air permeability comprises the net effect of both TH and THM processes. For example, the TH simulation results may predict an increase in air permeability after going through a minimum as a result of fracture drying after an initial saturation increase. The measured permeability, however, may increase much later than the TH prediction indicates, because fracture closure continues to occur if the rock temperatures are still high.

First, to illustrate the dynamic movement of the drying and condensation fronts, the simulated contours of fracture saturation are presented in a vertical cross section containing hydrology boreholes 57 through 61. Figures 7.4.3.3-1a through 7.4.3.3-1d show fracture saturation at 12 months, 18 months, 24 months, and at end of heating, respectively. In the end of this section, the measured changes in air permeability resulting from the saturation changes are analyzed, selecting boreholes 59, 60, and 61 for illustration. These boreholes, because of their proximity to the heat sources, experience the most drying and wetting and should exhibit the most prominent changes in air permeability. The numbers along the boreholes indicate the location of injection intervals for air-permeability testing. Typically, the borehole packers used to create separate borehole sections for injection are placed right next to temperature sensors that are shown as circular symbols. Thus, the injection intervals extend roughly either between the deepest sensor in the borehole and the bottom of the hole, between two displayed sensors, or between the borehole collar and the first sensor.

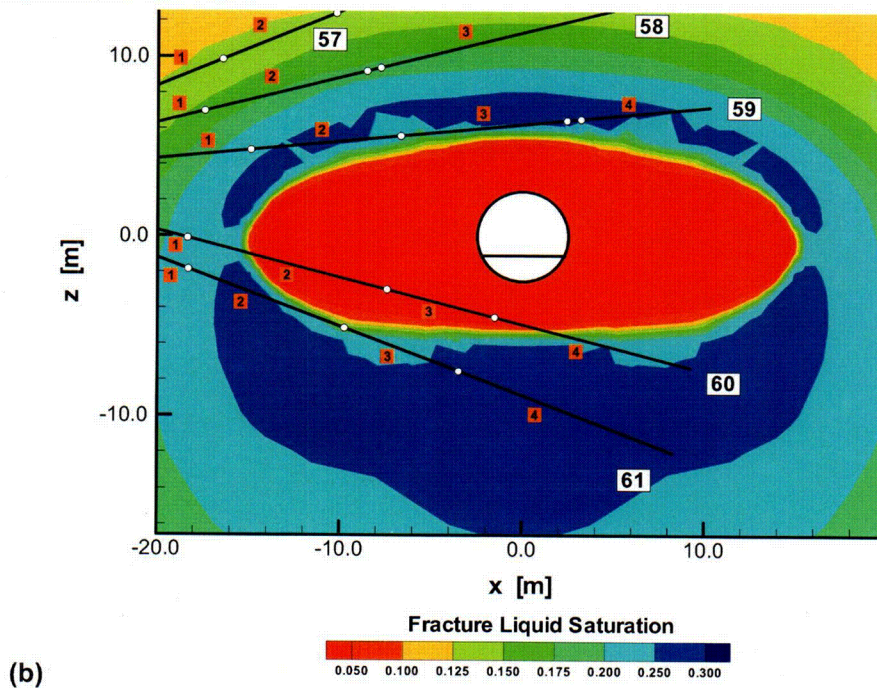
As shown in Figure 7.4.3.3-1a, significant drying (red color) can be seen in the fractures extending about 2 m above and below the Heated Drift and around the wing heaters at 12 months of heating. (Note that the ambient fracture saturation is about 0.08 to 0.09.) Areas of saturation increase (green and blue color) begin at the boundary of the drying zone and extend to about 5 m above and more than 15 m below the Heated Drift. The asymmetric buildup of the condensate zone above and below the Heated Drift is caused by gravity drainage through the fractures. Above the heaters, condensate is draining toward the boiling zone, while condensate below the heaters drains downward away from the boiling zone. The air-permeability changes expected from this saturation field are as follows: hydrology boreholes 57 and 58 should show little change because they are still residing in almost ambient-like saturation condition. In contrast, intervals 2, 3, and 4 in boreholes 59 and 61 are entering the condensate zone at 12 months of heating. These boreholes should exhibit some decrease in air permeability at this time. In borehole 60, interval 2 is partially in the dryout zone, interval 3 is in a transition state, and

interval 4 is in the condensate zone. In Figure 7.4.3.3-1b, which shows fracture saturation contours at 18 months, the dryout zone has expanded. For example, interval 4 in borehole 60, which was in the condensate zone at 12 months, is now partially in the dryout region. Interval 3, in a transition state earlier, is now fully dry. At 24 months (Figure 7.4.3.3-1c), the dryout zone has expanded enough to fully encompass interval 3 of borehole 59. On the other hand, wetting is possibly occurring in various intervals of borehole 58. Finally, Figure 7.4.3.3-1d shows the fracture saturation at the end of heating. Here, intervals 2, 3, and 4 of boreholes 59, 60, and 61 are mainly in dry-rock regions. Wetting signals should be observed in boreholes 57 and 58.



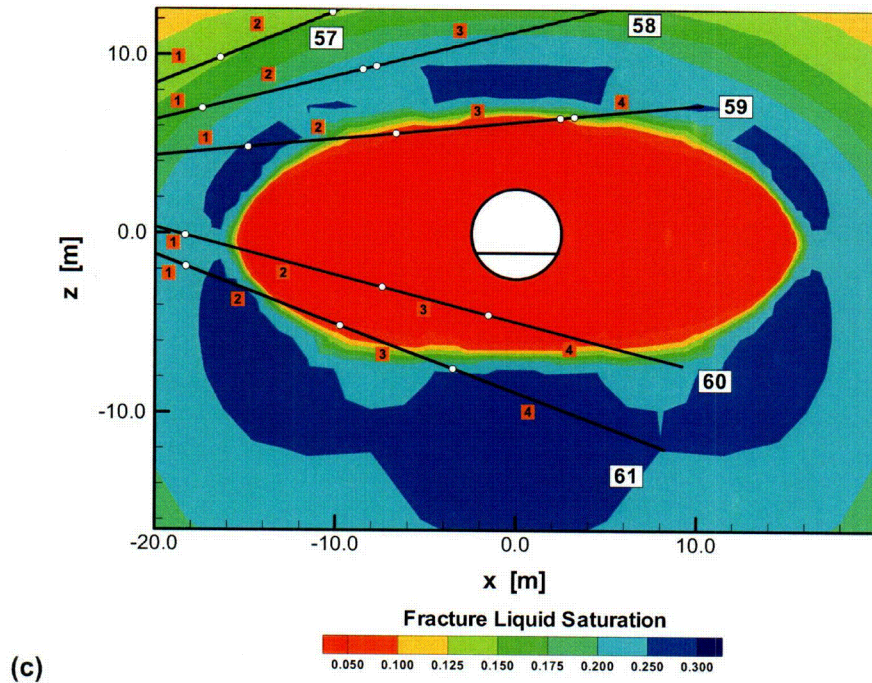


Output DTN: LB0303DSCPDSTV.001.

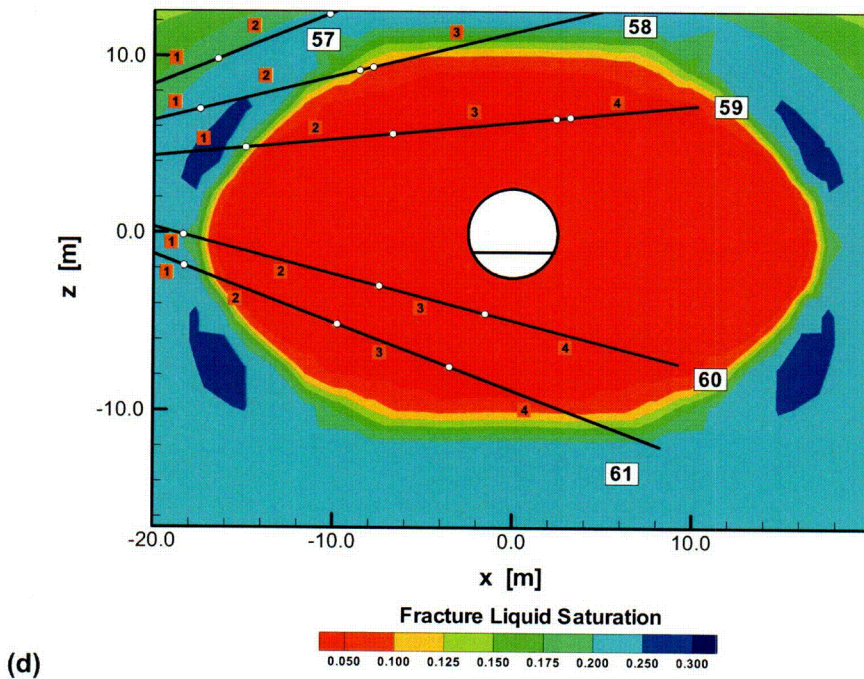


Output DTN: LB0303DSCPDSTV.001.

Figure 7.4.3.3-1. Simulated Contours of Fracture Saturation in Hydrology Boreholes 57 to 61 at Different Times of Heating (a) 12 Months, (b) 18 Months, (c) 24 Months, and (d) at End of Heating Period



Output DTN: LB0303DSCPDSTV.001.



Output DTN: LB0303DSCPDSTV.001.

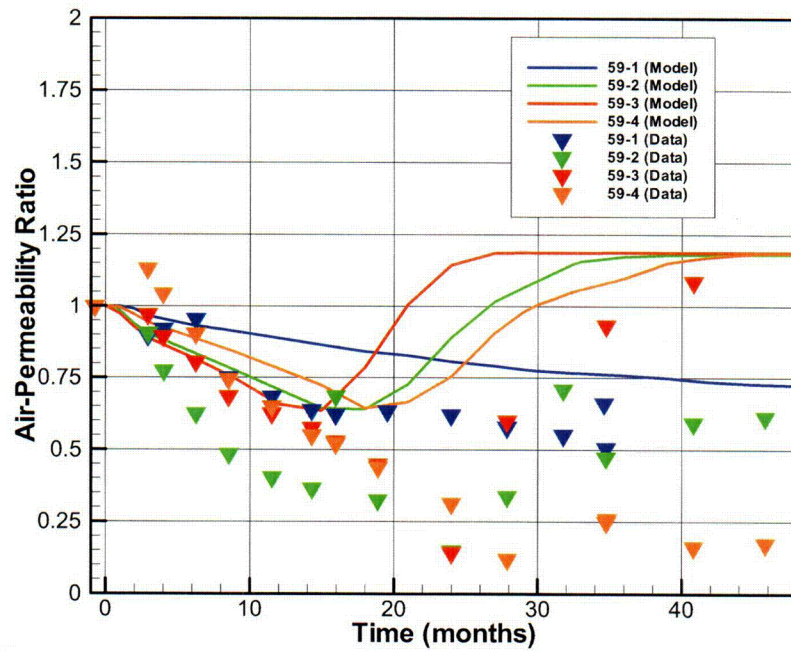
Figure 7.4.3.3-1 (Continued). Simulated Contours of Fracture Saturation in Hydrology Holes 57-61 at Different Times of Heating (a) 12 Months, (b) 18 Months, (c) 24 Months, and (d) at End of Heating Period



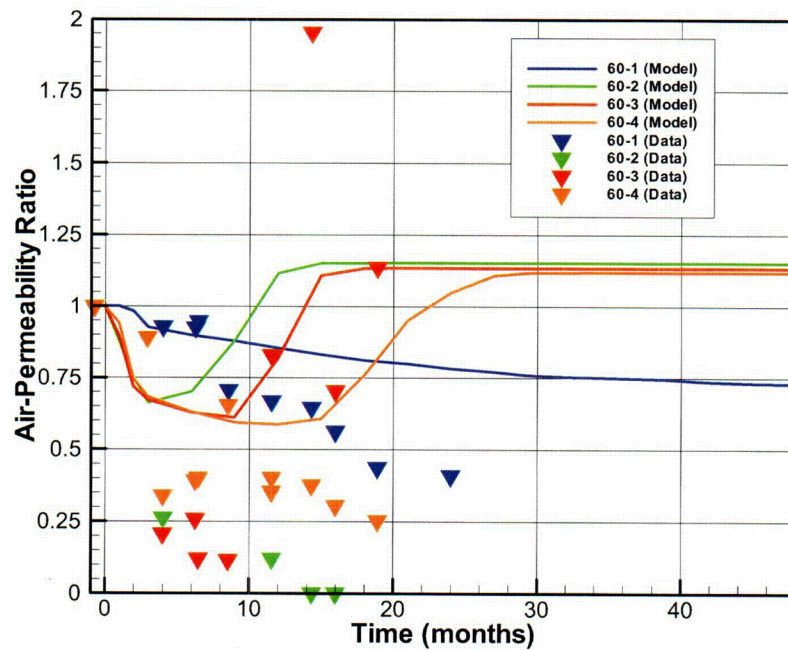
Figures 7.4.3.3-2a through 7.4.3.3-2c show the measured and simulated air-permeability data as a function of time in boreholes 59, 60, and 61, respectively. Air-injection tests were carried out before start of heating, and preheating ambient air permeabilities were determined for each of the intervals mentioned above. The vertical axis is the ratio of the time-varying air permeability and the preheating ambient air permeability. For the simulated results, air permeabilities have been calculated from simulated water saturation using the modified Brooks-Corey formulation given in Equation 6.2.1.1-13. The saturation value is extracted from those gridblocks of the numerical discretization that are nearest to the center of the injection interval. In some cases, where the injection interval is long and may comprise areas with strongly varying saturation, this procedure may lead to a misinterpretation of the results.

Consider first Figure 7.4.3.3-2a for air-injection test data in borehole 59. Measured air-permeability data in intervals 1, 2, and 3 show a monotonically decreasing trend from preheat values through at least the first two years of heating. Afterwards, they either stabilize (interval 1) or begin to increase (intervals 2 and 3). While interval 2 remains below the pretest value, interval 3 builds up to a value higher than the pretest permeability. Interval 4 has a jump in air permeability in the first few months of heating (which is related to THM effects of fracture opening outside of the hot rock region), then exhibits a steady decline similar to the other intervals and eventually becomes fairly stable towards the very end of the heating phase. Thus, over all intervals, there is a consistent trend of air-permeability decrease, indicating saturation buildup from TH effects and fracture closure from THM effects. This is followed by a period in which air permeability either increases or at least stabilizes, showing that the injection interval measures a decrease in saturation as a result of the extending drying front. During the first heating years, the simulated trend of air-permeability decrease is reasonably consistent with the observations. That the simulated decrease is smaller than the measured change is a result of the additional effect of THM fracture closure. At later times, the simulated increase of air permeability starts too early for intervals 2, 3, and 4. This again is attributed to continued THM effects near the heat source. While the simulated air permeabilities increase as a result of the predicted drying, the measured air permeabilities remain depressed because of fracture closure due to the still-high temperatures. Note that simulations performed with a fully coupled THM model indicate good quantitative agreement between measured and simulated air-permeability data (BSC 2004 [DIRS 169864], Section 7.4.3). Other factors contributing to differences between observation and simulation are local heterogeneity effects and misinterpretations arising from calculating the simulated air permeability at one point in space (while the measured values are integrated over the borehole interval).

The results shown in Figures 7.4.3.3-2b and 7.4.3.3-2c can be similarly explained. The trends of decrease, as observed in the measured data, are qualitatively represented by the simulation results, while the subsequent increase in the simulated air permeabilities is too early in most cases, because THM changes are not considered in the DST TH model. Note that as a result of packer failure, measurements in borehole 60 were only possible during the first two years of heating.



(a)



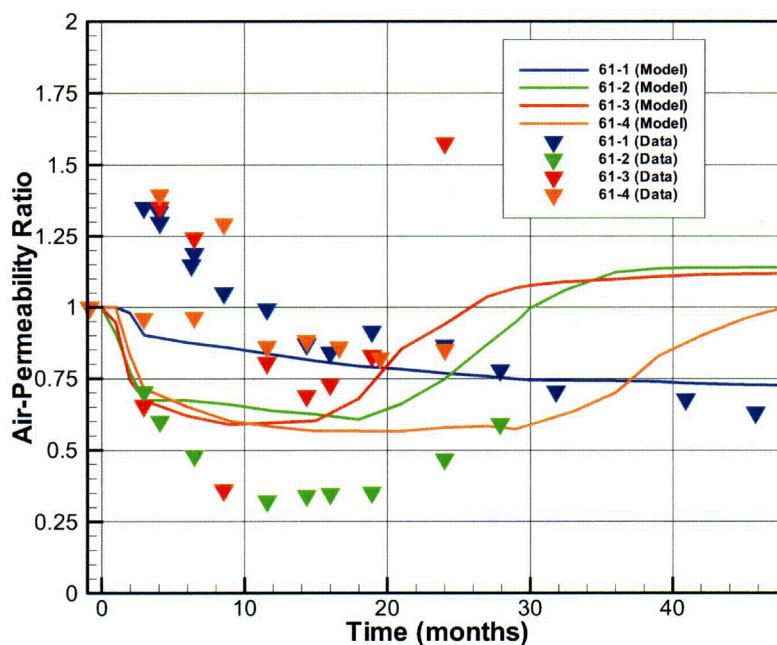
(b)

Input DTN (for Figures 7.4.3.3-2a through 2c): LB0208AIRKDSTH.001 [DIRS 160897].

Output DTN (for Figures 7.3.3.3-2a through 2c): LB0301DSCPDSTV.002.

Figure 7.4.3.3-2. Measured and Simulated Air-Permeability Ratios in Hydrology Boreholes (a) 59, (b) 60, and (c) 61



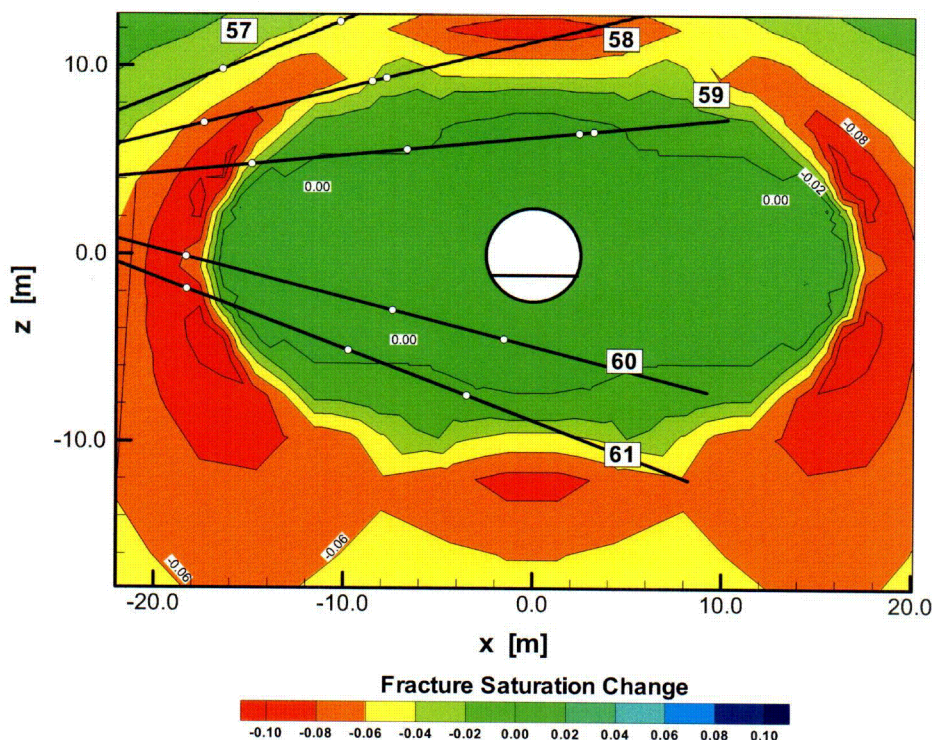


(c)

Figure 7.4.3.3-2 (Continued). Measured and Simulated Air-Permeability Ratios in Hydrology Boreholes (a) 59, (b) 60, and (c) 61

After heater turn-off in the DST, condensate water residing in the wetter zones of the rock should drain downward, away from the heated areas. Because little additional vapor is generated, the previously wetter zone should exhibit saturation decrease. This is observed from simulated contours of fracture saturation. For example, see Figure 7.4.3.3-3 for simulation results at 6 months of cooling, showing the difference in fracture saturation at this time from that at the end of heating. Some localized drying (decrease in saturation indicated by red color) is visible in the previously wet zones, just outside of the dryout region. Close to the heaters, fracture saturation remains unchanged, as rock temperature is still above boiling at 6 months of cooling. Thus, air-permeability data in most injection intervals should hardly change from the latest measurements during the heating phase. This is supported by preliminary analysis of air-injection tests conducted during cooling, indicating almost no permeability changes compared to tests performed at the end of the heating phase (Wang 2004 [DIRS 170510]). Results of these tests during cooling are therefore not presented in this report.





Output DTN: LB0303DSCPDSTV.001.

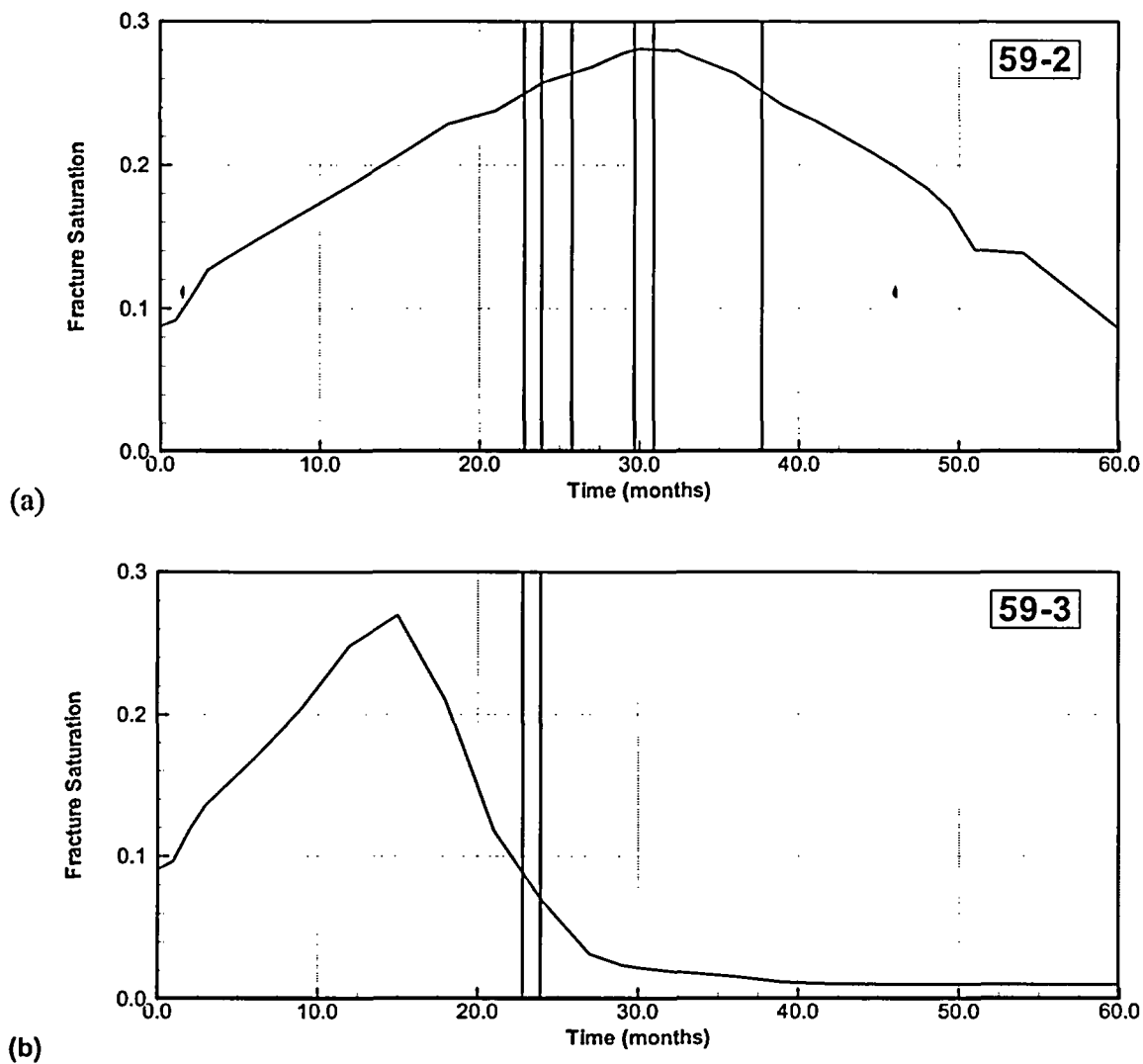
Figure 7.4.3.3-3. Contours of Change in Fracture Saturation from End of Heating to 6 Months of Cooling

In addition to air-permeability data, the temporal and spatial evolution of moisture buildup in fractures can also be evaluated by analysis of water collection in packed-off borehole intervals bracketing the Heated Drift. Increased liquid saturation in fractures within the condensation zone raises the plausibility of water seeping into borehole intervals residing at these locations. Water seepage into borehole intervals is typically promoted by increased water saturation, small-scale heterogeneity, and the presence of discrete fractures ending at the borehole wall. Since the numerical model does not explicitly account for these effects, it cannot predict the possibility of seepage into boreholes. Also, the specific location and rate of water flow into boreholes cannot be simulated in case seepage occurs. However, the general location of seepage into boreholes should coincide with regions of elevated fracture saturation. Thus, the water collection data can be used to analyze whether the simulated trends in fracture saturation are accurate. (This analysis is in addition to the model validation criteria established in BSC 2004 [DIRS 170236], Section 2.2.1.4.)

During the heating phase of the test, water samples were collected periodically (roughly every few months) from packed-off intervals in the three arrays of hydrology boreholes 57 to 61, 74 to 78, and 185 and 186. Water was produced in several intervals at several collection dates, as listed in Table 6.3.4.1-1 of *Thermal Testing Measurements Report* (BSC 2004 [DIRS 169900]). In some cases, water was collected in rock regions that were above boiling. In these cases, water vapor condensed while it was pumped through the cooler sample tubing and was collected as a sample of water. For the analysis below, these samples were not considered; i.e., only such samples were analyzed that clearly comprised water that had been in contact with the rock.

Categorization of water samples that stem from condensation of vapor in tubes is fairly straightforward because the chemistry of such samples typically exhibits very dilute mineral concentrations, consistent with distilled water. Also, such samples are typically collected at smaller pumping flow rates than the liquid water samples and often have a very low pH value.

Figures 7.4.3.3-4a through 7.4.3.3-4h show the evolution of fracture saturation extracted from the simulated results at a gridblock representative of the location of borehole intervals 59-2, 59-3, 59-4, 60-2, 60-3, 76-2, 76-3, and 186-3. These are the borehole intervals that produced liquid water samples from the start of the test through January 14, 2002. The vertical lines in these figures indicate the dates at which water was pumped out of the respective borehole intervals. (Thus at all other sample times except for these dates there was either no water in the borehole or the water was identified as water that had condensed in the tubing.) In most cases, the simulated time period of elevated saturation at the borehole interval corresponds reasonably well with the water collection times. The remaining differences can be attributed to small-scale heterogeneity, effects of discrete fractures and the fact that the simulated saturation evolution is calculated from one representative point in space (while the water may enter the borehole over the entire length of the interval). Note that no water was collected in some other instrumented borehole intervals with similar predicted saturation history. This suggests that the small-scale heterogeneity and fracture geometry in borehole vicinity are similarly important to water seepage as fracture saturation.



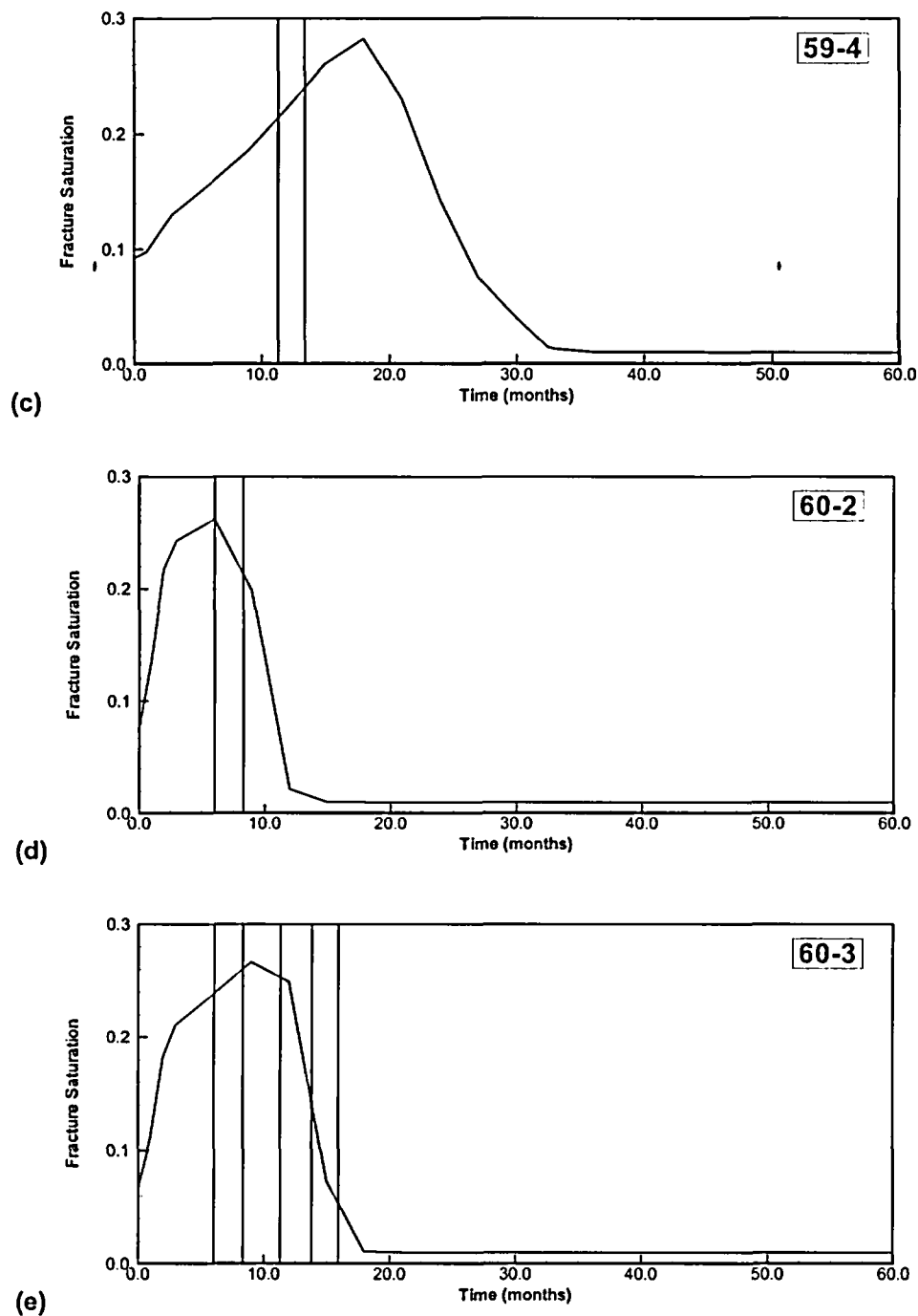
Input DTN for water collection times (for Figures 7.4.3.3-4a through 4h): SN0208F3903102.002 [DIRS 161246].

Output DTN (for Figures 7.4.3.3-4a through 4h): LB0303DSCPDTV.001.

NOTE: Vertical lines give water collection times.

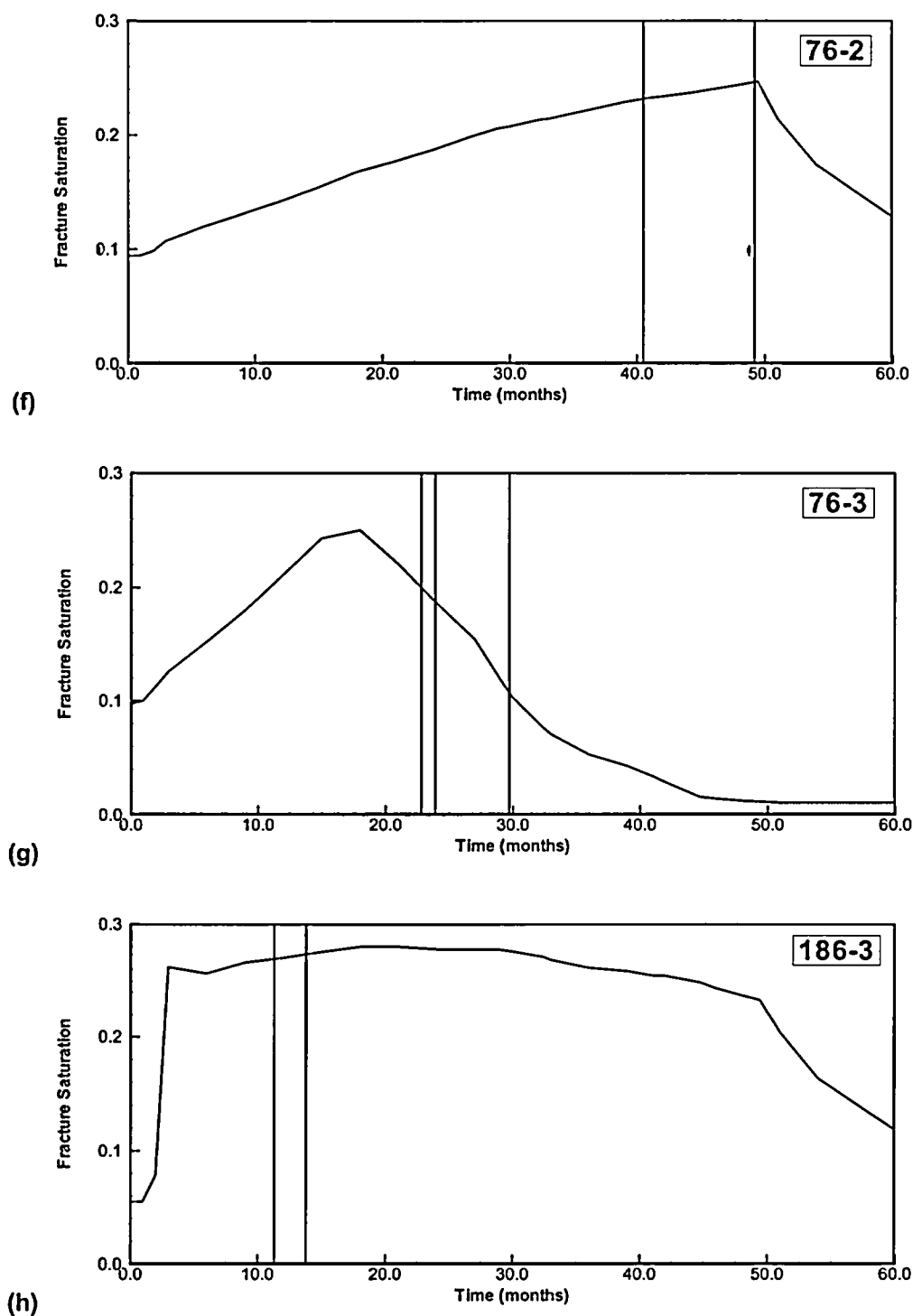
Figure 7.4.3.3-4. Simulated Fracture Saturation in Borehole Intervals (a) 59-2, (b) 59-3, (c) 59-4, (d) 60-2, (e) 60-3, (f) 76-2, (g) 76-3, and (h) 186-3





NOTE: Vertical lines give water collection times.

Figure 7.4.3.3-4 (Continued). Simulated Fracture Saturation in Borehole Intervals (a) 59-2, (b) 59-3, (c) 59-4, (d) 60-2, (e) 60-3, (f) 76-2, (g) 76-3, and (h) 186-3



NOTE: Vertical lines give water collection times.

Figure 7.4.3.3-4 (Continued). Simulated Fracture Saturation in Borehole Intervals (a) 59-2, (b) 59-3, (c) 59-4, (d) 60-2, (e) 60-3, (f) 76-2, (g) 76-3, and (h) 186-3. Vertical lines give water collection times.

Both the air-permeability results and the analysis of water collection data provide confidence in the model's capability to accurately represent the coupled TH processes. Though the predicted fracture saturation from the DST TH model are not always consistent with the pattern of measured air-permeability changes, the differences can be explained by THM effects that are not incorporated in the model. Also, the simulated fracture saturation evolution compares favorably with water collection in several hydrology boreholes.

#### **7.4.4 Comparative Analysis of the Site-Specific Property and the Calibrated Property Set**

The generally good agreement between simulated and measured results of temperature and moisture redistribution, as discussed in Section 7.4.3, indicates that the DST TH model has adequately represented the relevant TH processes in the DST. A remaining issue that needs to be addressed is that of the hydrological property set and the conceptual model for fracture-matrix interaction. The validation work in Section 7.4.3 is performed with the site-specific property set DKM-TT99 in conjunction with a standard DKM, while the predictions from the TH seepage model in Section 6 are based on the DS/AFM-UZ02-MEAN property set employing the AFM. Therefore, in this section, a comparative analysis of predictions from the DST TH model is provided with the two property sets and the two fracture-matrix interaction models. Since this comparative analysis is meant to be a sensitivity study, a two-dimensional version of the DST TH model is applied, because this considerably reduces the computational burden. This two-dimensional model is a representative vertical cross section from the three-dimensional model, identical to the three-dimensional model in every other way. Similar to Section 7.4.3, the data to be compared are temperature changes as well as matrix and fracture saturation changes, and only representative examples of these data can be presented below.

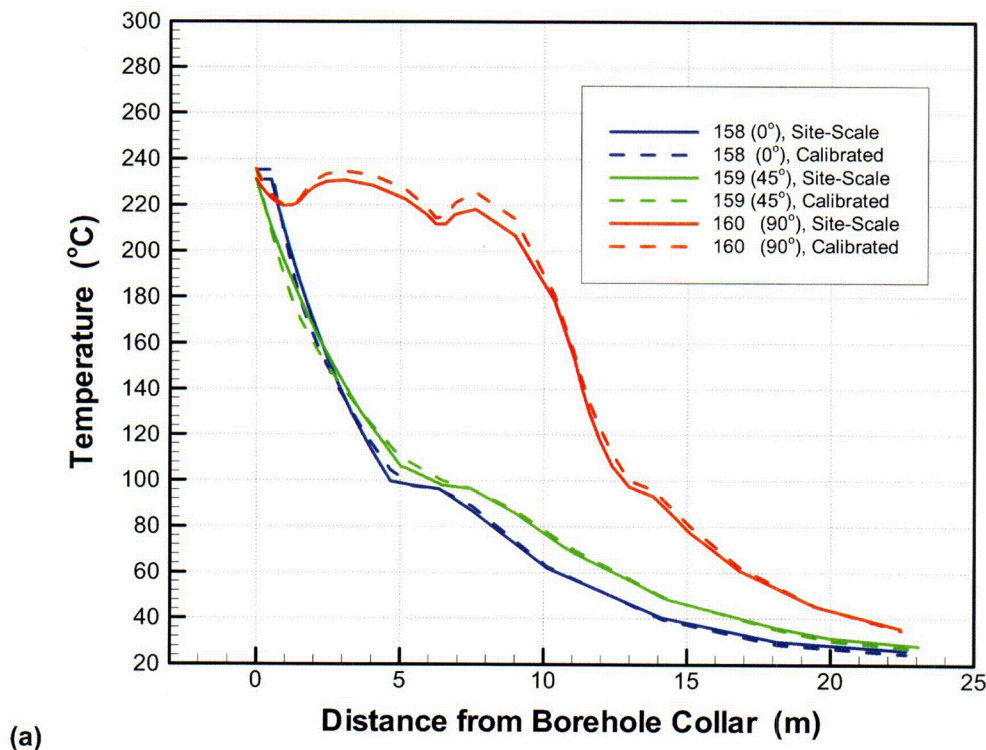
Note that a similar comparative analysis had also been conducted in the previous version of *Thermal Tests Thermal-Hydrological Analyses/Model Report* (BSC 2001 [DIRS 157330], Sections 6.2.2 and 6.3.2), comparing the same site-specific property set DKM-TT99 and a previous version of the mountain-scale calibrated property set. It was shown that both the property sets produce trends similar to the measured data, and that the differences in the model results represent sensitivity to the parameter values and not a disparity in the processes modeled. It was also shown that TH models based on both the AFM and the DKM produce TH results that compare well with measurements from the DST, and that the differences in the results given by the two conceptual models (AFM versus DKM) are not significant. The simulation results provided below support the conclusions of the previous report.

##### **7.4.4.1 Temperature**

Similar to Section 7.4.3.1, simulation results of temperature data are presented in two ways, using temperature profiles along boreholes and temperature history at selected sensors. The two-dimensional simulated results from the DKM-TT99 property set (with DKM) are directly compared with results from the DS/AFM-UZ02-Mean property set (with AFM). The selected boreholes and sensors are the same as those used in Section 7.4.3.

#### 7.4.4.1.1 Temperature Profile

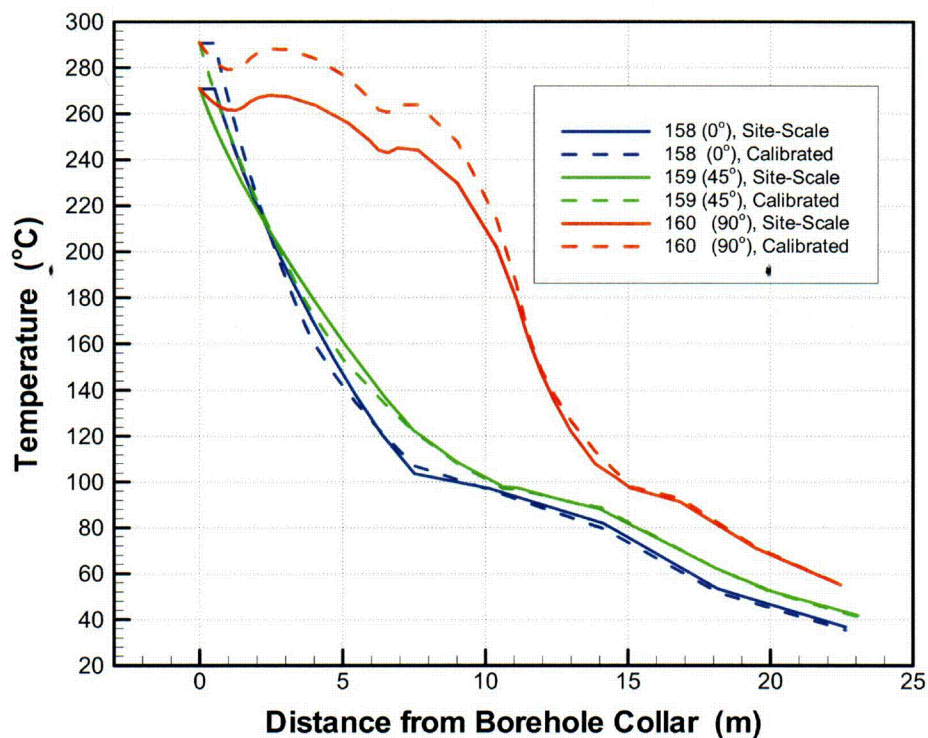
Figures 7.4.4.1-1a and 7.4.4.1-1b show simulated temperature profiles in boreholes 158, 159, and 160 at 24 months and at end of heating, respectively. The solid lines represent simulations performed with site-specific properties of the DKM-TT99 data set (Section 4.1.2.1), while the dashed lines are those with the DS/AFM-UZ02-Mean property set. The temperature profiles with the two property sets are similar in pattern. However, the simulated temperatures are slightly higher with the calibrated DS/AFM-UZ02-Mean property set, in particular close to the wing heaters in borehole 160 at the end of heating. This may in part be a result of the smaller dry thermal conductivity of the DS/AFM-UZ02-Mean, which allows less heat transfer away from the heat sources (see Section 4, Table 4.1-2). Another reason is the overall slower rate of boiling using this property set, as explained in Section 7.4.4.2 below. Heat-pipe signatures are almost identical—slightly more pronounced in the DKM-TT99 property set.



Output DTN: LB0303DSCPDSTV.001.

Figure 7.4.4.1-1. Comparison of Simulated Temperature Profiles in Boreholes 158, 159, and 160 Using the Site-Specific and DS/AFM-UZ02-Mean Property Sets at (a) 24 Months of Heating and at (b) the End of the Heating Period





(b)

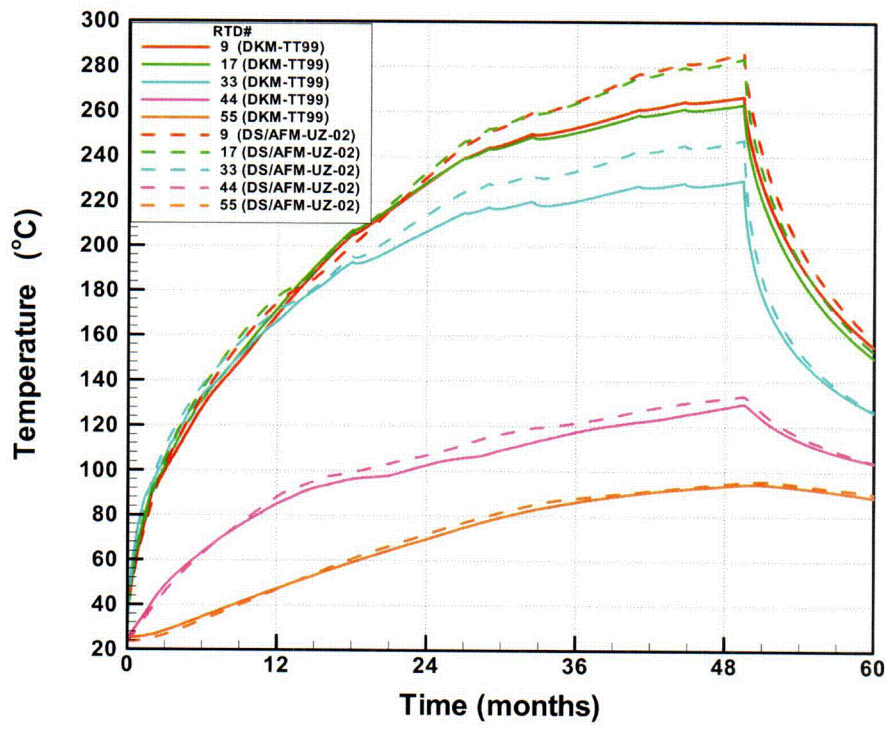
Output DTN: LB0303DSCPDSTV.001.

Figure 7.4.4.1-1 (Continued). Comparison of Simulated Temperature Profiles in Boreholes 158, 159, and 160 Using the Site-Specific and DS/AFM-UZ02-Mean Property Sets at (a) 24 Months of Heating and at (b) the End of the Heating Period

#### 7.4.4.1.2 Temperature History

Temporal evolution of temperatures is shown in Figures 7.4.4.1-2a through 7.4.4.1-2c for selected sensors of boreholes 160, 59, and 60, respectively. The solid lines are generated using the site-specific property set, and the dashed lines are generated using the DS/AFM-UZ02-Mean property set. In boreholes 160 and 59, the temperatures at above-boiling conditions are higher for the DS/AFM-UZ02-Mean property set compared to the site-specific property set. At below-boiling conditions, the temperature is similar for the two property sets. This again supports the hypothesis that the higher temperatures in the DS/AFM-UZ02-Mean results are caused by the smaller dry thermal conductivity. For the displayed sensors in boreholes 160 and 59, the observed heat-pipe signals are similar, indicating that vapor and liquid flow processes close to the sensor locations should be similar for the two simulation runs. In contrast, Figure 7.4.4.1-2c for borehole 60 shows that, while the overall agreement between the two simulation runs is good, there is a distinct difference in the heat-pipe signatures of sensors 60-3 and 60-4. The DKM-TT99 simulation—using the DKM model—shows clear heat-pipe effects, whereas there is almost no heat pipe in the DS/AFM-UZ02-Mean results—using the AFM model. This is attributed to the fact that boreholes 160 and 59 extend above the heaters, while borehole 60 extends below the Heated Drift. Vapor condensing below the drift can partially drain downward away from the heaters, thereby reducing the potential for heat pipes. It appears that the DS/AFM-UZ02-Mean results with the AFM show no heat-pipe signals because of

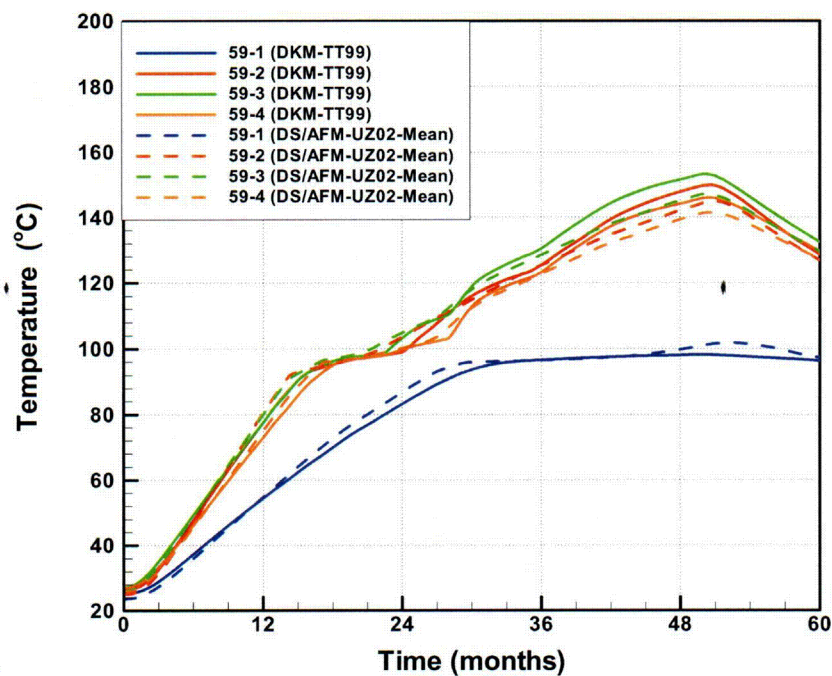
significant moisture loss from condensate drainage away from the boiling zone. Typically, the AFM features less fracture-matrix interaction compared to the DKM, so that less condensate imbibes into the rock matrix, where it would remain available for reflux back to the boiling zone as a result of capillary forces. It is shown in Section 7.4.4.3 that the fracture drainage behavior below the boiling region is indeed the main difference between simulation runs performed with the AFM and the DKM. In Figure 7.4.3.1-3c (Section 7.4.3.1.2) the measured temperature in borehole 60 is compared to the three-dimensional DST TH model results. It is noted that the measured temperatures show a minor heat-pipe signal that is clearly shorter and less pronounced than the one simulated with the DKM. It appears that the AFM model reproduces the behavior of sensors 60-3 and 60-4 somewhat better than the DKM model.



Output DTN: LB0303DSCPDSTV.001.

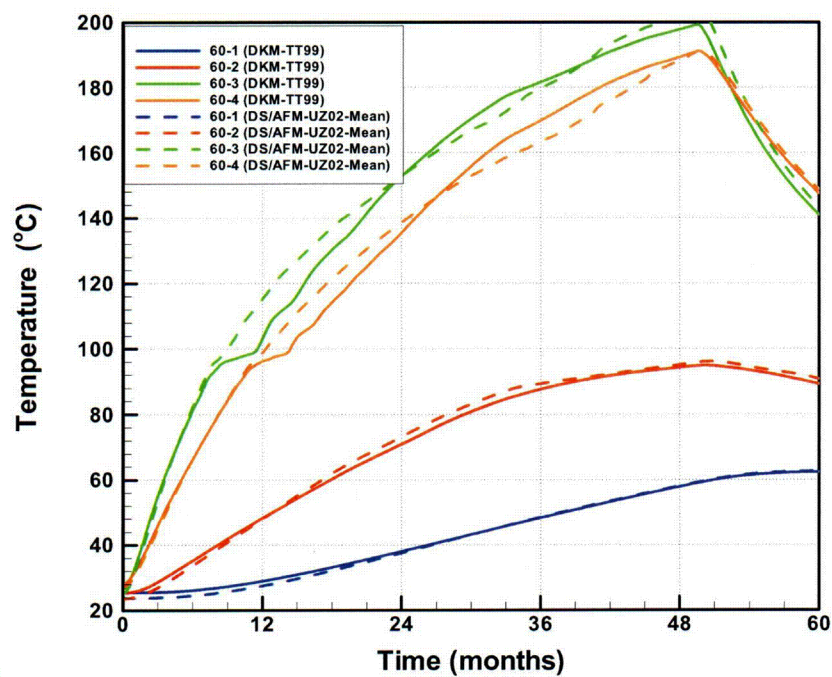
Figure 7.4.4.1-2. Comparison of Simulated Temporal Evolution of Temperature Using the Site-Specific and DS/AFM-UZ02-Mean Property Sets for Selected Sensors of (a) Borehole 160, (b) Hydrology Borehole 59, and (c) Hydrology Borehole 60





(b)

Output DTN: LB0303DSCPDSTV.001.



(c)

Output DTN: LB0303DSCPDSTV.001.

Figure 7.4.4.1-2 (Continued).

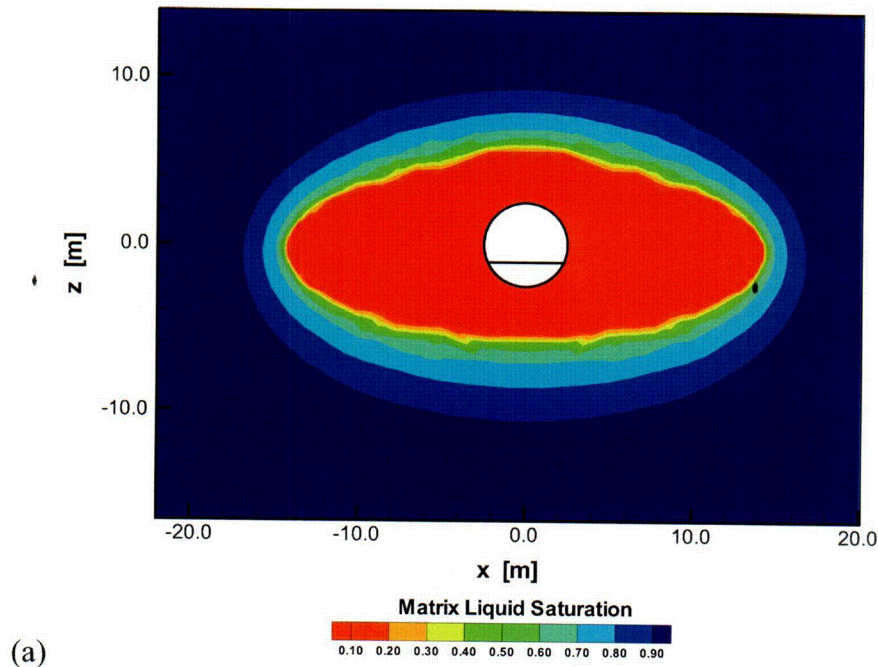
Comparison of Simulated Temporal Evolution of Temperature Using the Site-Specific and DS/AFM-UZ02-Mean Property Sets for Selected Sensors of (a) Borehole 160, (b) Hydrology Borehole 59, and (c) Hydrology Borehole 60

#### 7.4.4.2 Water Redistribution: Matrix Saturation

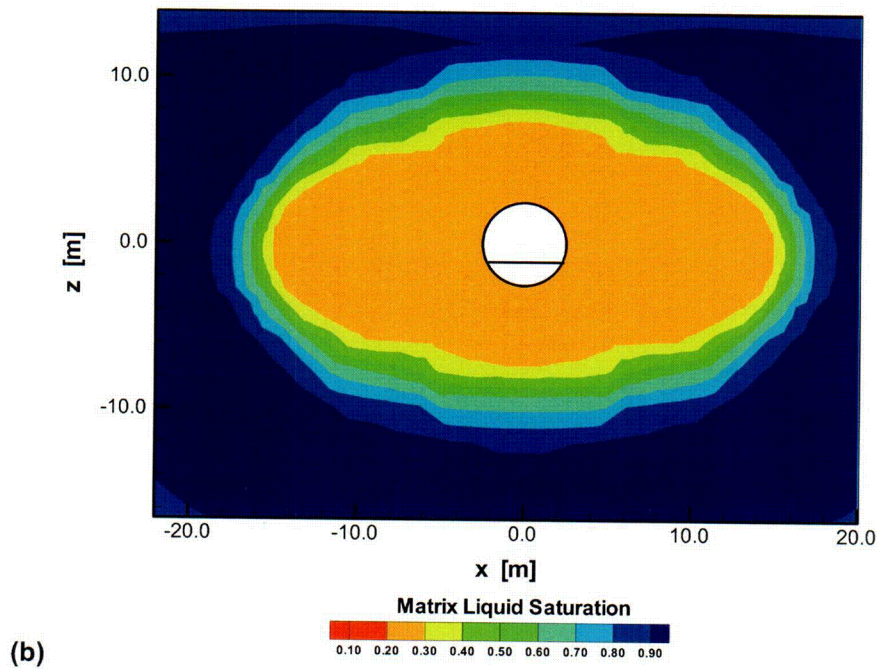
For comparison of moisture redistribution in the matrix, Figures 7.4.4.2-1a and 7.4.4.2-1b, respectively, show contours of matrix saturation at the end of heating using the DS/AFM-UZ02-Mean and the DKM-TT99 property sets. Qualitatively, the two plots show similar results. The main difference lies in the smaller dryout zone for the DS/AFM-UZ02-Mean property set compared to the site-specific property set. The smaller dryout zone arises out of slower boiling of water with the DS/AFM-UZ02-Mean properties, which can be attributed to the smaller matrix permeability in this property set compared to the site-specific property set. As a result, the vapor generated from boiling cannot move out of the pore spaces easily. Subsequently, the pressure in the matrix pores tends to substantially increase, leading to an increase in the nominal boiling temperature. This, in turn, means that boiling occurs at higher temperature, which would tend to slow down the overall boiling process and would also lead to a smaller dryout rock volume. The increase in gas pressure as a result of vigorous vaporization stems from the thermal perturbation applied to the DST rock. This is not expected to occur in the repository, where the thermal load will be smaller and applied over a much longer time period. This is confirmed by simulation results from the TH seepage model, in which the maximum gas-pressure buildup in matrix pores is a little more than one atmosphere. Also note that matrix permeability is one of the less important parameters affecting thermal seepage, compared to, for example, the fracture permeability, capillary-strength, and the percolation flux. Thus these differences between the two data sets do not impact the predictive capabilities of the TH seepage model with respect to the magnitude and evolution of thermal seepage.

The pressure increase in the matrix pores can also account for the higher simulated temperatures seen in the DS/AFM-UZ02-Mean results compared to the DKM-TT99 simulation, as discussed in Section 7.4.4.1.1. Since less water is vaporized, less energy is consumed as latent heat of vaporization, particularly in the early phases of heating. Instead, the energy is used in increasing the temperature of superheated water.





Output DTN: LB0303DSCPDSTV.001.



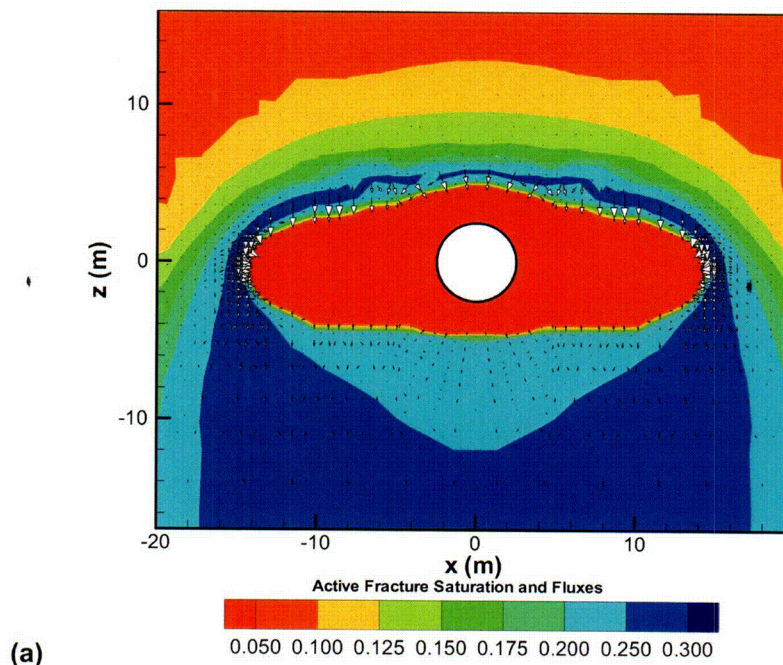
Output DTN: LB0303DSCPDSTV.001.

Figure 7.4.4.2-1. Simulated Contours of Matrix Liquid Saturation at End of Heating Using (a) the DS/AFM-UZ02-Mean Property Set and (b) the Site-Specific Property Set

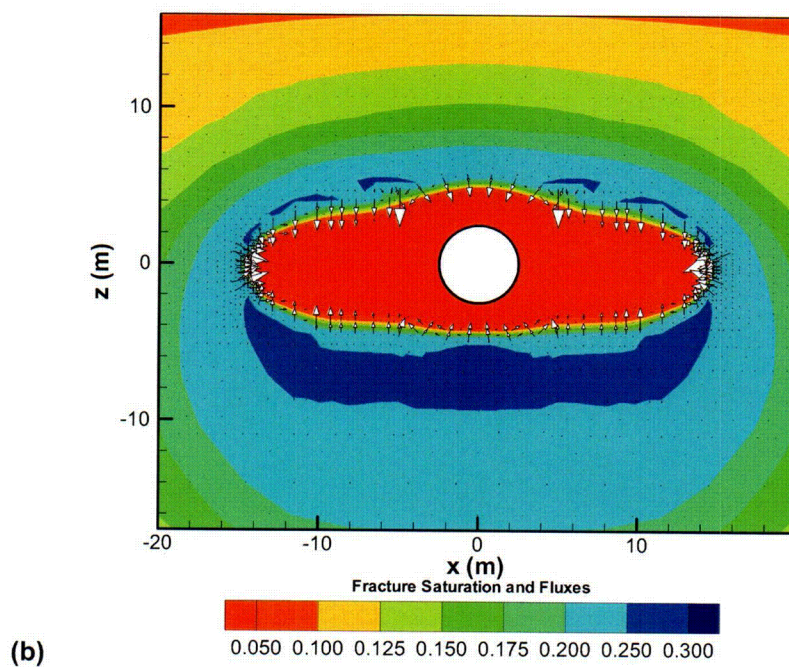
#### 7.4.4.3 Water Redistribution: Fracture Saturation and Water Flux

Figures 7.4.4.3-1a and 7.4.4.3-1b compare contours of fracture liquid saturation at 12 months of heating using the DS/AFM-UZ02-Mean and the DKM-TT99 property sets, respectively. For better comparison between simulation results from the DKM and the AFM model, the saturation of active fractures is presented in Figure 7.4.4.3-1a, instead of using the average saturation values of all active and nonactive fractures. The relationship between average saturation and active fracture saturation is given in Equation 6.2.1.1-11. The saturation contours indicate that the two simulation results give an almost identical dryout region and fairly similar condensation patterns above and to the sides of the heaters. Below the heater, however, the effect of downward drainage away from the boiling zone is significantly stronger for the DS/AFM-UZ02-Mean runs compared to the DKM-TT99 runs. The fracture-matrix interface area is smaller when using the AFM, so that less condensate imbibes from the fractures into the matrix.

To evaluate the potential effect of these differences between the DKM and the AFM model, vectors of fracture water flux are also plotted in Figures 7.4.4.3-1a and 7.4.4.3-1b. Similar to the results of the TH seepage model presented in Section 6, the maximum fluxes can be seen above the heaters, where condensate is driven towards the boiling zone by both gravitational and capillary forces. In this region, most important for thermal seepage, the DKM and the AFM fluxes are similar in magnitude, with the maximum flux in the DKM about 50 percent higher than in the AFM. (This difference in magnitude is mainly caused by the rate of boiling being smaller in the simulation using the DS/AFM-UZ02-Mean property set. There is less water produced from boiling, so that the water fluxes are somewhat smaller.) It is below the heaters where the main qualitative and quantitative differences in water flux occur. Here, the DKM model predicts larger fluxes in upward direction (from capillary suction) back towards the boiling zone, while downward drainage is less effective. The AFM, on the other hand, produces larger downward fluxes (from gravity) away from the heaters, with relatively small reflux processes towards the boiling zone. This explains why the saturation patterns below the Heated Drift are so different. It also explains why the two simulation methods produce different heat-pipe signals in sensors 60-3 and 60-4. Both these sensors are located below the heaters in a location where strong reflux of water occurs using the DKM, but rather small reflux of water with the AFM. Comparison with the measured temperature evolution at 60-3 and 60-4 seems to indicate that the water reflux predicted by the AFM is more accurate. However, other factors such as local heterogeneity effects may also play a role. Although, the air-permeability data measured in zones 3 and 4 of borehole 61 are not conclusive in defining the more accurate model for representing fracture saturation below the drift, the data are not relevant to seepage. The main conclusion from the above is that both conceptual models produce reasonably good agreement in comparison with data, and that the main differences occur in a region below the heaters that is not important for thermal seepage.



Output DTN: LB0303DSCPDSTV.001.



Output DTN: LB0303DSCPDSTV.001.

Figure 7.4.4.3-1. Simulated Contours of Fracture Saturation and Fracture Flux at 12 Months of Heating Using (a) the DS/AFM-UZ02-Mean Property Set and (b) the Site-Specific Property Set



## 7.5 DISCUSSION OF VALIDATION ACTIVITIES

Validation of the TH seepage model was conducted according to the strategy outlined in the “Modeling and Scientific Analysis Activities” given in the technical work plan (BSC 2004 [DIRS 170236], Section 2.2). The TH seepage model has been validated by applying acceptance criteria based the model’s intended uses and on an evaluation of the model’s relative importance to the potential performance of the repository system.

The purpose of the TH seepage model is to provide findings on the evolution of thermal seepage to form the basis for thermal seepage abstraction. These qualitative findings are (1) that water is prevented from entering drifts as long as the fractured rock near the drift wall is at above-boiling temperature and (2) that the amount of thermal seepage is bounded by the respective long-term ambient seepage rate. Based on these findings, two alternative abstraction methodologies for thermal seepage are developed in *Abstraction of Drift Seepage* (BSC 2004 [DIRS 169131], Sections 6.5.2 and 6.5.3) for further use in the total system performance assessment (TSPA). The selected abstraction methods use upper-bound estimates of thermal seepage to account for various sources of model uncertainty.

The main method of validation is to demonstrate that the conceptual model and the TH properties used in Section 6 can match TH data collected from the DST. Note that the validation plan introduced in Section 7.1.3 and documented in the TWP (BSC 2004 [DIRS 170236]) established quantitative criteria for temperature data (corroboration with temperature measurements) and qualitative criteria for hydrological data (corroboration with geophysical measurements and air permeability data). The three-dimensional TH model developed for this purpose, the DST TH model, has the same conceptualization and simulates the same relevant TH processes as the TH seepage model. Model evaluation was performed in two steps: first, a site-specific property set was applied and evaluated in direct comparison with measured data; second, simulation results using the site-specific property set were compared with results from the DS/AFM-UZ02-Mean property set. The latter property set was derived to better represent average ambient conditions across various stratigraphic layers of Yucca Mountain and is the one used in Section 6.2 for predicting the TH behavior of the repository.

Comparison of measured and simulated data in the DST is first presented for temperature. The agreement is generally good, both spatially and temporally—as demonstrated in various temperature plots—as well as quantitatively—as shown by statistical measures for the goodness of fit. The validation criteria for temperature data, as defined in Section 7.4.1, have been met. The temperature profiles and temperature history plots show similar heat-pipe behavior between the measured and the simulated data, providing evidence that TH coupling is well understood. The criterion here is that the predicted location and duration of these two-phase signals should also be observed in the measurements, which is demonstrated in Section 7.4.3.1.1. Also, the mean difference between measured and simulated temperatures at more than 1,700 temperature sensors does not exceed 2 percent of the maximum rock temperature. The good agreement establishes the fact that the DST TH model (and hence the TH seepage model) has successfully incorporated the relevant TH processes as far as temperature is concerned.

Apart from temperature analyses, TH processes are also evaluated by qualitatively tracking the time-varying location of the drying and condensation front in response to heating. In the DST,



this tracking was done using geophysical measurements, which measure saturation changes in the matrix, and by periodic air-injection tests, which measure saturation changes in the fractures. These methods are useful for estimating qualitative changes, whereas quantitative values of water saturation should be considered with caution because of measurement uncertainties. Thus the validation criterion for measurements of moisture redistribution, defined in Section 7.4.1, is a qualitative agreement between the trends and relative changes in dryout and condensation patterns, as indicated by simulated saturation changes and estimated from measurements. Comparison of geophysical data from GPR measurements with the simulated contours of matrix saturation at various times indicates that the time-varying location of the drying and condensation front is adequately represented by the model. Simulated fracture saturations—and predicted air-permeability changes calculated from these saturation changes—were compared with measured air-permeability data obtained at different times throughout the heating phase of the test. This comparison suggests that—while the main trends of air-permeability changes are captured by results of the TH model—a better agreement between simulated and measured values can only be achieved if thermal-mechanical processes are included. Since the DST TH model does not account for THM effects such as fracture closure and opening, some quantitative differences between simulated and measured air permeabilities remain. To provide additional confidence, the simulated fracture-saturation results were also compared to the location and timing of water collection from several packed-off borehole intervals. It was shown that water collection data correspond well with the predicted locations of high saturation from the model. This, and the overall good agreement of temperature and matrix saturation data, provides confidence that the relevant TH processes of moisture redistribution are accurately represented by the model, despite the fact that THM effects are neglected.

In Section 7.4.3, the DST TH model utilized the site-specific property set DKM-TT99 in conjunction with the DKM for fracture-matrix interaction. In Section 7.4.4, a sensitivity analysis was performed using the DS/AFM-UZ02-Mean property set and applying the AFM. Comparison of simulation results reveals minor differences in temperature and small differences in matrix saturation between the two property sets. Fracture saturation results, on the other hand, demonstrate noticeable differences in the flow patterns below the heated area, but show good agreement above and to the sides of the heaters. For the purpose of this report, both property sets and both underlying models—DKM and AFM—produced results that were within the acceptable limit around the measured data (see Section 7.4.1 for validation criteria), given that the fractured rock above the drift is most important for analysis of thermal seepage.

As mentioned in Section 7.1, the DST is only one out of three heater tests of different scales and geometry that have been conducted at Yucca Mountain. The successful modeling analyses performed for the Single Heater Test (SHT) and the Large Block Test (LBT) provide additional confidence in the TH models developed for the fractured rock at Yucca Mountain (Tsang and Birkholzer 1999 [DIRS 137577]; BSC 2001 [DIRS 157330]; Mukhopadhyay and Tsang 2002 [DIRS 160788]). In contrast to SHT and DST, which are located deep down in the ESF in an area of very small percolation, the LBT is a fractured rock block at the ground surface just southeast of Yucca Mountain. Here, a few intense rainfall events resulted in significant downward flow of water from the top of the block towards the boiling region in the center. Water was able to penetrate to the heater horizon and actually cooled the temperature below boiling for a short time. It was demonstrated that large conductive fractures connected the top of the block with the heater horizon, thereby providing a fast path for water fluxes of large

magnitude. These processes were accurately modeled by Mukhopadhyay and Tsang (2002 [DIRS 160788], Section 5), with a process model similar to the TH seepage model, demonstrating that the model used for thermal seepage is capable of simulating fast-flow effects.

Confidence is also gained by results from the alternative conceptual model of Section 6.3 that support the prediction of the TH seepage model. The alternative conceptual model, referred to as THMEFF, considers the possibility that unsaturated fracture flow may occur in fast-flowing preferential pathways (thin fingers) that drain downward intermittently. Such conditions may promote the potential of seepage during the thermal period at Yucca Mountain, because finger flow may penetrate far into the superheated rock zone (i.e., rock temperature above boiling point of water) around waste emplacement drifts. To test the impact of such flow concepts—which can be approximated by continuum models such as the TH seepage model—the THMEFF simulations in Section 6.3 analyzed the fate of episodic preferential-flow events that originate somewhere in the condensation zone above the repository and percolate downward towards the emplacement drifts. The assumed finger-flow events are fast and intense compared to the average flow conditions generally considered in process models like the TH seepage model, and vaporization effects are limited as a result of the small cross-sectional area between the draining water and the hot rock. These conditions, along with a simplified one-dimensional finger-flow model representing continuous vertical fractures, create an unfavorable environment for the vaporization barrier above heated waste emplacement drifts. In spite of this, the THMEFF results are reasonably consistent with the process model results obtained with the TH seepage model. Most importantly, the THMEFF demonstrates that finger flow is not able to penetrate through the superheated rock during the first several hundred years of heating, when rock temperature is high and boiling conditions exist in a sufficiently large region above the drifts. These are the conditions in which the largest thermal perturbation occurs, or, in other words, when the potential for episodic finger flow is highest. Only later, when the boiling zone is small and the impact of vaporization is limited, can finger flow arrive at the drift crown. However, the strong thermal perturbation observed at early heating stages has already diminished during this time period, and the net result of water arrival at the drift—considering the combined impact of water buildup in the condensation zone and vaporization in the superheated zone—is similar to ambient percolation. Seepage of water into the drift is not expected from this water arrival, because the flow should be effectively diverted around the drift by the capillary barrier capability of the open cavity. These findings are consistent over a wide range of finger flow characteristics studied in a sensitivity analysis, covering the potential uncertainty in finger flow patterns.

In summary, it can be concluded that the validation criteria established for demonstrating corroboration of model results with experimental data have been met. Other validation requirements concerning confidence building during model have also been fulfilled, including publications in refereed professional journals and corroboration with alternative conceptual models (Sections 6.3 and 7.1.2). In addition, activities requirements for confidence building during model development have been satisfied (Section 7.1.1). Altogether, the model development activities and post-development validation activities described establish the scientific bases for the drift scale TH models. Based on this, the drift scale TH models used in this report are considered to be sufficiently accurate and adequate for the intended purpose and to the level of confidence required by the model's relative importance to the potential performance of the repository system (see Section 7.1).

INTENTIONALLY LEFT BLANK

## 8. CONCLUSIONS

### 8.1 SUMMARY AND CONCLUSIONS

This report documents the conceptual model and results obtained from numerical simulation of the coupled thermal-hydrological (TH) processes in the vicinity of waste emplacement drifts. Heating of rock water to above-boiling conditions induces water saturation changes and perturbed water fluxes that affect the potential of water seepage into drifts. In addition to the capillary barrier at the rock-drift interface—-independent of the thermal conditions—a second barrier exists to downward percolation at above-boiling conditions, from vaporization of water in the fractured rock overlying the repository. A numerical model was developed in this report to analyze the combined effect of these two barriers (not to be construed as synonymous with regulatory definition of barriers). The TH seepage model is a model that accounts for all important TH processes in response to heating while incorporating the capillary barrier condition at the drift wall. The conceptual model for evaluating capillary barrier behavior was adopted from the simulation methods developed for ambient seepage, namely the seepage calibration model (SCM) and the seepage model for performance assessment (SMPA). The key elements in these models—fracture permeability heterogeneity, small capillary-strength parameter, and effects of discrete fractures at the drift wall—have all been included in the TH seepage model. Simulations are performed to explicitly calculate fluid flow down to the drift during the heating phase of the repository, and to directly calculate transient seepage rates into the drift. These transient rates for the thermally affected time period are compared to the respective long-term ambient seepage rates, the latter calculated from steady-state simulation runs applying the constant infiltration rates associated with the three climate periods.

Most simulations conducted with the TH seepage model consider the TH conditions near intact drifts that have not degraded or collapsed. Results from these simulations are presented in Sections 6.2.2, 6.2.3, and 6.2.4.2. Two main suites of simulation cases have been studied. The first suite of cases addresses the relevant thermal-hydrological conditions in the drift vicinity, mainly for informative purposes. The second suite of cases focuses specifically on the potential for thermal seepage for further use in seepage abstraction and TSPA, applying the specific modeling framework for seepage that was outlined above. Several sensitivity cases were conducted (see overview in Section 6.2.1.6), including:

- Different repository host rocks with the Tptpmn submodel (for a drift located in non-lithophysal rock) and the Tptpll submodel (for a drift located in lithophysal rock)
- Different thermal operating modes (including a case that never reaches boiling conditions and a case with maximum temperature as high as 143°C in the rock)
- Different percolation fluxes at upper boundary (considering climate changes and flow focusing, with resulting percolation fluxes as high as 2,500 mm/yr)
- Different capillary-strength parameter values for fractures in the drift vicinity (ranging from 400 Pa to about 10,000 Pa)



- Variations in key rock properties such as near-field fracture permeability and matrix thermal conductivity
- Active fracture model and standard dual-permeability method
- Different conceptual model choices for defining the interface thermal conductivity between fracture-fracture connections and matrix-fracture connections as well as in-drift properties
- Transient thermal representation and long-term ambient (steady-state) representation.

The thermal modes and the percolation fluxes considered cover a wide range of the variability and uncertainty in TH conditions expected in the repository. For a given set of TH rock properties, the predicted thermal conditions—maximum rock temperature, extent of the superheated rock zone, and duration of the boiling period—are mainly driven by the assumed heat load and the magnitude of percolation. One thermal mode, the low-temp mode, results in rock temperatures that never reach boiling conditions. It was shown that thermal effects on flow and seepage are negligible in this case, so that the potential for thermal seepage can be estimated from ambient seepage results. The other thermal modes give rise to boiling of water in the fractured rock close to waste emplacement drifts. Simulation results demonstrate that the thermal perturbation of the flow field—causing increased downward flux from the condensation zone towards the drifts—is strongest during the first few hundred years after closure, corresponding to the time period when rock temperature is highest and the vaporization barrier is most effective. Even for high percolation fluxes into the model domain, and strong flow channeling as a result of fracture heterogeneity, water cannot penetrate far into the superheated rock during the time that rock temperature is above boiling, and model results show no seepage. The majority of the vaporized (and subsequently condensed) matrix water is diverted around the dryout zone and drains away from the drift. The magnitude of percolation affects the temperature conditions in the fracture rock. For a given thermal load, high percolation fluxes tend to cool down the rock temperatures, result in a shorter boiling period, and cause more distinct heat-pipe effects compared to small percolation fluxes.

At the time when temperature has returned to below-boiling conditions and fractures start rewetting at the drift (for mean infiltration without flow focusing, this occurs around 1,000 years after emplacement), the capillary barrier at the drift wall continues to operate, reducing (or preventing) water seepage into the drift. Since the thermal and hydrological conditions in the fractured rock will be perturbed from heating for a long time, simulation of thermal seepage was performed for 4,000 years after waste emplacement. The performance of the capillary barrier during this time period was evaluated in comparison to results from long-term ambient seepage (steady-state) simulations that were conducted to provide reference values for seepage at different percolation rates. The results indicate that thermal seepage never occurs in simulation cases where the respective long-term ambient seepage is zero. In cases where long-term ambient seepage is obtained—typically, cases with high percolation fluxes, heterogeneous fracture permeability fields, small fracture-capillary strength parameter in the drift vicinity, and inclusion of the effect of discrete fractures in the immediate drift vicinity using a specific drift wall boundary condition—thermal seepage is possible. (These are cases that have been identified as promoting seepage in ambient seepage studies: e.g., Birkholzer et al. 1999 [DIRS 105170]; BSC

2004 [DIRS 167652]) In such cases, seepage is predicted to begin several hundred to a few thousand years after rock temperature has returned below boiling, the delay caused by the slow saturation buildup in fractures; there is no seepage during the time period of above-boiling temperatures in the rock. Thermal-seepage percentages are always smaller than the respective ambient reference values, indicating that there is no enhanced seepage as a result of reflux of water (because most of the condensate has long drained down away from the drift), and that the long-term ambient seepage values provide an asymptotic upper limit for thermal seepage. Note that these general conclusions apply for all above-boiling thermal operating modes and for both the Tptpmn and the Tptpll repository horizons. Mainly because of the smaller thermal conductivity in this unit, the Tptpll submodel—for the same thermal mode—has slightly higher maximum temperatures, a larger superheated zone, and a longer boiling period than the Tptpmn submodel, giving rise to a more effective vaporization barrier. The key conclusions from the analyses for intact drifts are:

- For the low-temp thermal operating mode, thermal effects on flow and seepage are negligible, and the potential for long-term seepage can be estimated from ambient seepage results.
- For the other thermal operating modes discussed in this report, including the base case operating mode, percolation fluxes at the top of the model domain plays a significant role.
- For a given thermal load, higher percolation fluxes result in cooler rock temperatures, shorter duration of boiling, and earlier occurrence of drift seepage.
- Thermal seepage never occurs for cases where the long-term ambient seepage is zero.
- For cases where thermal seepage takes place, it is predicted to begin several hundred to a few thousand years after rock temperature has returned below boiling, the delay caused by the slow saturation buildup in fractures; there is no seepage during the time period of above-boiling temperatures in the rock.
- Thermal-seepage percentages are always smaller than the respective ambient reference values, indicating that there is no enhanced seepage as a result of reflux of water.
- Reduced fracture capillary strength parameter, reduced near-field fracture permeability, increased percolation fluxes, and the presence of discrete fractures in the vicinity of the drift wall tend to enhance both long-term ambient seepage and thermal seepage.

Additional TH simulations were conducted with the TH seepage model to analyze the TH conditions within and around collapsed drifts and to determine the impact on seepage abstraction. The drift collapse was assumed to occur shortly after emplacement of the radioactive waste. Results from the collapsed drift simulations can be summarized as follows:

- In contrast to open drifts, where a combined capillary and vaporization barrier at the drift crown prevents water seepage during the period of above-boiling temperatures, vaporization is not effective at the crown of collapsed drifts.

- With ambient rock water boiling off in the rubble material, in-drift flux perturbation gives rise to moderate reflux of condensate in the upper half of collapsed drifts. However, water drainage down to the waste packages is not possible, a result of the vaporization barrier forming in the vicinity of the waste package.
- The vaporization and reflux processes cease after a few thousand years or less, and the TH conditions slowly approach steady-state (ambient) behavior. During this transition phase, the fluxes in the lower half of the collapsed drift remain zero at all times. Later, when steady-state conditions have been reached, the entire collapsed drift is characterized by zero fluxes, as the void spaces are essentially dry (at residual saturation).
- The above in-drift flow processes are largely unaffected by changes in the percolation flux because the capillary barrier at the drift crown limits water flux from the intact rock into the rubble material.

## 8.2 IMPLICATIONS FOR ABSTRACTION OF THERMAL SEEPAGE IN INTACT DRIFTS

Based on the consistent trends observed in the thermal seepage results, abstraction methods for transient seepage into intact drifts were recommended in Section 6.2.4.1. These abstraction methods use the long-term ambient seepage rate calculated for each climate period as reference values for thermal seepage. The abstraction method used for licence application (LA) is documented in *Abstraction of Drift Seepage* (BSC 2004 [DIRS 169131]). As a basis for the abstraction rationale, several thermal seepage simulation scenarios, including sensitivity analyses to percolation fluxes, heat loads, key rock parameters, and conceptual model choices, were presented in Sections 6.2.2, 6.2.3, and 6.2.4.2. It was demonstrated that the potential variability of boundary conditions and rock properties results in considerable differences in the TH conditions, e.g., in the duration of the boiling period or the predicted maximum rock temperature at the drift wall. However, the general conclusions about the magnitude and evolution of thermal seepage, and thus the recommended abstraction procedures, are valid over the required range of boundary conditions and parameter values used in TSPA (i.e., extreme percolation fluxes, different repository temperature conditions, varying near-field rock properties).

The abstraction methodologies proposed in the above paragraph utilize simplified transient thermal-seepage rates based on the long-term ambient seepage estimates. It is recommended that the long-term ambient seepage rates used for such thermal seepage abstraction are the ones provided by the SMPA. This ambient seepage model, computationally much less demanding compared to the TH seepage model, can be applied to a wide range of parameters and flux boundary conditions. Also, the SMPA results are considered quantitatively more reliable than the ones from the TH seepage model, due to the three-dimensional model representation and the large number of realizations considered. Thus, the qualitative evolution of thermal seepage relative to the long-term ambient seepage would be derived from the TH seepage model, while the quantitative magnitude of seepage would be predicted by the SMPA.

### 8.3 MODEL VALIDATION AND UNCERTAINTIES

The validation activities conducted for the TH seepage model are described in Section 7 of this report. The TH seepage model has been validated by applying acceptance criteria based on an evaluation of the model's intended use and the model's relative importance to the potential performance of the repository system. All validation requirements defined in the TWP (BSC 2004 [DIRS 170236], Section 2.2.1) have been fulfilled, including corroboration of model results with experimental data, publications in refereed professional journals, and corroboration with an alternative conceptual model (Sections 6.3 and 7). Requirements for confidence building during model development have also been satisfied. The model development activities and post-development validation activities described establish the scientific bases for the drift scale TH models. Based on this, the drift scale TH models used in this report are considered to be sufficiently accurate and adequate for the intended purpose and to the level of confidence required by the model's relative importance to the potential performance of the repository system.

The most important validation method in this report is corroboration with experimental data; i.e., to demonstrate a good agreement between model results and appropriate experimental data, using measurements from the Drift Scale Test (DST). The DST TH model was developed for this purpose; it is a three-dimensional drift-scale process model that has the same model conceptualization as the TH seepage model. The model was applied to the DST using the DKM-TT99 property set, specific for the DST test block, and the DS/AFM-UZ02-Mean property set, representing average properties over the repository. To test the different methods for fracture-matrix interaction, simulations were performed using the standard dual-permeability method (DKM) and the active fracture model (AFM), respectively. Comparison with measured data from the DST indicated good overall agreement for temperature values and moisture redistribution patterns, implying that the models considered are valid for the purposes of this report. Both property sets and both the DKM/AFM methods are suitable for simulating the thermally perturbed conditions in the test block of the DST. The qualitative and quantitative assessment of model agreement with data—including evaluation of subtle temperature signals showing TH coupling, comparison with geophysical measurements, air-permeability data, and occurrence of fracture flow at water collection points—indicates that uncertainty in predicting temperature, saturation, and water flux is within acceptable ranges. Though not presented in this report, the TH process models have also been applied to the Single Heater Test (SHT) and the Large Block Test (LBT) at Yucca Mountain, also resulting in good agreement between simulation and measurements (Tsang and Birkholzer 1999 [DIRS 137577]; BSC 2001 [DIRS 157330]; Mukhopadhyay and Tsang 2002 [DIRS 160788]). This provides additional confidence in the suitability of the predictive model.

Note that the geometry and the in-drift heat source setup of the DST are similar to the proposed design of waste emplacement drifts. Therefore, the TH processes measured and simulated in the DST occur on the same spatial scale as the ones predicted to occur in the repository drifts. With respect to the time scale, however, it is recognized that the DST provides observations on temperatures and water redistribution for a time frame of four years while the intended application of the thermal-hydrologic modeling prediction is for many centuries. It is not possible to perform such tests similar to the DST for time frames even approaching the intended time frame for predictions. However, the TH seepage model is considered valid for the intended



time frame of interest beyond four years because of the following: (1) The governing TH processes leading to moisture redistribution—vaporization, vapor transport, condensation, and reflux—are the same over four years and over much longer time frames; only the duration of these processes is different. (2) The conceptual framework used for describing these processes, i.e., the energy and mass balances, are valid for all times; these principles do not change. (3) The observations from the DST for both temperatures (energy) and mass are consistent with the current understanding of these processes as demonstrated by comparison with model predictions. Furthermore, it is reasonable to expect that the scientific understanding of these processes in the intended application will not change because the state of knowledge of these processes has been developed extensively for many years, as illustrated by successful predictions for similar processes.

All three thermal tests have been conducted in the Tptpmn unit at Yucca Mountain; however, there has been no testing in the Tptpll unit. Thus, validation of the TH seepage model does not include direct comparison with measured data from the Tptpll. However, the good agreement of the model predictions with data from the Tptpmn provides confidence that the TH processes in the fractured rock are well captured by the model. Therefore, application of the model to the Tptpll unit is appropriate since similar TH processes will occur in that unit. Some uncertainty, however, remains about the rock properties of the Tptpll unit and the influence of lithophysal cavities. This uncertainty is propagated to TSPA by the choice of upper-bound estimates of thermal seepage in the seepage abstraction (BSC 2004 [DIRS 169131], Sections 6.5.2 and 6.5.3).

As discussed in Section 7.1, no seepage of liquid water has been observed in the Heated Drift of the DST. The DST results allow for a unique model validation with respect to the near-field TH conditions in the rock mass, but offer no seepage data (observed seepage rates) that can be used directly for thermal seepage validation purposes. Thus, validation of the seepage part of the TH seepage model is an indirect one. First, the better the overall TH behavior can be predicted by the DST TH model, the more confidence is gained for the seepage results obtained with the TH seepage model. In other words, the successful validation of the DST TH model with respect to coupled processes (i.e., saturation distribution, temperature signals) adds confidence in the seepage part of the TH seepage model because the thermally perturbed water fluxes are accurately represented. Second, the modeling framework for the capillary barrier treatment in the TH seepage model can already be considered validated, because the conceptual model is identical to the one validated and successfully applied in the ambient seepage studies. As described in *Seepage Calibration Model and Seepage Testing Data* (BSC (2004 [DIRS 171764], Section 7), the conceptual model developed in the SCM was tested by performing blind predictions of seepage rates for niche liquid release tests that had not been used for model calibration and that were conducted in a different drift section. It was demonstrated that the measured ambient seepage data (seepage threshold and seepage rate) were accurately represented by the simulated results. Validation of the coupled TH processes (using the DST data) together with validation of the ambient seepage conceptual model (using liquid-release data) provides confidence in the thermal seepage results of the TH seepage model. However, some uncertainty remains, since no direct test data on thermal seepage at extreme flux conditions are available. This uncertainty is propagated to TSPA by the choice of upper-bound estimates of thermal seepage in the seepage abstraction (BSC 2004 [DIRS 169131], Sections 6.5.2 and 6.5.3).

Uncertainties regarding the effectiveness of the vaporization barrier have also been addressed in Section 6.3 of this report, where an alternative conceptual model of water flow in the superheated rock environment is introduced, the TH model for episodic finger flow (THMEFF). The THMEFF conceptualizes that the thermally perturbed downward flux from the condensation zone towards the superheated rock zone drains in episodic finger-flow patterns. The effectiveness of the vaporization barrier is then tested for these extreme conditions where downward flux is fast and large in magnitude compared to average flow, and where vaporization is limited by the small cross-sectional area between the narrow finger and the rock surface. Analyses were performed using finger-flow characteristics from experimental work described in the literature, applied to the thermal conditions in the Tptpmn and Tptpll units at several selected times after emplacement. It was demonstrated that results of the alternative conceptual model are consistent with the process-model results obtained with the TH seepage model. Most importantly, the THMEFF results show that finger flow is not able to penetrate through the superheated rock during the first several hundred years of heating, when rock temperature is high and boiling conditions exist in a sufficiently large region above the drifts. These are the conditions when the largest thermal perturbation occurs, or, in other words, when the potential for episodic finger flow is highest. Note that the THMEFF includes a number of limitations that are valid for a qualitative evaluation, but should not be interpreted as an exact quantitative representation of system behavior at Yucca Mountain. For example, one such limitation is that experimental data from a granite fracture at Stripa are used to represent the characteristics of episodic finger flow in fractured tuff at Yucca Mountain (remember though that the flow processes are similar).

For numerical models, the main sources of uncertainty are uncertainty in model input parameters and uncertainty in the conceptual model. As discussed in the above paragraph, uncertainty with respect to the conceptual model has been addressed in this report, building confidence in the validity of the conceptual model for thermal seepage. Remaining uncertainties are propagated to TSPA by the choice of upper-bound estimates of thermal seepage in the seepage abstraction (BSC 2004 [DIRS 169131], Sections 6.5.2 and 6.5.3). Uncertain and spatially variable model input parameters are the rock properties and the model boundary conditions. Sensitivity to all parameters relevant for thermal seepage was explicitly studied with the TH seepage model by assessing seepage in two host rock units with different thermal and hydrological properties, by varying the seepage relevant fracture capillary-strength parameter, by analyzing infiltration scenarios with different flux multiplication factors, by changing host rock thermal conductivities and fracture permeabilities, and by simulating several different thermal loads (see Section 6.2.1.6 for overview of simulation cases). In all these cases, covering a wide range of property values and conditions, the main conclusions regarding thermal seepage were similar, in that no seepage is predicted to occur during the period of above-boiling temperatures in the rock and that thermal seepage is always less in magnitude compared to the respective long-term ambient values. This confirms that these main conclusions hold for all relevant TSPA parameter cases.

#### **8.4 HOW THE APPLICABLE ACCEPTANCE CRITERIA ARE ADDRESSED**

The following information describes how this analysis addresses the acceptance criteria in the Yucca Mountain Review Plan (NRC 2003 [DIRS 163274], Sections 2.2.1.3.3 and 2.2.1.3.6.3). Only those acceptance criteria that are applicable to this report (see Section 4.2) are discussed. In most cases, the applicable acceptance criteria are not addressed solely by this report; rather, the

acceptance criteria are fully addressed when this report is considered in conjunction with other analysis and model reports that describe quantity and chemistry of water contacting engineered barriers and waste forms, and flow in the unsaturated zone. Where a subcriterion includes several components, only some of those components may be addressed. How these components are addressed is summarized below. The acceptance criteria and subcriteria listed in Section 4.2 and here are consistent with those mentioned in Section 3.2.1 of *Technical Work Plan for: Near-Field Environment and Transport: Near-Field Coupled Processes (TH Seepage and THM) Model Report Integration* (BSC 2004 [DIRS 170236]), except for the following deviation. For “Quantity and Chemistry of Water Contacting Waste Packages and Waste Forms (Section 2.2.1.3.3),” *Acceptance Criteria 5: Model Abstraction Output is Supported by Objective Comparisons* is included here though not present in the technical work plan (BSC 2004 [DIRS 170236], Section 3.2.1).

**Acceptance Criteria from Section 2.2.1.3.3.3, *Quantity and Chemistry of Water Contacting Engineered Barriers and Waste Forms***

**Acceptance Criterion 1: *System Description and Model Integration Are Adequate.***

- (1) The design features, physical phenomena, and couplings for this report (see Sections 5, 6.1, and 6.2.1) are consistent with those in other related model reports, see for example, *Drift-Scale Coupled Processes (DST and TH Seepage) Models* (BSC 2004 [DIRS 169856] and *Drift-Scale THM Model* (BSC 2004 [DIRS 169864])). The abstraction procedure for determining quantity of water entering the emplacement drifts is given in *Abstraction of Drift Seepage* (BSC 2004 [DIRS 169131], Sections 6.5 and 6.7).
- (2) The abstraction of quantity of water entering the emplacement drifts is provided in *Abstraction of Drift Seepage* (BSC 2004 [DIRS 169131], Sections 6.5 and 6.7). The technical bases (see Sections 5, 6.1 and 6.2.1) for thermal seepage in this report are identical to those in *Abstraction of Drift Seepage* (BSC 2004 [DIRS 169131]).
- (3) Thermal line load and decay of radioactive heat, parameters important for estimating quantity of water entering the emplacement drifts, have been obtained from controlled sources (see Section 4.1.1.3). The adopted values for these parameters are identical to those in other related model reports (see item (1) above).
- (4) The physics of the coupled thermal-hydrological processes and the thermal seepage phenomenon (Section 6.1) are adequately incorporated into an appropriate process model based on a sufficient technical basis (Section 6.2.1), supported by field data (Sections 4.1 and 7) and sensitivity analyses (Sections 6.2.2, 6.2.3, and 6.2.4).
- (5) The technical bases, assumptions, data, and models used in this report to determine the quantity of water entering the emplacement drifts are consistent with those used in analyzing the flow paths in the unsaturated zone. Sufficient technical bases and justifications have been provided for modeling coupled thermal-hydrological effects on seepage and flow (Sections 5, 6.1 and 6.2.1).

- (6) Seepage of water into the emplacement drifts promotes corrosion of engineered barriers and degradation of waste packages. The potential for water seepage into emplacement drifts under different thermal conditions is addressed in Section 6.2 (particularly in Section 6.2.4).
- (7) The modeling approach in this report is consistent with the dimensionality of seepage abstractions (Section 6.2.1.2) and detailed information on engineered barrier design and other engineered features (Sections 4.1.1.6 and 6.2.1.2).
- (8) Adequate technical bases (see Sections 6.1 and 6.2.1) have been provided for the TH seepage model in this report. The coupling of thermal and hydrological processes, which determine quantity of water entering emplacement drifts, has been elaborately discussed (see Sections 6.2.1, 6.2.2, and 6.2.3) through numerical modeling. Sensitivity studies including alternative parameter choices have been discussed in Section 6.2.4. Alternative conceptual models have been discussed in Section 6.3. Model validation of coupled TH processes against field thermal tests are provided in Section 7.
- (9) Performance affecting processes that have been observed in thermal-hydrologic tests and experiments have been conceptually included in the TH seepage model (Section 6.2.1). Model validation against measured TH data (from field thermal tests) are discussed in Section 7. The approach and model is documented in a transparent and traceable manner by adopting input data from controlled sources and by thorough record keeping.

**Acceptance Criterion 2: *Data Are Sufficient for Model Justification.***

- (1) Geological, hydrological, and thermal property data used in this report are adequately justified and described (Sections 4.1, 5, and 6.2.1). Adequate description of how the data were used, interpreted, and appropriately synthesized into the parameters is provided in Sections 4.1, 5, and 6.2.1.
- (2) Sufficient data (see Sections 4.1) were collected on the relevant characteristics of the natural system for conceptual models of TH coupled processes, that affect seepage and flow into emplacement drifts.
- (3) Heater tests were designed and conducted with the objective of observing TH processes for the temperature ranges expected for repository conditions and making measurements for mathematical models. Section 7 provides discussion of TH data collected from the DST, the largest Yucca Mountain thermal test. Section 7 also provides validation of the conceptual TH seepage model against measured TH data from the DST.
- (4) Sufficient data were collected for the formulation of the conceptual framework and for the validation of the TH process model (Section 7). Sufficient data were collected to characterize the TH properties of the natural system and to observe critical TH processes (Section 7).



**Acceptance Criterion 3: *Data Uncertainty Is Characterized and Propagated Through the Model Abstraction.***

- (1) Parameter values, assumed ranges, probability distributions, and bounding assumptions (see Sections 4.1.1, 5, 6.1, 6.2.1, 6.2.2, and 6.2.3) used in this report are technically defensible, reasonably account for uncertainty, and do not result in an under-representation of the risk estimate (see Sections 8.1, 8.2, and 8.3).
- (2) The parameters used in and the coupled processes modeled by the process model are technically defensible; they are based on and are consistent with available data from Yucca Mountain (see Section 4.1.1).
- (3) Parameters used to define initial conditions (Section 6.2.1.3), boundary conditions (Sections 4.1.1.2 and 6.2.1.3), and computational domain (Sections 4.1.1.5 and 6.2.12) in sensitivity analyses (Section 6.2.4.2) involving coupled TH effects on seepage and flow are consistent with available data.
- (4) Uncertainties and variabilities in the coupled TH processes are evaluated, reasonably accounted for and adequately represented (Sections 6.2, 6.3, and 8.3), providing a sufficient basis for incorporating data uncertainty in downstream reports on seepage abstraction.
- (6) Where sufficient data do not exist, the definition of parameter values is based on other appropriate sources (see Section 5).

**Acceptance Criterion 4: *Model Uncertainty Is Characterized and Propagated Through the Model Abstraction.***

- (1) Alternative modeling choices have been adequately addressed (see Sections 6.2.4.2.3 through 6.2.4.2.6). Selected modeling approaches are consistent with available data and current scientific understanding.
- (2) An alternative conceptual model has been developed consistent with available data and current scientific understanding (see Section 6.3). Modeling approaches have been discussed (see Sections 6.1 and 6.2). Model uncertainty is evaluated by sensitivity studies with the TH seepage model (Sections 6.2.4.2.3 through 6.2.4.2.6).
- (3) Consideration of conceptual model uncertainty is consistent with available data, laboratory experiments, and field measurements (see Sections 6.2.4.2.3 through 6.2.4.2.6, 6.3, and 7).
- (4) Adequate consideration is given to effects of TH coupled processes in the assessment of alternative conceptual models (Section 6.2 and 6.3).
- (5) A dual-permeability model (DKM) has been adopted for the TH seepage model (see Section 6.1 and 6.2.1).

**Acceptance Criterion 5: *Model Abstraction Output Is Supported by Objective Comparisons.***

- (1) The recommended abstraction methodologies are based on detailed process-level models (Sections 6.2.4.1 and 8.2).
- (2) The assumptions and approximations are demonstrated to be appropriate for process-level models (Sections 5, 6.1.1, and 6.2.1)
- (3) Accepted and well-documented procedures are used to construct and test the numerical models that simulate coupled TH effects on seepage and flow (Sections 6.1.1 and 6.2.1).

**Acceptance Criteria from Section 2.2.1.3.6.3, *Flow Paths in the Unsaturated Zone.***

**Acceptance Criterion 1: *System Description and Model Integration Are Adequate.***

- (1) The design features, physical phenomena, and couplings for this report (see Sections 5, 6.1, and 6.2.1) are consistent with those in other related model reports; see for example, *Drift-Scale Coupled Processes (DST and TH Seepage) Models* (BSC 2004 [DIRS 169856]) and *Drift-Scale THM Model* (BSC 2004 [DIRS 169864]).
- (2) The aspects of geology, hydrology, physical phenomena, and TH couplings that may affect flow paths in the unsaturated zone are adequately considered (see Sections 6.1, 6.2.1, 6.2.2, and 6.2.3)
- (3) In the context of abstraction of flow paths in the unsaturated zone, the assumptions (Section 5), technical bases (Sections 6.1 and 6.2.1), data (Section 4.1.1), and models (Sections 6.1 and 6.2) in this report are consistent with other related abstractions.
- (5) Sufficient technical bases have been provided to assess the degree to which features, events, and processes have been included (see Section 6).
- (6) Adequate spatial and temporal variability of model parameters are employed in the TH seepage model to investigate flow paths in the unsaturated zone (Sections 6.1, 6.2.1, 6.2.2, and 6.2.3).
- (7) The average parameter values used in the TH seepage model are representative of the temporal and spatial discretizations (Sections 4.1.1).
- (9) Data from qualified sources have been used. Further confidence is gained through thorough record keeping.

**Acceptance Criterion 2: *Data Are Sufficient for Model Justification.***

- (1) Hydrological and thermal property values used in this report have been adequately justified (Sections 4.1.1 and 5)
- (2) Geology and hydrology data used in this report are obtained from controlled sources (Section 4.1.1).
- (3) Estimates of percolation fluxes were obtained from controlled and qualified sources (Section 4.1.1.4 and Appendix B).
- (4) Appropriate thermal-hydrologic tests were designed and conducted, so that critical thermal-hydrologic processes could be observed; Section 7 provides discussion of validation of the TH seepage model against measured thermal-hydrologic data from the largest thermal test at Yucca Mountain.
- (5) Sensitivity and uncertainty analyses have been performed (Sections 6.2.4.2.3 through 6.2.4.2.6, and 6.3).
- (6) Accepted and well-documented procedures are used to construct numerical models (Sections 4.1.1 and 6).
- (7) Mathematical models (Section 6.2.1.1.3) are provided that are consistent with conceptual models (Sections 6.1 and 6.2.1.1.1). The robustness of results from different mathematical models is compared (Sections 6.2 and 6.3).

**Acceptance Criterion 3: *Data Uncertainty Is Characterized and Propagated Through the Model Abstraction.***

- (1) Parameter values, assumed ranges, probability distributions, and bounding assumptions (see Sections 4.1.1, 5, 6.1, 6.2.1, 6.2.2, and 6.2.3) used in this report are technically defensible, reasonably account for uncertainty, and do not result in an under-representation of the risk estimate (see Sections 8.1, 8.2, and 8.3).
- (2) Adequate technical bases for the parameter values have been provided (Sections 4.1.1, 5, 6.2.1, and 6.2.4.2).
- (3) Possible statistical correlations between parameter values have been discussed, when appropriate (Section 4.1.1).
- (4) The sensitivity analyses (Sections 6.2.4.2.3 through 6.2.4.2.6) in this report are consistent with available data.
- (5) Coupled TH processes have been adequately represented (Sections 6.1 and 6.2).
- (6) Uncertainties in the characteristics of the natural system are considered (Sections 6.2.4.2.3 through 6.2.4.2.6).

**Acceptance Criterion 4: *Model Uncertainty Is Characterized and Propagated Through the Model Abstraction.***

- (1) Alternative modeling choices have been adequately addressed (see Sections 6.2.4.2.3 through 6.2.4.2.6). Selected modeling approaches are consistent with available data and current scientific understanding.
- (2) The bounds of uncertainty considered by the TH seepage model are considered (Sections 8.1, 8.2, and 8.3).
- (3) Consideration of conceptual model uncertainty is consistent with available data, laboratory experiments, and field measurements (see Sections 6.2.4.2.3 through 6.2.4.2.6, 6.3, and 7).

## **8.5 OUTPUT DTNS**

Thermal properties for the UZ model layers (see Section 4.1.1.1 and Appendix F) are developed in this report. These thermal properties for the UZ model layers have been submitted to the TDMS as output from this report. These thermal properties can be found in DTN: LB0402THRMLPRP.001.

Several of the many simulation cases presented in this model report have been selected for submittal to the Technical Data Management System (TDMS). The simulation cases that were submitted to the TDMS are those cases deemed relevant to downstream users. The rationale for selecting simulation cases for the TDMS is given below:

### **TH Seepage Model**

- Simulation cases that mainly serve informative purposes and provide intermediary or supplementary results are not submitted to the TDMS. These are the simulation cases in Sections 6.2.2.1 and 6.2.3.1, where drift-scale TH conditions are presented without specific focus on thermal seepage, and in Sections 6.2.4.2.4 and 6.4.2.4.5, where different alternative model choices are tested for comparison.
- Simulation cases that are specifically intended to calculate thermal seepage and to evaluate the combined barrier effectiveness are submitted to the TDMS. These are all simulation cases presented in Sections 6.2.2.2, 6.2.3.2, and 6.2.4.2.1 through 6.2.4.2.3 of this report, and also include selected simulation cases in Appendix C. The DTNs comprise both transient thermal runs and long-term ambient (steady-state) runs. The following DTNs have been submitted:
  - Thermal seepage results for intact drifts: LB0303DSCPTHSM.001 (TOUGH2 files) and LB0301DSCPTHSM.002 (developed data); LB0309DSCPTHSM.001 (TOUGH2 files) and LB0309DSCPTHSM.002 (developed data)
  - TH Conditions for Collapsed Drifts: LB0310DSCPTHSM.001 (TOUGH2 files) and LB0310DSCPTHSM.002 (developed data)



- Thermal seepage results for intact drifts with revised thermal properties (Appendix): LB0404DSCPTHSM.001 (TOUGH2 files) and LB0404DSCPTHSM.002 (developed data)

#### **THMEFF (Alternative Conceptual Model)**

- Data from the THMEFF are not submitted to the TDMS. The THMEFF is an alternative conceptual model providing corroborative information to support the TH seepage model.
- Specific results of this model are intermediary results and are not relevant as direct input for downstream users.

#### **DST TH Model**

- All simulation cases conducted with the DST TH model and presented in this report are submitted to the TDMS. The DTNs are: LB0303DSCPDSTV.001 (TOUGH2 files) and LB0301DSCPDSTV.002 (developed data).

For the selected simulation cases, all computer files needed to reproduce the model results were submitted to the TDMS. For both the TH seepage model and the DST TH model runs, the input files needed to perform a TOUGH2 simulation and the respective output files obtained from the respective TOUGH2 simulation have been submitted. Data developed from these simulations have been submitted in addition to the simulation files. These data comprise computer files giving the transient or steady-state seepage rates, extracted from the TH seepage model, and computer files providing predicted air-permeability results, calculated from saturation data simulated with the DST TH model. Reproducibility by an appropriately qualified individual is possible by consulting this report and the pertinent scientific notebook pages as listed in Table 6-1.

## 9. INPUTS AND REFERENCES

The following is a list of the references cited in this document. Column 2 represents the unique six-digit numerical identifier (the Document Input Reference System [DIRS] number), which is placed in the text following the reference callout (e.g., BSC 2002 [DIRS 160780]). The purpose of these numbers is to assist the reader in locating a specific reference. Within the reference list, multiple sources by the same author (e.g., BSC 2002) are sorted alphabetically by title.

### 9.1 DOCUMENTS CITED

- |   |        |
|---|--------|
| Ang, A.H-S. and Tang, W.H. 1975. "Basic Principles." Volume I of <i>Probability Concepts in Engineering Planning and Design</i> . New York, New York: John Wiley & Sons. TIC: 8346.   | 160321 |
| Birkholzer, J.; Li, G.; Tsang, C-F.; and Tsang, Y. 1999. "Modeling Studies and Analysis of Seepage into Drifts at Yucca Mountain." <i>Journal of Contaminant Hydrology</i> , 38, (1-3), 349-384. New York, New York: Elsevier. TIC: 244160.   | 105170 |
| Birkholzer, J.T. 2002. <i>TH_PULSE: Program for Calculating Infiltration of Episodic Liquid Fingers in Superheated Rock Fractures, Theory, User's Manual, and Sample Applications</i> . LBNL/PUB-3277. Berkeley, California: Lawrence Berkeley National Laboratory. TIC: 253581.                | 160748 |
| Birkholzer, J.T. and Tsang, Y.W. 1997. <i>Pretest Analysis of the Thermal-Hydrological Conditions of the ESF Drift Scale Test</i> . Milestone SP9322M4. Berkeley, California: Lawrence Berkeley National Laboratory. ACC: MOL.19971201.0810.  | 100597 |
| Birkholzer, J.T. and Tsang, Y.W. 2000. "Modeling the Thermal-Hydrologic Processes in a Large-Scale Underground Heater Test in Partially Saturated Fractured Tuff." <i>Water Resources Research</i> , 36, (6), 1431-1447. Washington, D.C.: American Geophysical Union. TIC: 248278.             | 154608 |
| Brooks, R.H. and Corey, A.T. 1966. "Properties of Porous Media Affecting Fluid Flow." <i>Journal of the Irrigation and Drainage Division, Proceedings of the American Society of Civil Engineers</i> , 92, (IR2), 61-89. Ann Arbor, Michigan: American Society of Civil Engineers. TIC: 216867. | 119392 |
| BSC (Bechtel SAIC Company) 2001. <i>FY 01 Supplemental Science and Performance Analyses, Volume 1: Scientific Bases and Analyses</i> . TDR-MGR-MD-000007 REV 00 ICN 01. Las Vegas, Nevada: Bechtel SAIC Company. ACC: MOL.20010801.0404; MOL.20010712.0062; MOL.20010815.0001.                  | 155950 |
| BSC 2001. <i>FY01 Supplemental Science and Performance Analyses, Volume 2: Performance Analyses</i> . TDR-MGR-PA-000001 REV 00. Las Vegas, Nevada: Bechtel SAIC Company. ACC: MOL.20010724.0110.  | 154659 |

BSC 2001. <i>Multiscale Thermohydrologic Model</i> . ANL-EBS-MD-000049 REV 00 ICN 02. Las Vegas, Nevada: Bechtel SAIC Company. ACC: MOL.20020123.0279.	158204
BSC 2001. <i>Thermal Tests Thermal-Hydrological Analyses/Model Report</i> . ANL- NBS-TH-000001 REV 00 ICN 02. Las Vegas, Nevada: Bechtel SAIC Company. ACC: MOL.20011116.0025.	157330
BSC 2001. <i>UZ Flow Models and Submodels</i> . MDL-NBS-HS-000006 REV 00 ICN 01. Las Vegas, Nevada: Bechtel SAIC Company. ACC: MOL.20020417.0382.	158726
BSC 2002. <i>Geologic Framework Model (GFM2000)</i> . MDL-NBS-GS-000002 REV 01. Las Vegas, Nevada: Bechtel SAIC Company. ACC: MOL.20020530.0078.	159124
BSC 2002. <i>Invert Effective Thermal Conductivity Calculation</i> . 000-00C-WIS0- 00100-000-00A. Las Vegas, Nevada: Bechtel SAIC Company. ACC: MOL.20020828.0178.	159906
BSC 2002. <i>Repository Design, Repository/PA IED Subsurface Facilities Plan Sht.</i> <i>1 of 5, Sht. 2 of 5, Sht. 3 of 5, Sht. 4 of 5, and Sht. 5 of 5</i> . DWG-MGR-MD-000003 REV A. Las Vegas, Nevada: Bechtel SAIC Company. ACC: MOL.20020601.0194.	159527
BSC 2002. <i>Ventilation Model</i> . ANL-EBS-MD-000030 REV 01 ICN 01. Las Vegas, Nevada: Bechtel SAIC Company. ACC: MOL.20021106.0055.	160975
BSC 2003. <i>Advection Versus Diffusion in the Invert</i> . ANL-EBS-MD-000063 REV 00. Las Vegas, Nevada: Bechtel SAIC Company. ACC: DOC.20040217.0004; Replacement for 165686.	170881
BSC 2003. <i>Development of Numerical Grids for UZ Flow and Transport</i> <i>Modeling</i> . ANL-NBS-HS-000015 REV 01. Las Vegas, Nevada: Bechtel SAIC Company. ACC: DOC.20030404.0005.	160109
BSC 2003. <i>Drift-Scale Coupled Processes (DST and THC Seepage) Models</i> . MDL-NBS-HS-000001 REV 02. Las Vegas, Nevada: Bechtel SAIC Company. ACC: DOC.20030804.0004.	162050
BSC 2003. <i>Repository Design Project, RDP/PA IED Typical Waste Package</i> <i>Components Assembly 1 of 9</i> . 800-IED-WIS0-00201-000-00A. Las Vegas, Nevada: Bechtel SAIC Company. ACC: ENG.20030702.0001.	164053
BSC 2003. <i>Repository Design Project, Repository/PA IED Emplacement Drift</i> <i>Committed Materials 1 of 2</i> . 800-IED-WIS0-00301-000-00A. Las Vegas, Nevada: Bechtel SAIC Company. ACC: ENG.20030627.0003.	164052

BSC 2003. <i>Repository Design, Repository/PA IED Subsurface Facilities</i> . 800-IED-EBS0-00403-000-00B. Las Vegas, Nevada: Bechtel SAIC Company. ACC: MOL.20030109.0147.	161731
BSC 2004. <i>Abstraction of Drift Seepage</i> . MDL-NBS-HS-000019, Rev. 01. Las Vegas, Nevada: Bechtel SAIC Company.	169131
BSC 2004. <i>Analysis of Hydrologic Properties Data</i> . ANL-NBS-HS-000042, Rev. 00. Las Vegas, Nevada: Bechtel SAIC Company.	170038
BSC 2004. <i>Calibrated Properties Model</i> . MDL-NBS-HS-000003, Rev. 02. Las Vegas, Nevada: Bechtel SAIC Company.	169857
BSC 2004. <i>Conceptual Model and Numerical Approaches for UZ Flow and Transport</i> . MDL-NBS-HS-000005 REV 01. Las Vegas, Nevada: Bechtel SAIC Company.	170035
BSC 2004. <i>D&amp;E / PA/C IED Emplacement Drift Configuration and Environment</i> . 800-IED-MGR0-00201-000-00B. Las Vegas, Nevada: Bechtel SAIC Company. ACC: ENG.20040326.0001.	168489
BSC 2004. <i>D&amp;E / PA/C IED Typical Waste Package Components Assembly</i> . 800-IED-WIS0-00204-000-00B. Las Vegas, Nevada: Bechtel SAIC Company. ACC: ENG.20040202.0012.	167369
BSC 2004. <i>D&amp;E / PA/C IED Typical Waste Package Components Assembly</i> . 800-IED-WIS0-00205-000-00C. Las Vegas, Nevada: Bechtel SAIC Company. ACC: ENG.20040202.0013.	167758
BSC 2004. <i>Data Qualification Report: Heat Capacity Values for Rock and Lithostratigraphic Layers of the Geologic Framework Model for Use on the Yucca Mountain Project</i> . TDR-NBS-GS-000028 REV 00. Las Vegas, Nevada: Bechtel SAIC Company. ACC: DOC.20040805.0007.	171504
BSC 2004. <i>Design and Engineering, Drip Shield Plate - 1</i> . 000-M00-SSE0-00601-000-00A. Las Vegas, Nevada: Bechtel SAIC Company. ACC: ENG.20040310.0027.	168283
BSC 2004. <i>Development of Numerical Grids for UZ Flow and Transport Modeling</i> . ANL-NBS-HS-000015 REV 02. Las Vegas, Nevada: Bechtel SAIC Company. ACC: DOC.20040901.0001.	169855
BSC 2004. <i>Drift Degradation Analysis</i> . ANL-EBS-MD-000027, Rev. 03. Las Vegas, Nevada: Bechtel SAIC Company. ACC: DOC.20040915.0010.	166107
BSC 2004. <i>Drift Scale THM Model</i> . MDL-NBS-HS-000017, Rev. 01. Las Vegas, Nevada: Bechtel SAIC Company.	169864



BSC 2004. <i>Drift-Scale THC Seepage Model</i> . MDL-NBS-HS-000001, Rev. 03. Las Vegas, Nevada: Bechtel SAIC Company.	169856
BSC 2004. <i>Geologic Framework Model (GFM2000)</i> . MDL-NBS-GS-000002 REV 02. Las Vegas, Nevada: Bechtel SAIC Company. ACC: DOC.20040827.0008.	170029
BSC 2004. <i>Heat Capacity Analysis Report</i> . ANL-NBS-GS-000013, Rev. 01. Las Vegas, Nevada: Bechtel SAIC Company.	170003
BSC 2004. <i>In Situ Field Testing of Processes</i> . ANL-NBS-HS-000005, Rev. 03. Las Vegas, Nevada: Bechtel SAIC Company.	170004
BSC 2004. <i>In-Drift Natural Convection and Condensation</i> . MDL-EBS-MD- 000001, Rev. 00. Las Vegas, Nevada: Bechtel SAIC Company.	164327
BSC 2004. <i>Multiscale Thermohydrologic Model</i> . ANL-EBS-MD-000049, Rev. 02. Las Vegas, Nevada: Bechtel SAIC Company.	169565
BSC 2004. <i>Q-List</i> . 000-30R-MGR0-00500-000-000 REV 00. Las Vegas, Nevada: Bechtel SAIC Company. ACC: ENG.20040721.0007.	168361
BSC 2004. <i>Repository Subsurface Emplacement Drifts Steel Invert Structure Sect. &amp; Committed Materials</i> . 800-SS0-SSE0-00102-000-00B. Las Vegas, Nevada: Bechtel SAIC Company. ACC: ENG.20040520.0005.	169776
BSC 2004. <i>Seepage Calibration Model and Seepage Testing Data</i> . MDL-NBS- HS-000004 REV 03. Las Vegas, Nevada: Bechtel SAIC Company. ACC: DOC.20040922.0003.	171764
BSC 2004. <i>Seepage Model for PA Including Drift Collapse</i> . MDL-NBS-HS- 000002, Rev. 03. Las Vegas, Nevada: Bechtel SAIC Company.	167652
BSC 2004. <i>Technical Work Plan for: Near-Field Environment and Transport: Near-Field Coupled Processes (TH Seepage and THM) Model Report Integration</i> . TWP-MGR-PA-000015 REV 00. Las Vegas, Nevada: Bechtel SAIC Company. ACC: DOC.20040610.0001.	170236
BSC 2004. <i>Technical Work Plan for: Performance Assessment Unsaturated Zone</i> . TWP-NBS-HS-000003 REV 02 [Errata 001]. Las Vegas, Nevada: Bechtel SAIC Company. ACC: MOL.20030102.0108; DOC.20040121.0001.	167969
BSC 2004. <i>Thermal Conductivity of Non-Repository Lithostratigraphic Layers</i> . MDL-NBS-GS-000006, Rev. 01. Las Vegas, Nevada: Bechtel SAIC Company.	170033

BSC 2004. <i>Thermal Conductivity of the Potential Repository Horizon</i> . MDL-NBS-GS-000005, Rev. 01. Las Vegas, Nevada: Bechtel SAIC Company. ACC: MOL.20040630.0641	169854
BSC 2004. <i>Thermal Testing Measurements Report</i> . TDR-MGR-HS-000002 REV 00. Las Vegas, Nevada: Bechtel SAIC Company.	169900
BSC 2004. <i>UZ Flow Models and Submodels</i> . MDL-NBS-HS-000006, Rev. 02. Las Vegas, Nevada: Bechtel SAIC Company.	169861
BSC 2004. <i>Ventilation Model and Analysis Report</i> . ANL-EBS-MD-000030, Rev. 04. Las Vegas, Nevada: Bechtel SAIC Company.	169862
Buscheck, T.A. and Nitao, J.J. 1993. "Repository-Heat-Driven Hydrothermal Flow at Yucca Mountain, Part I: Modeling and Analysis." <i>Nuclear Technology</i> , 104, (3), 418-448. La Grange Park, Illinois: American Nuclear Society. TIC: 224039.	100617
Buscheck, T.A.; Rosenberg, N.D.; Gansemer, J.; and Sun, Y. 2002. "Thermohydrologic Behavior at an Underground Nuclear Waste Repository." <i>Water Resources Research</i> , 38, (3), 10-1 through 10-19. Washington, D.C.: American Geophysical Union. TIC: 253566.	160749
Canori, G.F. and Leitner, M.M. 2003. <i>Project Requirements Document</i> . TER-MGR-MD-000001 REV 02. Las Vegas, Nevada: Bechtel SAIC Company. ACC: DOC.20031222.0006.	166275
Carslaw, H.S. and Jaeger, J.C. 1959. <i>Conduction of Heat in Solids</i> . 2nd Edition. Oxford, Great Britain: Oxford University Press. TIC: 206085.	100968
CRWMS (Civilian Radioactive Waste Management System) M&O (Management and Operating Contractor) 1997. <i>Ambient Characterization of the Drift Scale Test Block</i> . BADD00000-01717-5705-00001 REV 01. Las Vegas, Nevada: CRWMS M&O. ACC: MOL.19980416.0689.	101539
CRWMS M&O 1997. <i>Drift Scale Test Design and Forecast Results</i> . BAB000000-01717-4600-00007 REV 01. Las Vegas, Nevada: CRWMS M&O. ACC: MOL.19980710.0155.	146917
CRWMS M&O 1998. <i>Drift Scale Test As-Built Report</i> . BAB000000-01717-5700-00003 REV 01. Las Vegas, Nevada: CRWMS M&O. ACC: MOL.19990107.0223.	111115
CRWMS M&O 1998. <i>Near-Field/Altered Zone Coupled Effects Expert Elicitation Project</i> . Las Vegas, Nevada: CRWMS M&O. ACC: MOL.19980729.0638.	100351

CRWMS M&O 1998. <i>Thermal Test Progress Report #1</i> . Las Vegas, Nevada: CRWMS M&O. ACC: MOL.19991104.0269.	159512
CRWMS M&O 1999. <i>Thermal Test Progress Report #2</i> . BABEAF000-01717-5700-00001 REV 00. Las Vegas, Nevada: CRWMS M&O. ACC: MOL.19991104.0270.	154585
CRWMS M&O 1999. <i>Thermal Test Progress Report #3</i> . Las Vegas, Nevada: CRWMS M&O. ACC: MOL.19991104.0271.	159513
CRWMS M&O 1999. <i>Thermal Test Progress Report #4</i> . Las Vegas, Nevada: CRWMS M&O. ACC: MOL.20020131.0342.	160806
CRWMS M&O 2000. <i>Geologic Framework Model (GFM3.1)</i> . MDL-NBS-GS-000002 REV 00 ICN 01. Las Vegas, Nevada: CRWMS M&O. ACC: MOL.20000121.0115.	138860
CRWMS M&O 2000. <i>Seepage Model for PA Including Drift Collapse</i> . MDL-NBS-HS-000002 REV 01. Las Vegas, Nevada: CRWMS M&O. ACC: MOL.20010221.0147.	153314
CRWMS M&O 2000. <i>Tabulated In-Drift Geometric and Thermal Properties Used in Drift-Scale Models for TSPA-SR</i> . CAL-EBS-HS-000002 REV 00. Las Vegas, Nevada: CRWMS M&O. ACC: MOL.20020212.0257.	171790
CRWMS M&O 2000. <i>Thermal Test Progress Report #5</i> . Las Vegas, Nevada: CRWMS M&O. ACC: MOL.20020131.0308.	160807
CRWMS M&O 2000. <i>Total System Performance Assessment for the Site Recommendation</i> . TDR-WIS-PA-000001 REV 00 ICN 01. Las Vegas, Nevada: CRWMS M&O. ACC: MOL.20001220.0045.	153246
CRWMS M&O 2000. <i>Unsaturated Zone Flow and Transport Model Process Model Report</i> . TDR-NBS-HS-000002 REV 00 ICN 02. Las Vegas, Nevada: CRWMS M&O. ACC: MOL.20000831.0280.	151940
CRWMS M&O 2001. <i>Seepage Calibration Model and Seepage Testing Data</i> . MDL-NBS-HS-000004 REV 01. Las Vegas, Nevada: CRWMS M&O. ACC: MOL.20010122.0093.	153045
CRWMS M&O 2001. <i>Water Distribution and Removal Model</i> . ANL-EBS-MD-000032 REV 01. Las Vegas, Nevada: CRWMS M&O. ACC: MOL.20010214.0031.	152016
de Marsily, G. 1986. <i>Quantitative Hydrogeology: Groundwater Hydrology for Engineers</i> . San Diego, California: Academic Press. TIC: 208450.	100439

- Doughty, C. 1999. "Investigation of Conceptual and Numerical Approaches for Evaluating Moisture, Gas, Chemical, and Heat Transport in Fractured Unsaturated Rock." *Journal of Contaminant Hydrology*, 38, (1-3), 69-106. New York, New York: Elsevier. TIC: 244160. 135997
- Edlefsen, N.E. and Anderson, A.B.C. 1943. "Thermodynamics of Soil Moisture." *Hilgardia*, 15, (2), 31-298. Berkeley, California: California Agricultural Experiment Station. TIC: 235679. 138932
- Finsterle, S. 2000. "Using the Continuum Approach to Model Unsaturated Flow in Fractured Rock." *Water Resources Research*, 36, (8), 2055-2066. Washington, D.C.: American Geophysical Union. TIC: 248769. 151875
- Francis, N.D. 1997. "The Base-Case Thermal Properties for TSPA-VA Modeling." Memorandum from N.D. Francis (SNL) to Distribution, April 16, 1997. ACC: MOL.19980518.0229. 127326
- Glass, R.J. 1993. "Modeling Gravity-Driven Fingering in Rough-Walled Fractures Using Modified Percolation Theory." *High Level Radioactive Waste Management, Proceedings of the Fourth Annual International Conference, Las Vegas, Nevada, April 26-30, 1993*. 2, 2042-2052. La Grange Park, Illinois: American Nuclear Society. TIC: 208542. 160751
- Grant, S.A. 2003. "Extension of a Temperature Effects Model for Capillary Pressure Saturation Relations." *Water Resources Research*, 39, (1), SBH 1-1 - SBH 1-10. Washington, D.C.: American Geophysical Union. TIC: 56355. 171054
- Hakami, E. 1995. *Aperture Distribution of Rock Fractures*. Doctoral thesis. Stockholm, Sweden: Royal Institute of Technology, Department of Civil and Environmental Engineering. TIC: 253610. 160760
- Hakami, E. and Barton, N. 1990. "Aperture Measurements and Flow Experiments Using Transparent Replicas of Rock Joints." *Rock Joints, Proceedings of the International Symposium on Rock Joints, Loen, Norway, 4-6 June 1990*. Barton, N. and Stephansson, O., eds. Pages 383-390. Brookfield, Vermont: A.A. Balkema. TIC: 103532. 160754
- IFC (International Formulation Committee) 1967. *The 1967 IFC Formulation for Industrial Use, A Formulation of the Thermodynamic Properties of Ordinary Water Substance*. Düsseldorf, Germany: International Formulation Committee of the Sixth International Conference on the Properties of Steam. TIC: 224838. 156448
- Kneafsey, T.J. and Pruess, K. 1998. "Laboratory Experiments on Heat-Driven Two-Phase Flows in Natural and Artificial Rock Fractures." *Water Resources Research*, 34, (12), 3349-3367. Washington, D.C.: American Geophysical Union. TIC: 247468. 145636



- LeCain, G.D. 1995. *Pneumatic Testing in 45-Degree-Inclined Boreholes in Ash-Flow Tuff Near Superior, Arizona*. Water-Resources Investigations Report 95-4073. Denver, Colorado: U.S. Geological Survey. ACC: MOL.19960715.0083. 101700
- Lichtner, P.C. and Walton, J.C. 1994. *Near-Field Liquid-Vapor Transport in a Partially Saturated High-Level Nuclear Waste Repository*. CNWRA 94-022. San Antonio, Texas: Center for Nuclear Waste Regulatory Analyses. TIC: 216007. 152609
- Lin, W.; Blair, S.C.; Wilder, D.; Carlson, S.; Wagoner, J.; DeLoach, L.; Danko, G.; Ramirez, A.L.; and Lee, K. 2001. *Large Block Test Final Report*. UCRL-ID-132246, Rev. 2. Livermore, California: Lawrence Livermore National Laboratory. TIC: 252918. 159069
- Liu, H.H.; Doughty, C.; and Bodvarsson, G.S. 1998. "An Active Fracture Model for Unsaturated Flow and Transport in Fractured Rocks." *Water Resources Research*, 34, (10), 2633-2646. Washington, D.C.: American Geophysical Union. TIC: 243012. 105729
- Mualem, Y. 1976. "A New Model for Predicting the Hydraulic Conductivity of Unsaturated Porous Media." *Water Resources Research*, 12, (3), 513-522. Washington, D.C.: American Geophysical Union. TIC: 217339. 100599
- Mukhopadhyay, S. and Tsang, Y.W. 2002. "Understanding the Anomalous Temperature Data from the Large Block Test at Yucca Mountain, Nevada." *Water Resources Research*, 38, (10), 28-1 through 28-12. Washington, D.C.: American Geophysical Union. TIC: 253867. 160788
- Mukhopadhyay, S. and Tsang, Y.W. 2003. "Uncertainties in Coupled Thermal-Hydrological Processes Associated with the Drift Scale Test at Yucca Mountain, Nevada." *Journal of Contaminant Hydrology*, 62-63, 595-612. New York, New York: Elsevier. TIC: 254205. 160790
- Nicholl, M.J.; Glass, R.J.; and Nguyen, H.A. 1993. "Small-Scale Behavior of Single Gravity-Driven Fingers in an Initially Dry Fracture." *High Level Radioactive Waste Management, Proceedings of the Fourth Annual International Conference, Las Vegas, Nevada, April 26-30, 1993*. 2, 2023-2032. La Grange Park, Illinois: American Nuclear Society. TIC: 208542. 160759
- Nicholl, M.J.; Glass, R.J.; and Wheatcraft, S.W. 1994. "Gravity-Driven Infiltration Instability in Initially Dry Nonhorizontal Fractures." *Water Resources Research*, 30, (9), 2533-2546. Washington, D.C.: American Geophysical Union. TIC: 243493. 141580
- Nitao, J.J. 2000. *Documentation of the Thermal Energy Balance Equation Used in the USNT Module of the NUFT Flow and Transport Code*. UCRL-ID-139836. Livermore, California: Lawrence Livermore National Laboratory. ACC: MOL.20020711.0161. 159883

- NRC (U.S. Nuclear Regulatory Commission) 2003. *Yucca Mountain Review Plan, Final Report*. NUREG-1804, Rev. 2. Washington, D.C.: U.S. Nuclear Regulatory Commission, Office of Nuclear Material Safety and Safeguards. TIC: 254568. 163274
- Oldenburg, C.M. and Pruess, K. 1993. "On Numerical Modeling of Capillary Barriers." *Water Resources Research*, 29, (4), 1045-1056. Washington, D.C.: American Geophysical Union. TIC: 238834. 141594
- Perry, R.H.; Green, D.W.; and Maloney, J.O., eds. 1984. *Perry's Chemical Engineers' Handbook*. 6th Edition. New York, New York: McGraw-Hill. TIC: 246473. 125806
- Persoff, P. and Pruess, K. 1995. "Two-Phase Flow Visualization and Relative Permeability Measurement in Natural Rough-Walled Rock Fractures." *Water Resources Research*, 31, (5), 1175-1186. Washington, D.C.: American Geophysical Union. TIC: 229697. 160758
- Philip, J.R.; Knight, J.H.; and Waechter, R.T. 1989. "Unsaturated Seepage and Subterranean Holes: Conspectus, and Exclusion Problem for Circular Cylindrical Cavities." *Water Resources Research*, 25, (1), 16-28. Washington, D.C.: American Geophysical Union. TIC: 239117. 105743
- Phillips, O.M. 1996. "Infiltration of a Liquid Finger Down a Fracture into Superheated Rock." *Water Resources Research*, 32, (6), 1665-1670. Washington, D.C.: American Geophysical Union. TIC: 239025. 152005
- Pruess, K. 1987. *TOUGH User's Guide*. NUREG/CR-4645. Washington, D.C.: U.S. Nuclear Regulatory Commission. TIC: 217275. 100684
- Pruess, K. 1991. *TOUGH2—A General-Purpose Numerical Simulator for Multiphase Fluid and Heat Flow*. LBL-29400. Berkeley, California: Lawrence Berkeley Laboratory. ACC: NNA.19940202.0088. 100413
- Pruess, K. 1997. "On Vaporizing Water Flow in Hot Sub-Vertical Rock Fractures." *Transport in Porous Media*, 28, (3), 335-372. Boston, Massachusetts: Kluwer Academic Publishers. TIC: 238922. 144794
- Pruess, K. 1998. "On Water Seepage and Fast Preferential Flow in Heterogeneous, Unsaturated Rock Fractures." *Journal of Contaminant Hydrology*, 30, 333-362. New York, New York: Elsevier. TIC: 238921. 107843
- Pruess, K.; Oldenburg, C.; and Moridis, G. 1999. *TOUGH2 User's Guide, Version 2.0*. LBNL-43134. Berkeley, California: Lawrence Berkeley National Laboratory. TIC: 253038. 160778

- Pruess, K.; Tsang, Y.W.; and Wang, J.S.Y. 1984. *Numerical Studies of Fluid and Heat Flow Near High-Level Nuclear Waste Packages Emplaced in Partially Saturated Fractured Tuff*. LBL-18552. Berkeley, California: Lawrence Berkeley Laboratory. TIC: 211033. 144801
- Pruess, K.; Wang, J.S.Y.; and Tsang, Y.W. 1990. "On Thermohydrologic Conditions Near High-Level Nuclear Wastes Emplaced in Partially Saturated Fractured Tuff, 2. Effective Continuum Approximation." *Water Resources Research*, 26, (6), 1249-1261. Washington, D.C.: American Geophysical Union. TIC: 224854. 100819
- Ross, B. 1990. "The Diversion Capacity of Capillary Barriers." *Water Resources Research*, 26, (10), 2625-2629. Washington, D.C.: American Geophysical Union. TIC: 225235. 141790
- Su, G.W.; Geller, J.T.; Pruess, K.; and Wen, F. 1999. "Experimental Studies of Water Seepage and Intermittent Flow in Unsaturated, Rough-Walled Fractures." *Water Resources Research*, 35, (4), 1019-1037. Washington, D.C.: American Geophysical Union. TIC: 245798. 107846
- Tsang, Y.W. and Birkholzer, J.T. 1999. "Predictions and Observations of the Thermal-Hydrological Conditions in the Single Heater Test." *Journal of Contaminant Hydrology*, 38, (1-3), 385-425. New York, New York: Elsevier. TIC: 244160. 137577
- Tsang, Y.W.; Birkholzer, J.T.; Sonnenthal, E.; Spycher, N.; Apps, J.; Peterson, J.E., Jr.; and Williams, K.H. 1998. *Drift Scale Test Progress Report Lawrence Berkeley National Laboratory, Version 0.0*. Milestone SP2930M4. Berkeley, California: Lawrence Berkeley National Laboratory. ACC: MOL.19980825.0268. 144941
- USGS (U.S. Geological Survey) 2003. *Simulation of Net Infiltration for Modern and Potential Future Climates, with Errata*. ANL-NBS-HS-000032 REV 00 ICN 02. Denver, Colorado: U.S. Geological Survey. ACC: MOL.20011119.0334; DOC.20031014.0004; DOC.20031015.0001. 166518
- van Genuchten, M.T. 1980. "A Closed-Form Equation for Predicting the Hydraulic Conductivity of Unsaturated Soils." *Soil Science Society of America Journal*, 44, (5), 892-898. Madison, Wisconsin: Soil Science Society of America. TIC: 217327. 100610
- Wang, J. 2004. Scientific Notebooks Referenced in Model Report U0240 Drift-Scale Coupled Processes Model, MDL-NBS-HS-000015 REV 01 "Memorandum from J.S. Wang (BSC) to File, July 17, 2004, with attachment. ACC: MOL.20040809.0113. 170510

Wang, J.S. 2003. "Scientific Notebooks Referenced in Model Report U0240, Drift-Scale Coupled Processes (DST and TH Seepage) Models, MDL-NBS-HS-000015 REV 00." Interoffice correspondence from J.S. Wang (BSC) to File, March 25, 2003, with attachments. ACC: MOL.20030407.0010. 161123

Williams, N.H. 2001. "Contract #: DE-AC08-01RW12101--Thermal Test Progress Report #7." Letter from N.H. Williams (BSC) to S.P. Mellington (DOE/YMSCO), November 9, 2001, NHW:TJV:bm-1025010261, with enclosure. ACC: MOL.20011207.0060. 160809

Williams, N.H. 2001. "Contract #: DE-AC08-01NV12101 -- Thermal Test Progress Report #6." Letter from N.H. Williams (BSC) to S.P. Mellington (DOE/YMSCO), April 19, 2001, PROJ.04/01.030, with enclosure. ACC: MOL.20010612.0531. 156323

Williams, N. H. 2002. Contract No. DE-AC28-01RW12101 - Key Technical Issue (KTI) Agreement Item Thermal Effects on Flow (TEF) 2.01. ACC: MOL.20030213.0147. 171270

## 9.2 CODES, STANDARDS, REGULATIONS, AND PROCEDURES

10 CFR 63. Energy: Disposal of High-Level Radioactive Wastes in a Geologic Repository at Yucca Mountain, Nevada. Readily available 156605

AP-2.22Q, Rev. 1, ICN 1. *Classification Analyses and Maintenance of the Q-List*. Washington, D.C.: U.S. Department of Energy, Office of Civilian Radioactive Waste Management. ACC: DOC.20040714.0002.

AP-2.27Q, Rev. 1, ICN 4. *Planning for Science Activities*. Washington, D.C.: U.S. Department of Energy, Office of Civilian Radioactive Waste Management. ACC: DOC.20040610.0006

AP-SIII.2Q, Rev. 1, ICN 2. *Qualification of Unqualified Data*. Washington, D.C.: U.S. Department of Energy, Office of Civilian Radioactive Waste Management. ACC: DOC.20040127.0008.

AP-SIII.3Q, Rev. 2 ICN 1. *Submittal and Incorporation of Data to the Technical Data Management System*. Washington, D.C.: U.S. Department of Energy, Office of Civilian Radioactive Waste Management. ACC: DOC.20040226.0001.

AP-SIII.9Q, Rev. 1, ICN 7. *Scientific Analyses*. Washington, D.C.: U.S. Department of Energy, Office of Civilian Radioactive Waste Management. ACC: DOC.20040920.0001.

AP-SIII.10Q, Rev. 2, ICN 7. *Models*. Washington, D.C.: U.S. Department of Energy, Office of Civilian Radioactive Waste Management. ACC: DOC.20040920.0002.

AP-SV.1Q, Rev. 1, ICN 1. *Control of the Electronic Management of Information*. Washington, D.C.: U.S. Department of Energy, Office of Civilian Radioactive Waste Management. ACC: DOC.20030929.0004.

LP-SI.11Q-BSC, Rev. 0, ICN 0. *Software Management*. Washington, D.C.: U.S. Department of Energy, Office of Civilian Radioactive Waste Management. ACC: DOC.20040225.0007.

YMP-LBNL-QIP-SV.0, Rev. 2, Mod. 1. *Management of LBNL Electronic Data*. Berkeley, California: Lawrence Berkeley National Laboratory. ACC: MOL.20020717.0319.

### 9.3 SOURCE DATA, LISTED BY DATA TRACKING NUMBER

GS000308311221.005. Net Infiltration Modeling Results for 3 Climate Scenarios for FY99. Submittal date: 03/01/2000.	147613
GS000483351030.003. Thermal Properties Measured 12/01/99 to 12/02/99 Using the Thermolink Soil Multimeter and Thermal Properties Sensor on Selected Potential Candidate Backfill Materials Used in the Engineered Barrier System. Submittal date: 11/09/2000.	152932
LB000300123142.001. Thermal-Hydrological Simulations of the Drift Scale Test. AMR N0000, Thermal Tests Thermal Hydrological Analysis/Model Report. Submittal date: 03/24/2000.	148120
LB0205REVUZPRP.001. Fracture Properties for UZ Model Layers Developed from Field Data. Submittal date: 05/14/2002.	159525
LB0208AIRKDSTH.001. Air Permeability Data for the Heating Phase of the DST. Submittal date: 08/09/2002.	160897
LB0208UZDSCPMI.002. Drift-Scale Calibrated Property Sets: Mean Infiltration Data Summary. Submittal date: 08/26/2002.	161243
LB0210GPRDSTCP.001. DST GPR Monitoring of Water Content Over Time (Cooling Phase). Submittal date: 10/31/2002.	160896
LB0210GPRDSTHP.001. DST GPR Monitoring of Water Content Over Time (Heating Phase). Submittal date: 10/31/2002.	160895
LB0210THRMLPRP.001. Thermal Properties of UZ Model Layers: Data Summary. Submittal date: 10/25/2002.	160799
LB03023DKMGRID.001. UZ 3-D Site Scale Model Grids. Submittal date: 02/26/2003.	162354



LB0302SCMREV02.002. Seepage-Related Model Parameters K and 1/A: Data Summary. Submittal date: 02/28/2003.	162273
LB0303THERMSIM.001. UZ Thermal Modeling: Simulations. Submittal date: 03/28/2003.	165167
LB0310AMRU0120.001. Supporting Calculations and Analysis for Seepage Abstraction and Summary of Abstraction Results. Submittal date: 10/23/2003.	166409
LB990501233129.004. 3-D UZ Model Calibration Grids for AMR U0000, "Development of Numerical Grids of UZ Flow and Transport Modeling". Submittal date: 09/24/1999.	111475
LB991131233129.004. Modeling of Thermo-Hydrological Data to Simulate Flow, Transport, and Geothermal Conditions of the UZ Model. AMR U0050, "UZ Flow Models and Submodels". Submittal date: 03/11/2000.	162183
LL000114004242.090. TSPA-SR Mean Calculations. Submittal date: 01/28/2000.	142884
MO0001SEPDSTPC.000. Drift Scale Test (DST) Temperature, Power, Current, and Voltage Data for June 1, 1999 through October 31, 1999. Submittal date: 01/12/2000.	153836
MO0002ABBLSLDS.000. As-Built Borehole Locations and Sensor Locations for the Drift Scale Test Given in Local (DST) Coordinates. Submittal date: 02/01/2000.	147304
MO0003RIB00071.000. Physical and Chemical Characteristics of Alloy 22. Submittal date: 03/13/2000.	148850
MO0007SEPDSTPC.001. Drift Scale Test (DST) Temperature, Power, Current, and Voltage Data for November 1, 1999 through May 31, 2000. Submittal date: 07/13/2000.	153707
MO0012SEPDSTPC.002. Drift Scale Test (DST) Temperature, Power, Current, and Voltage Data for June 1, 2000 through November 30, 2000. Submittal date: 12/19/2000.	153708
MO0107SEPDSTPC.003. Drift Scale Test (DST) Temperature, Power, Current, and Voltage Data for December 1, 2000 through May 31, 2001. Submittal date: 07/06/2001.	158321
MO0202SEPDSTTV.001. Drift Scale Test (DST) Temperature, Power, Current, and Voltage Data for June 1, 2001 through January 14, 2002. Submittal date: 02/28/2002.	158320

MO0208SEPDSTTD.001. Drift Scale Test (DST) Temperature Data for January 15, 2002 through June 30, 2002. Submittal date: 08/29/2002.	161767
MO0307MWDAC8MV.000. Analytical-La-Coarse-800M Ventilation. Submittal date: 07/15/2003.	165395
MO0307MWDAC8VD.000. Analytical-LA-Coarse-800M Ventilation with the Delta Method Analysis. Submittal date: 07/15/2003.	167396
MO0407SEPFELA.000. LA FEP List. Submittal date: 07/20/2004.	170760
MO9807DSTSET01.000. Drift Scale Test (DST) Temperature, Power, Current, Voltage Data for November 7, 1997 through May 31, 1998. Submittal date: 07/09/1998.	113644
MO9810DSTSET02.000. Drift Scale Test (DST) Temperature, Power, Current, Voltage Data for June 1 through August 31, 1998. Submittal date: 10/09/1998.	113662
MO9901MWDGFM31.000. Geologic Framework Model. Submittal date: 01/06/1999.	103769
MO9906DSTSET03.000. Drift Scale Test (DST) Temperature, Power, Current, Voltage Data for September 1, 1998 through May 31, 1999. Submittal date: 06/08/1999.	113673
SN0206T0503102.005. Thermal Conductivity of the Non-Repository Layers of Yucca Mountain. Submittal date: 06/27/02.	160258
SN0208F3903102.002. Summary of Thermal Test Water Samples and Field Measurements through 1/14/2002. Submittal date: 08/16/2002.	161246
SN0208T0503102.007. Thermal Conductivity of the Potential Repository Horizon Rev 3. Submittal date: 08/26/2002.	160257
SN0303T0503102.008. Revised Thermal Conductivity of the Non-Repository Layers of Yucca Mountain. Submittal date: 03/19/2003.	162401
SN0307T0510902.003. Updated Heat Capacity of Yucca Mountain Stratigraphic Units. Submittal date: 07/15/2003.	164196
SN0402T0503102.010. Heat Capacity Values for Lithostratigraphic Layers of Yucca Mountain. Submittal date: 02/24/2004.	170993
SN0404T0503102.011. Thermal Conductivity of the Potential Repository Horizon Rev 3. Submittal date: 04/27/2004.	169129

SN9908T0872799.004. Tabulated In-Drift Geometric and Thermal Properties Used in Drift-Scale Models for TSPA-SR (Total System Performance Assessment-Site Recommendation). Submittal date: 08/30/1999. 108437

#### 9.4 OUTPUT DATA, LISTED BY DATA TRACKING NUMBER

LB0301DSCPDSTV.002. Drift-Scale Coupled Process Model Validation: Data Summary.

LB0301DSCPTHSM.002. Drift-Scale Coupled Process Model for Thermohydrologic Seepage: Data Summary. Submittal date: 01/29/2003.

LB0303DSCPDSTV.001. Drift-Scale Coupled Process Model Validation: Simulation Files. Submittal date: 03/20/2003.

LB0303DSCPTHSM.001. Drift-Scale Coupled Process Model for Thermohydrologic Seepage: Simulation Files. Submittal date: 03/20/2003.

LB0309DSCPTHSM.001. Drift-Scale Coupled Process Model For Thermohydrologic Seepage: Simulation Files for Additional Simulation Scenarios. Submittal date: 09/19/2003.

LB0309DSCPTHSM.002. Drift-Scale Coupled Process Model for Thermohydrologic Seepage: Data Summary for Additional Simulation Scenarios. Submittal date: 09/19/2003.

LB0310DSCPTHSM.001. Drift-Scale Coupled Process Model for Thermohydrologic Seepage: Simulation Files for Collapsed Drift Scenarios. Submittal date: 10/21/2003.

LB0310DSCPTHSM.002. Drift-Scale Coupled Process Model for Thermohydrologic Seepage: Data Summary for Collapsed Drift Scenarios. Submittal date: 10/21/2003.

LB0402THRMLPRP.001. Thermal Properties of UZ Model Layers: Data Summary. Submittal date: 02/20/2004.

LB0404DSCPTHSM.001. Drift-Scale Coupled Process Model for Thermohydrologic Seepage: Simulation Files for Additional Simulation Scenarios. Submittal Date: 04/14/2004.

LB0404DSCPTHSM.002. Drift-Scale Coupled Process Model for Thermohydrologic Seepage: Data Summary for Additional Simulation Scenarios. Submittal Date: 04/14/2004.

#### 9.5 SOFTWARE CODES

LBNL (Lawrence Berkeley National Laboratory) 1999. *Software Code: AMESH*. V1.0. Sun, DEC O.S. 5.5.1, V4.0. 10045-1.0-00. 147561

LBNL 1999. *Software Code: EXT*. V1.0. Sun Ultra Sparc, Sun OS 5.5.1. 10047-1.0-00. 147562

LBNL 1999. *Software Code: EXT*. V1.1. Sun, UNIX. 10005-1.1-00. 160768

LBNL 1999. <i>Software code: TOUGH2. V1.3MEOS4V1.0. SUN, DEC ALPHA, SUN O.S. 5.5.1, OSF1 V4.0. 10062-1.3MEOS4V1.0-00.</i>	147569
LBNL 2000. <i>Software Routine: 2KGRIDVI.F. V1.0. SUN Ultra Sparc, SUN OS 5.5.1. 10244-1.0-00.</i>	147553
LBNL 2000. <i>Software Routine: 2kgridv1a.for. V1.0. PC, DOS Emulation. 10382-1.0-00.</i>	153067
LBNL 2000. <i>Software Routine: assign.f. V1.0. SUN, SUN O.S. 5.5.1. 10315-1.0-00.</i>	153090
LBNL 2000. <i>Software Routine: exclude.f. V1.0. SUN, SUN O.S. 5.5.1. 10316-1.0-00.</i>	153089
LBNL 2000. <i>Software Routine: merggrid.f. V1.0. SUN, SUN O.S. 5.5.1. 10230-1.0-00.</i>	148352
LBNL 2000. <i>Software Routine: MK_3DINTER*.F. V1.0. Sun, SUN O.S. 5.5.1. 10241-1.0-00.</i>	147550
LBNL 2000. <i>Software Routine: MK_3DSLIZE.F. V1.0. Sun, SUN O.S. 5.5.1. 10232-1.0-00.</i>	147539
LBNL 2000. <i>Software Routine: MK_CAN_POWER.F. V1.0. Sun, SUN O.S. 5.5.1. 10247-1.0-00.</i>	147557
LBNL 2000. <i>Software Routine: mk_circ.f. V1.0. Sun, SUN O.S. 5.5.1. 10229-1.0-00.</i>	148349
LBNL 2000. <i>Software Routine: MK_CLUSTER*.F. V1.0. Sun, SUN O.S. 5.5.1. 10240-1.0-00.</i>	147548
LBNL 2000. <i>Software Routine: MK_DUAL.F. V1.0. Sun, SUN O.S. 5.5.1. 10236-1.0-00.</i>	147544
LBNL 2000. <i>Software Routine: MK_EVALUATE_*.F. V1.0. Sun, SUN O.S. 5.5.1. 10243-1.0-00.</i>	147552
LBNL 2000. <i>Software Routine: MK_GENER.F. V1.0. Sun, SUN O.S. 5.5.1. 10234-1.0-00.</i>	147542
LBNL 2000. <i>Software Routine: mk_grav2.f. V1.0. SUN, SUN O.S. 5.5.1. 10379-1.0-00.</i>	153068
LBNL 2000. <i>Software Routine: MK_GRAV2D.F. V1.0. Sun, SUN O.S. 5.5.1. 10231-1.0-00.</i>	147538

LBNL 2000. <i>Software Routine: MK_GRAV3D.F.</i> V1.0. Sun, SUN O.S. 5.5.1. 10233-1.0-00.	147540
LBNL 2000. <i>Software Routine: MK_INCON_3D_DUAL.F.</i> V1.0. Sun, SUN O.S. 5.5.1. 10250-1.0-00.	147560
LBNL 2000. <i>Software Routine: MK_OBS3D.F.</i> V1.0. Sun, SUN O.S. 5.5.1. 10238-1.0-00.	147546
LBNL 2000. <i>Software Routine: MK_OBSERV.F.</i> V1.0. Sun, SUN O.S. 5.5.1. 10235-1.0-00.	147543
LBNL 2000. <i>Software Routine: mk_rect.f.</i> V1.0. Sun, SUN O.S. 5.5.1. 10228-1.0-00.	148351
LBNL 2000. <i>Software Routine: MK_TEC*.F.</i> V1.0. Sun, SUN O.S. 5.5.1. 10239-1.0-00.	147547
LBNL 2000. <i>Software Routine: MK_TEMP3D_ALL.F.</i> V1.0. Sun, SUN O.S. 5.5.1. 10242-1.0-00.	147551
LBNL 2000. <i>Software Routine: MK_TIME*.F.</i> V1.0. Sun, SUN O.S. 5.5.1. 10237-1.0-00.	147545
LBNL 2000. <i>Software Routine: MK_WING_POWER.F.</i> V1.0. Sun, SUN O.S. 5.5.1. 10248-1.0-00.	147558
LBNL 2000. <i>Software Routine: MK_YSW_CONNE.F.</i> V1.0. Sun, SUN O.S. 5.5.1. 10246-1.0-00.	147556
LBNL 2000. <i>Software Routine: MK_YSW_ELEME.F.</i> V1.0. Sun, SUN O.S. 5.5.1. 10245-1.0-00.	147554
LBNL 2000. <i>Software Routine: mrgdrift.f.</i> V1.0. SUN, SUN O.S. 5.5.1. 10380-1.0-00.	153082
LBNL 2002. <i>Software Code: TH_PULSE.F.</i> V1.0. Sun, SUN O.S. 5.5.1. 10851-1.0-00.	160767
LBNL 2003. <i>Software Code: TOUGH2.</i> V1.6. PC/MS-DOS Windows 98, Sun UltraSparc/Sun OS 5.5.1, DEC-Alpha OSF1 V4.0. 10007-1.6-01.	161491



INTENTIONALLY LEFT BLANK

## **APPENDIX A**

### **RANDOM PERMEABILITY FIELDS GENERATED WITH EXCEL**

## Drift-Scale Coupled Processes (DST and TH Seepage) Models

---

The heterogeneous fracture permeability fields for the drift scale TH seepage model were generated using Excel 97 SR-1. Four different realizations of the heterogeneous fracture permeability field were generated, three for the Tptpmn submodel and one for the Tptpll submodel. All realizations of the Tptpmn submodel have a mean permeability of  $3.3 \times 10^{-13} \text{ m}^2$  (see Table 4.1-2) and a standard deviation (in log10 space) of 0.84 (see Section 6.2.2.2.2). The mean fracture permeability for the Tptpll submodel is  $9.1 \times 10^{-13} \text{ m}^2$  (see Table 4.1-2). The standard deviation for the Tptpll submodel is assumed to be the same as that for the Tptpmn submodel (see Section 6.2.3.2.1).

To generate random permeability fields, a workbook was opened in Excel. Under the “Tools” drawdown menu, the option “Data Analysis”<sup>a</sup> was used and “Random Number Generation” was selected. Then the following input information was entered to the algorithm:

1. *Number of Variables:* 1
2. *Number of Random Numbers:* 440 (for the number of heterogeneous elements)
3. *Distribution:* From the drawdown menu, “normal” was selected
4. *Mean:* Since lognormal distribution was desired, the mean was provided as  $\ln(10) \times \log(3.3 \times 10^{-13}) \sim -28.74$  for the Tptpmn submodel. The mean for the Tptpll submodel was similarly  $\ln(10) \times \log(9.1 \times 10^{-13}) \sim -27.72$
5. The standard deviation was provided in the natural log space as  $0.84 \times \ln(10) \sim 1.934$
6. Random Seed: A random seed was provided

Once the distributions were generated in natural log space, they were converted into permeability values using the “EXP” function. The resulting distributions were saved in four different output Excel files with the following names:

1. *liste\_rel1\_tptpmn.xls:* First realization for the Tptpmn submodel
2. *liste\_rel2\_tptpmn.xls:* Second realization for the Tptpmn submodel
3. *liste\_rel3\_tptpmn.xls:* Third realization for the Tptpmn submodel
4. *liste\_rel1\_tptpll.xls:* First realization for the Tptpll submodel

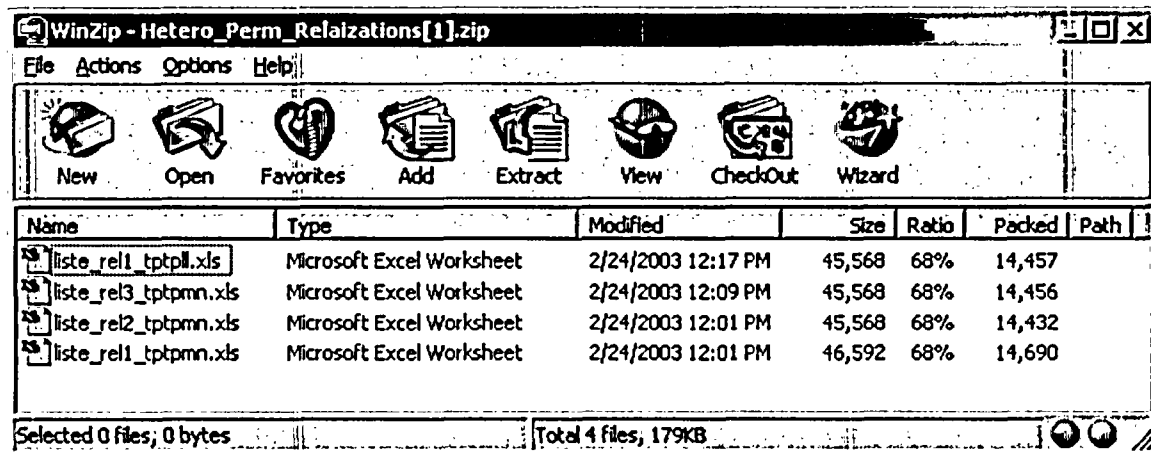
These four files have been submitted to the TDMS (Output DTN: LB0303DSCPTHSM.001). Note that the random seeds required for generating the permeability fields in Excel were not recorded. Thus, it may not be possible to reproduce the individual numbers in the distributions. However, what is more important from a statistical standpoint is that the distribution itself is reproduced statistically (rather than the individual numbers). As proof of the fact that the desired

---

a If the Data Analysis command is not on the Tools menu, the Analysis ToolPak in Microsoft Excel needs to be installed. To install the Analysis ToolPak: 1) On the Tools menu, click Add-Ins; 2) Select the Analysis ToolPak check box.

statistical distribution has been generated, the actual mean and standard deviation of the numbers generated is calculated in each of the above submitted files. These are consistent with the desired mean and standard deviation of the respective distribution. The slight mismatch occurs because of the finite sample number used in generating the distributions.

The dates, times, and file sizes of the four Excel data files, as included in the TDMS are listed below.





**APPENDIX B**

**ARITHMETIC AVERAGE FOR INFILTRATION VALUES**



The infiltration values (6, 16, and 25 mm/year for the present-day, monsoon, and glacial transition periods, respectively) represent repository-wide averages of percolation; the values are calculated as an arithmetic average of the 31 repository locations considered in *Multiscale Thermohydrologic Model* (BSC 2001 [DIRS 158204], Section 6.3.1). The infiltration values at 31 locations are provided in DTN: LL000114004242.090 [DIRS 142884] (file “chimney\_infiltration\_fluxes,” median infiltration cases) (see Section 4.1.1.5). The calculation for deriving the repository-wide averages is conducted in an Excel spreadsheet as listed below. The first column gives the 31 locations, the other three columns give infiltration values in mm/yr for the present-day, the monsoon, and the glacial transition climate periods as extracted from the DTN. The calculated averages have been rounded to 6 mm/yr, 16 mm/yr, and 25 mm/yr, respectively, for further use in this report.

Table B-1. Average Infiltration Values for Different Climate Periods

Column	Present Day	Monsoon	Glacial
I7c4	1.493	3.252	5.211
I7c3	4.677	10.71	18.418
I7c2	5.554	13.726	22.42
I7c1	1.7	4.588	7.013
I6c5	9.41	17.746	30.732
I6c4	11.302	32.651	47.872
I6c3	4.18	10.303	16.574
I6c2	3.147	7.163	10.986
I6c1	3.879	9.432	15.079
I5c5	8.428	17.265	29.872
I5c4	14.412	40.972	60.237
I5c3	5.68	13.12	19.949
I5c2	7.395	17.707	27.097
I5c1	0.663	0.436	0.816
I4c5	5.449	14.472	20.214
I4c4	10.132	28.876	41.998
I4c3	10.144	24.091	38.66
I4c2	6.909	16.9	27.923
I4c1	4.794	12.093	18.881
I3c4	15.877	43.993	65.028
I3c3	1.304	2.637	4.194
I3c2	0.485	0.492	1.271

Table B-1. Average Infiltration Values for Different Climate Periods (Continued)

<b>Column</b>	<b>Present Day</b>	<b>Monsoon</b>	<b>Glacial</b>
I3c1	6.335	18.869	27.005
I2c4	15.998	42.285	58.627
I2c3	12.011	40.749	63.168
I2c2	1.416	9.154	23.399
I2c1	0.406	0.25	0.733
I1c4	3.015	11.575	19.057
I1c3	7.809	21.854	32.439
I1c2	0.877	0.94	2.13
I1c1	0.574	10.004	13.523
	<b>Average</b>	<b>Average</b>	<b>Average</b>
	<b>5.941625</b>	<b>16.07435</b>	<b>24.85568</b>

## **APPENDIX C**

### **SENSITIVITY TO REVISED MATRIX POROSITY AND THERMAL PROPERTIES**





This appendix provides a description of additional simulation runs that were conducted using revised thermal property data for the various stratigraphic layers in the UZ at Yucca Mountain. Some of the DTNs providing input parameters in Section 4 were changed after the simulation runs in Section 6.2 had been completed. The simulation results in this appendix demonstrate that the impact of these parameter changes on the near-field TH response is negligible, and that all the conclusions regarding thermal seepage summarized in Section 8.1 still hold, even when using the revised properties. The following provides a comparative analysis of selected simulation runs with the new property set (given in DTN: LB0402THRMLPRP.001) and the previous property set (given in DTN: LB0210THRMLPRP.001 [DIRS 160799]).

## C.1 INPUT DATA

The revised thermal properties used here are given in DTN: LB0402THRMLPRP.001 (see Appendix F). As noted in Section 4.1.1.1, the original thermal properties were provided in DTN: LB0210THRMLPRP.001 [DIRS 160799]. The simulation runs in this appendix use the following properties from these DTNs: matrix porosity, matrix rock grain density, matrix specific heat capacity, bulk dry thermal conductivity, and bulk wet thermal conductivity. The revisions to the properties affected only the matrix porosity, the rock grain density, and the dry and wet heat conductivities; minor changes in heat capacity stem from rounding-off differences. Only the nonrepository units were affected by these changes (Table C-1). The properties of the repository units remain essentially unchanged (shaded data on Table C-1). Thus, it can be expected that the impact of these property changes on the TH conditions near emplacement drifts is small (see Sections C.3 and C.4 for the comparative analysis); most emplacement drifts are separated from the affected nonrepository units by thick layers of rock.

Adjustments in DTN: LB0210THRMLPRP.001 [DIRS 160799] became necessary because a new revision of *Thermal Conductivity of Non-Repository Lithostratigraphic Layers* (BSC 2004 [DIRS 170033]) became available, providing a new DTN: SN0303T0503102.008 [DIRS 162401] with revised porosity, density and thermal conductivity values for all nonrepository layers (different from those used for the simulations presented in Section 6.2). The revised values were used to derive DTN: LB0402THRMLPRP.001, which contain adjustments from the source data provided in DTN: SN0303T0503102.008 [DIRS 162401]. The source data are defined for the stratigraphic units of the geologic framework model (BSC 2002 [DIRS 159124]), while the thermal seepage model uses the slightly different layering of the UZ model (e.g., BSC 2003 [DIRS 160109], Table 11). When UZ layers comprise two or more GFM layers, the thermal properties were averaged. The procedures followed in developing these revised thermal properties can be found in Appendix F.

For the simulations in this appendix, the same heat capacity values as those presented in Section 6.2 are used. However, an alternative set of heat capacity and grain density values are also provided in *Heat Capacity and Thermal Expansion Coefficients Analysis Report* (BSC 2004 [DIRS 170003]), as contained in DTN: SN0307T0510902.003 [DIRS 164196]. The alternative values were derived from a mineral summation method, based on the mineral composition of the grain. Heat capacity and grain density are calculated as the sum of heat capacities and grain densities of the minerals weighted by their abundance. For thermal modeling purposes, the product of heat capacity and grain density define the thermal storage capacity in a given volume of rock. It can be shown that the product of heat capacity and grain density calculated from this

alternative set is similar (less than a few percent) to that used in Section 6.2 and in this appendix. Considering that the thermal response of the near-field environment is rather insensitive to heat capacity (BSC 2001 [DIRS 155950], Sections 5.3.1.2.3 and 5.3.1.4.9), the impact of using these slightly different alternative values is expected to be negligibly small. While not documented in this report, a selected simulation case was conducted using the alternative values for heat capacity and grain density, giving TH results that were virtually identical to those presented in Section 6.2.

## C.2 MODELING PROCEDURE AND SIMULATION CASES

Except for using the revised property set, the modeling procedures of the simulation runs in this appendix are identical to those described in Section 6.2.1. A subset of the suite of simulations conducted in Section 6.2 was repeated in this appendix using the revised properties. It was not necessary to repeat all original simulation runs because the impact of the property changes was expected (and turned out) to be very small. The selected simulation cases are listed in Table C-2.

Similar to Section 6.2.1.6, each new simulation case is denoted by a specific name code as follows. The first two letters are either MN (for the *Tptpmn* submodel) or LL (for the *Tptpll* submodel), followed by HOM (for *homogeneous* representation of permeability) or HET (for *heterogeneous* representation of permeability), followed by NEW (indicating the use of revised properties), followed by a two-digit number. For example, a simulation name MN-HET-NEW-01 denotes the first simulation case with the *Tptpmn* submodel using a heterogeneous permeability field and revised thermal properties. Results from this simulation case can be directly compared with the original simulation MN-HET-01.

The rationale for selecting simulation cases is as follows: Simulation Case MN-HOM-NEW-01 was chosen because it corresponds to the primary simulation case (base case) for studying the drift-scale TH processes in Section 6.2.1.1. Simulation Cases MN-HET-NEW-01 through -04 were selected as representative of the many cases presented in Sections 6.2.2.2 and 6.2.4.2 that focus on the potential for thermal seepage with related sensitivities. With flux multiplication factors of 1, 5, 10, and 20, they cover sufficient variation of the most important parameter for thermal seepage, i.e., percolation flux. All the above cases use the *Tptpmn* submodel, i.e., where the emplacement drift is located in the *Tptpmn* stratigraphic unit. As it turned out, the impact of adjusting properties in nonrepository units was negligibly small for all the *Tptpmn* simulation cases, in particular when considering the primary focus of this report, which is the evolution of thermal seepage. Due to the small impact, only one additional simulation was selected for the *Tptpll* submodel (LL-HOM-NEW-01). The reason for analyzing both submodels is that, depending on the stratigraphy and the vertical location of the drifts, the *Tptpmn* and the *Tptpll* submodel may be slightly more or slightly less affected from parameter changes in nonrepository units.

Table C-1. Summary of Revised and Original Rock Matrix Properties

UZ Model Layer	Matrix Porosity		Grain Density (kg/m <sup>3</sup> )		Heat Capacity (J/Kg-K)		Bulk Dry Conductivity (W/m-K)		Bulk Wet Conductivity (W/m-K)	
	Revised	Original	Revised	Original	Revised	Original	Revised	Original	Revised	Original
tcw11	0.119	0.118	2486	2514	985.0	985.0	1.30	1.30	1.81	1.80
tcw12	0.119	0.118	2486	2514	985.0	985.0	1.30	1.30	1.81	1.80
tcw13	0.211	0.0457	2385	2274	1040	1040	0.572	0.670	0.909	0.794
ptn21	0.385	0.354	2374	2288	1040	1040	0.490	0.489	1.06	1.07
ptn22	0.385	0.354	2374	2288	1040	1040	0.490	0.489	1.06	1.07
ptn23	0.385	0.354	2374	2288	1040	1040	0.490	0.489	1.06	1.07
ptn24	0.385	0.354	2374	2288	1040	1040	0.490	0.489	1.06	1.07
ptn25	0.385	0.354	2374	2288	1040	1040	0.490	0.489	1.06	1.07
ptn26	0.385	0.251	2374	2283	1040	1040	0.490	0.537	1.06	0.957
tsw31	0.0775	0.0457	2441	2274	1012	1040	0.900	0.670	1.11	0.794
tsw32	0.119	0.118	2486	2514	985.0	985.0	1.30	1.30	1.81	1.80
tsw33	0.143	0.143	2344	2358	985.0	985.0	1.16	1.16	1.68	1.68
tsw34	0.129	0.129	2466	2466	985.0	985.0	1.42	1.42	2.07	2.07
tsw35	0.149	0.149	2325	2325	985.0	985.0	1.28	1.28	1.89	1.89
tsw36	0.106	0.106	2473	2473	985.0	985.0	1.49	1.49	2.13	2.13
tsw37	0.106	0.106	2473	2473	985.0	985.0	1.54	1.49	2.20	2.13
tsw38	0.0360	0.046	2396	2274	1040	1040	0.688	0.670	0.796	0.794
tsw39	0.385	0.046	2374	2274	1040	1040	0.490	0.670	1.06	0.794
ch1(v,z)	0.385	0.354	2374	2288	1040	1040	0.490	0.489	1.06	1.07
ch2(v,z)	0.333	0.328	2504	2256	1038	1038	0.595	0.600	1.26	1.27
ch3(v,z)	0.333	0.328	2504	2256	1038	1038	0.595	0.600	1.26	1.27
ch4(v,z)	0.333	0.328	2504	2256	1038	1038	0.595	0.600	1.26	1.27
ch5(v,z)	0.333	0.328	2504	2256	1038	1038	0.595	0.600	1.26	1.27
ch6(v,z)	0.333	0.328	2504	2256	1038	1038	0.595	0.600	1.26	1.27
pp4	0.300	0.297	2557	2103	1040	1040	0.569	0.538	1.13	1.11
pp3	0.300	0.297	2557	2103	1040	1040	0.569	0.538	1.13	1.11
pp2	0.255	0.233	2587	2385	1012	1009	0.741	0.733	1.33	1.34
pp1	0.277	0.273	2519	2038	1040	1040	0.596	0.564	1.15	1.13
bf3	0.194	0.188	2485	2106	1021	1018	0.788	0.757	1.34	1.33
bf2	0.264	0.262	2506	2012	1040	1040	0.611	0.576	1.16	1.14

NOTES: Revised data are from DTN: LB0402THRMLPRP.001 (rounded to the number of significant digit shown).

Original data are from DTN: LB0210THRMLPRP.001 (rounded to the number of significant digit shown).

Fracture thermal properties are derived using matrix properties as discussed in Section 6.2.1.1.3. Other rock properties data are identical to those listed in Table 6.1-2. The data for repository units are shaded.

Table C-2. List of Simulation Cases Using Revised Properties

New Simulation Case	Thermal Load	Flux multiplication factor	Property Set	Permeability in Drift Vicinity	Capillary Strength in Drift Vicinity	Previous Simulation Case	Previous Case Shown in Section	Output DTN for New Simulation
<b>Tptpmn Submodel</b>								
MN-HOM-NEW-01	Reference Mode	1	DS/AFM-UZ02-Mean	Homogeneous	From DS-AFM-UZ02-Mean	MN-HOM-01	6.2.2.1.1	NA (see Section 8.5)
MN-HET-NEW-01	Reference Mode	1	DS/AFM-UZ02-Mean	Heterogeneous (Realization 1)	From SCM ( $1/\alpha = 589$ Pa)	MN-HET-01	6.2.2.2.3	LB0404DSCPTHSM.001
MN-HET-NEW-02	Reference Mode	5	DS/AFM-UZ02-Mean	Heterogeneous (Realization 1)	From SCM ( $1/\alpha = 589$ Pa)	MN-HET-02	6.2.2.2.4	LB0404DSCPTHSM.001 LB04041DSCPTHSM.002
MN-HET-NEW-03	Reference Mode	10	DS/AFM-UZ02-Mean	Heterogeneous (Realization 1)	From SCM ( $1/\alpha = 589$ Pa)	MN-HET-03	6.2.2.2.4	LB0404DSCPTHSM.001 LB0404DSCPTHSM.002
MN-HET-NEW-04	Reference Mode	20	DS/AFM-UZ02-Mean	Heterogeneous (Realization 1)	From SCM ( $1/\alpha = 589$ Pa)	MN-HET-04	6.2.4.2	LB0404DSCPTHSM.001 LB04041DSCPTHSM.002
<b>Tptpll Submodel</b>								
LL-HOM-NEW-01	Reference Mode	1	DS/AFM-UZ02-Mean	Homogeneous	From DS-AFM-UZ02-Mean	LL-HOM-01	6.2.3.1	NA (see Section 8.5)

NOTE: The steady-state ambient simulation cases that are required to compare the thermal seepage results to their steady-state ambient counterparts were not repeated. This is not necessary because the steady-state ambient situation is not affected by changes in porosity, density, or thermal conductivity.

### **C.3 SIMULATION RESULTS – REVISED VERSUS ORIGINAL PROPERTIES (TPTPMN SUBMODEL)**

The first simulation case that is analyzed for the impact of thermal property changes is the base case simulation MN-HOM-NEW-01. This simulation assumes a drift emplaced in the Tptpmn stratigraphic unit, uses homogeneous properties, applies a thermal load representative of average conditions (reference mode, see Section 6.2.1.3.3), and uses the mean infiltration scenario without flow focusing (see Section 6.2.1.4). Except for the property changes, this simulation case is similar to simulation case MN-HET-01 presented in Section 6.2.2.1.1. Figures C-1, C-2, and C-3 show the evolution of matrix temperature, matrix saturation, and fractures saturation, respectively, for both property sets. It is evident that the differences between the two simulations are negligibly small. Temperatures at the drift crown differ by less than one degree between the original and revised simulation results, the revised results showing a minor temperature decrease. Rewetting of matrix and fractures at the drift crown is predicted to occur at around the same time for the two simulation cases. The small impact of changes in thermal properties on TH conditions is also demonstrated in Figure C-4, where fracture saturations and downward fluxes are plotted along a vertical line above the drift crown. Again, the simulated results are virtually identical. No seepage occurs in either case.

The following simulation cases for the Tptpmn submodel focus on the potential for thermal seepage. According to the conceptual model introduced in Section 6.2.1.1.2, they incorporate a heterogeneous fracture permeability field (using Realization 1 of the heterogeneous field) and apply the fracture capillary-strength parameter suggested from the SCM. Again, the reference mode thermal load is applied. The cases studied have flux multiplication factors of 1, 5, 10, and 20. Consistent with the original simulation described in Section 6.2.2.2.3, there is no seepage in the first case (MN-HET-NEW-01), where the imposed percolation fluxes are relatively small (i.e., 6 mm/year during present-day climate, 16 mm/yr during the monsoon climate, and 25 mm/year during glacial transition climate). Figures C-5 and C-6 demonstrate that the temperature and fractures saturation histories for this case are almost identical to the original simulation results (MN-HET-01). For higher percolation flux cases, seepage was predicted to occur in the original simulation runs (flux multiplication factors of 5 and 10 in Section 6.2.2.4 and flux multiplication factor 20 in Section 6.2.4.2), and the same result is obtained with the revised property set. For the first case with flux multiplication factor 5, the temperature and saturation plots in Figures C-7 and C-8 confirm that the TH conditions close to the drift wall are not affected by the property changes. Since the saturation pattern at the drift wall is directly linked to the onset and the evolution of seepage, there is also no difference in the predicted seepage rates. Figure C-8 shows virtually identical seepage rates resulted from simulations with the revised and previous property sets. Figures C-9 and C-10 give a comparison of seepage rates obtained for the simulation cases with flux multiplication factors of 10 and 20, demonstrating that the “no-impact” conclusion holds for rather high percolation flux cases too.

### **C.4 SIMULATION RESULTS – REVISED VERSUS ORIGINAL PROPERTIES (TPTPLL SUBMODEL)**

Because of the negligible impact of the revised property set on TH conditions in the Tptpmn submodel (see Section C.3), only one simulation was performed for the Tptpll submodel. The selected simulation case is the base case simulation LL-HOM-NEW-01. This simulation



assumes a drift emplaced in the Tptpll stratigraphy unit, uses homogeneous properties, applies a thermal load representative of average conditions (reference mode), and uses the mean infiltration scenario without flow focusing. Except for the property changes, this simulation case is identical to simulation case LL-HET-01 presented in Section 6.2.3.1. Figures C-11, C-12, and C-13 show the evolution of matrix temperature, matrix saturation, and fractures saturation, respectively, for the revised and the original property set. The differences between the two property sets are small, yet slightly larger than those obtained for the Tptpmn submodel. Temperatures differ by a little more than one degree between the original and revised simulation results, the revised results showing a small temperature decrease. As a result, the onset of rewetting in the fractures at the drift crown is predicted to occur about 50 years earlier using the revised properties. However, the differences in fracture saturation vanish soon after initiation of rewetting; except for a time period of about 50 years (at about 1,200 years after waste emplacement), the saturation evolution of the two cases is identical. The slightly earlier rewetting can also be seen in Figure C-14, where fracture saturations and fluxes are plotted along a vertical line above the drift crown. While the saturation profiles are very similar for time steps of 100 years, 500 years, and 2,000 years, the 1,000-year profiles indicate a slightly smaller dry-out zone compared to the previous property set. No seepage is predicted to occur in both cases.

The observed differences between the two property sets are slightly larger using the Tptpll submodel compared to those predicted for the Tptpmn submodel. This finding can be explained when analyzing the vertical distance between the emplacement drifts and the stratigraphic units that have been affected by thermal property changes. Table C-1 suggests that the tsw31 layer is the first unit above the repository with thermal conductivity changes, while the tsw37 layer is the first unit below the repository with such changes. As explained in Section 6.2.1.2, the Tptpmn submodel stratigraphy is adopted from a location close to borehole USW SD-9. Here, the center of the emplacement drift (located in the tsw34 unit) is roughly 150 m below the tsw31 layer, and roughly 150 m above the tsw37 unit.<sup>b</sup> The Tptpll submodel uses a stratigraphy near the center of the repository, close to the area of the proposed Cross-Drift Thermal Test. Here, the center of the emplacement drift (located in the tsw35 unit) is roughly 200 m below the tsw31 layer, but only about 90 m above the tsw37 unit.<sup>1</sup> That the Tptpll submodel is more sensitive to the property changes than the Tptpmn submodel is a result of the relatively smaller distance between the drift and the underlying tsw37 unit.

While the observed differences between the two property sets are slightly larger than those predicted for the Tptpmn submodel, they are much smaller than differences stemming from the spatial variability of input parameters and boundary conditions for the thermal seepage model.

---

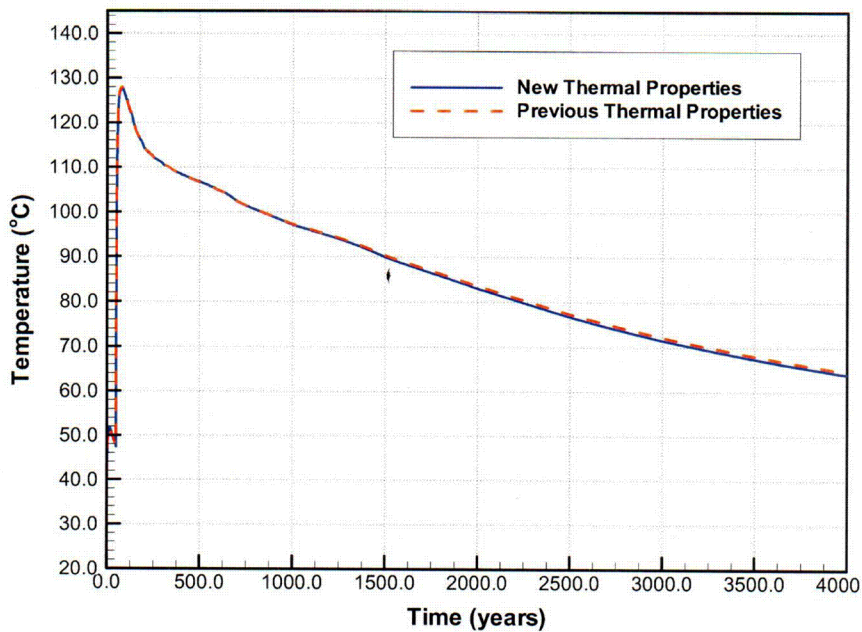
<sup>b</sup> This calculation is conducted using the simulation MESH files for the Tptpmn and Tptpll submodels, respectively, as given in DTN: LB0404DSCPTISM.001. Using a MESH file for the Tptpmn submodel from one of the respective data directories, one can extract the vertical distances as follows: The distance between the center of the repository and the tsw31/tsw32 interface is given by the average vertical coordinates of elements F 610 (tsw31) and F 603 (tsw32), respectively. The distance between the center of the repository and the tsw36/tsw37 interface is given by the average vertical coordinates of elements F1004 (tsw36) and F1006 (tsw37), respectively. Using a MESH file for the Tptpll submodel from one of the respective data directories, one can extract the vertical distances as follows: The distance between the center of the repository and the tsw31/tsw32 interface is given by the average vertical coordinates of elements F 584 (tsw31) and F 579 (tsw32), respectively. The distance between the center of the repository and the tsw36/tsw37 interface is given by the average vertical coordinates of elements F 773 (tsw36) and F 781 (tsw37), respectively. The vertical distances are given in the MESH file in the ELEMENT block, in the last column to the right.

Figures 6.2.4.2-1 through 6.2.4.2-4, for example, demonstrate the bandwidth of temperature and thermal seepage responses for simulation cases with different thermal loads or different percolation fluxes. Compared to this, the discrepancies occurring from the property revision are negligibly small.

## C.5 CONCLUSIONS REGARDING THE ABSTRACTION OF THERMAL SEEPAGE

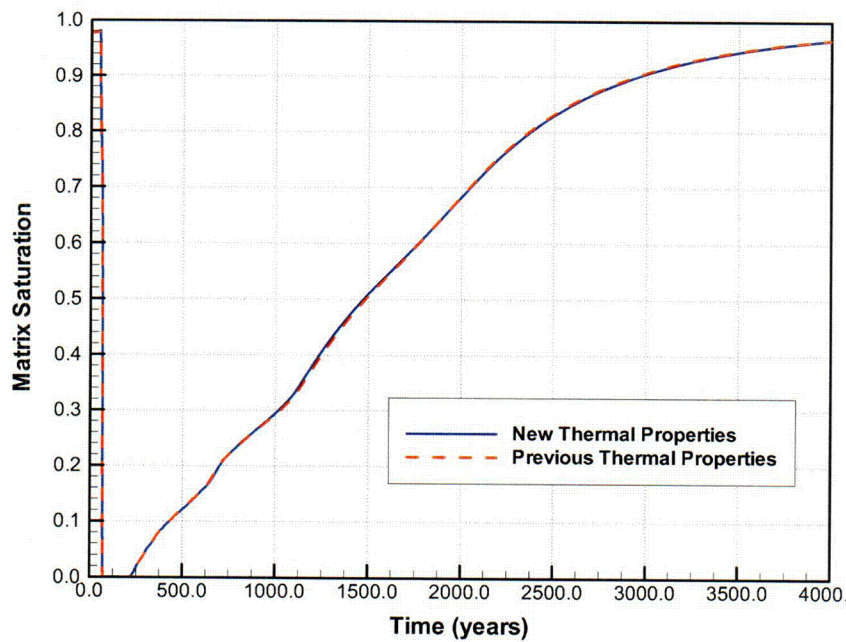
The model results shown in Sections C.3 and C.4 demonstrate that the differences between TH conditions predicted with revised thermal properties vs. original thermal properties are either almost undetectable (for the Tptpmn submodel) or very small (for the Tptpll submodel). In the latter case, rewetting occurs somewhat earlier using the revised properties, as a result of the small temperature decrease, compared to the original properties. However, these differences are not large enough to change the main output generated in REV 00 of this report. The main output of the report is the consistent result that (1) seepage during the thermal period does not occur at above-boiling temperatures, and (2) that, in case seepage occurs at later times, the thermal seepage rate is always smaller than the respective long-term ambient seepage rate for the considered time period (see Section 6.2.4.1). This consistency in thermal seepage results over many simulation cases is utilized in *Abstraction of Drift Seepage* (BSC 2004 [DIRS 169131]) to develop an abstraction methodology for thermal seepage.

Two alternative abstraction methodologies for thermal seepage are proposed in Section 6.5.2 of *Abstraction of Drift Seepage* (BSC 2004 [DIRS 169131]). Both are based on the qualitative results of the thermal seepage model given in Section 6.2, and also incorporate quantitative results from other sources. These quantitative results are (1) the ambient seepage rates with related spatial variability over the repository provided by the SMPA (BSC 2004 [DIRS 167652]), and (2) the duration of the boiling period near emplacement drifts with related spatial variability over the repository provided by the multiscale thermohydrologic model (BSC 2004 [DIRS 169565]). Therefore, as long as the main outputs from the thermal seepage model remain unchanged in a qualitative sense, the abstraction of drift seepage and the seepage calculation in TSPA are unaffected. This is clearly true for the small differences obtained using the revised vs. the previous property sets. As a result, there is no impact on the proposed abstraction methodology for thermal seepage.



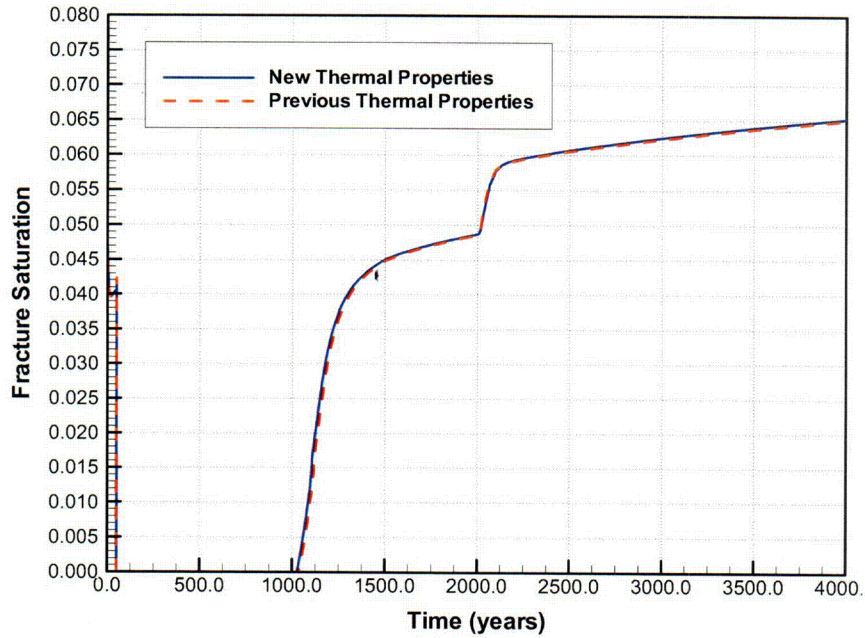
Output DTN: NA (See Section 8.5).

Figure C-1. Evolution of Rock Temperature at the Drift Crown for Tptpmn Submodel, Comparing New vs. Previous Thermal Properties (Simulation Cases MN-HOM-NEW-01 vs. MN-HOM-01)



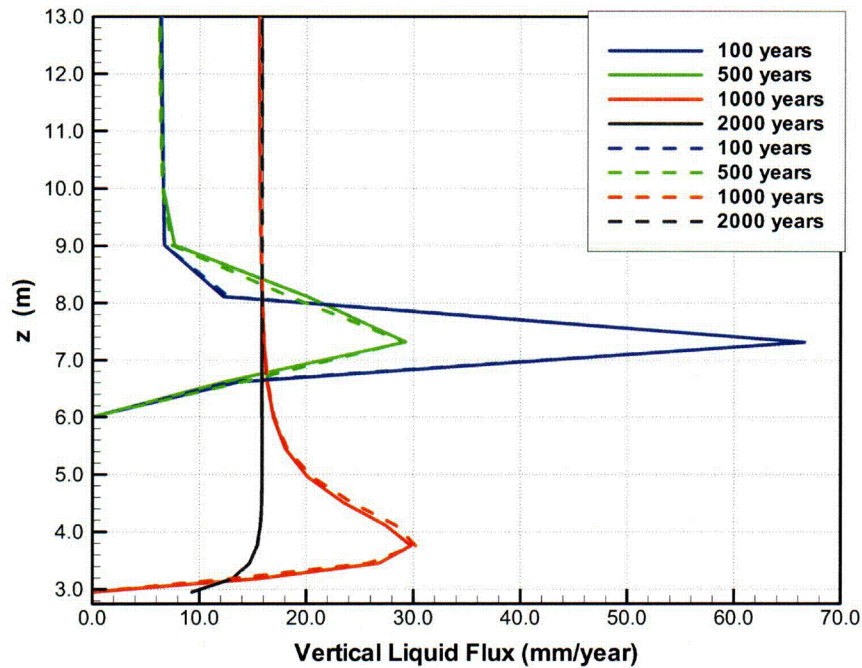
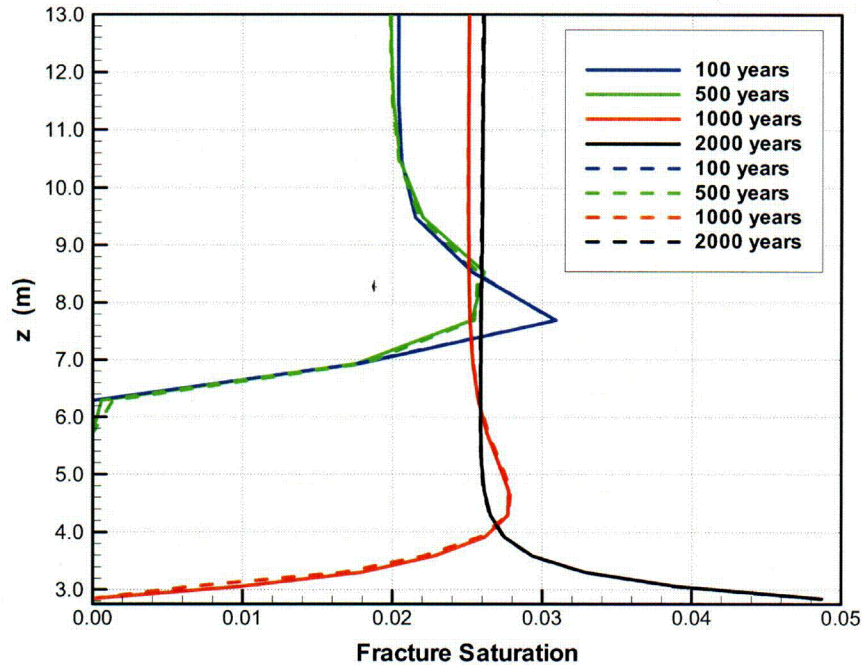
Output DTN: NA (See Section 8.5).

Figure C-2. Evolution of Matrix Saturation at the Drift Crown for Tptpmn Submodel, Comparing New vs. Previous Thermal Properties (Simulation Cases MN-HOM-NEW-01 vs. MN-HOM-01)



Output DTN: NA (See Section 8.5).

Figure C-3. Evolution of Fracture Saturation at the Drift Crown for Tptpmn Submodel, Comparing New vs. Previous Thermal Properties (Simulation Cases MN-HOM-NEW-01 vs. MN-HOM-01)

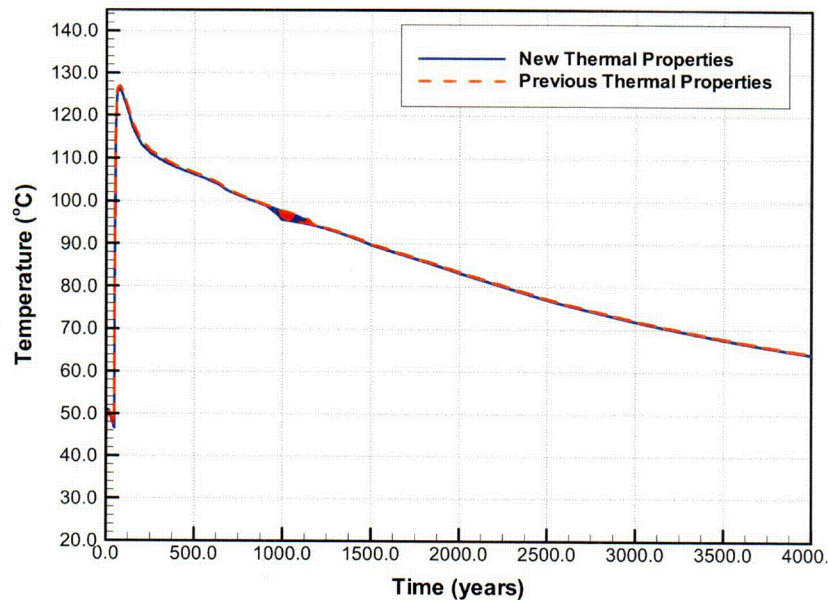


Output DTN: NA (See Section 8.5).

NOTE: The solid blue line represents new thermal properties; the dashed red line represents previous thermal properties.

Figure C-4. (a) Fracture Saturation and (b) Vertical Liquid Flux in a Vertical Cross Section above Drift Crown for Tptpmn Submodel, Comparing New vs. Previous Thermal Properties (Simulation Cases MN-HOM-NEW-01 vs. MN-HOM-01)

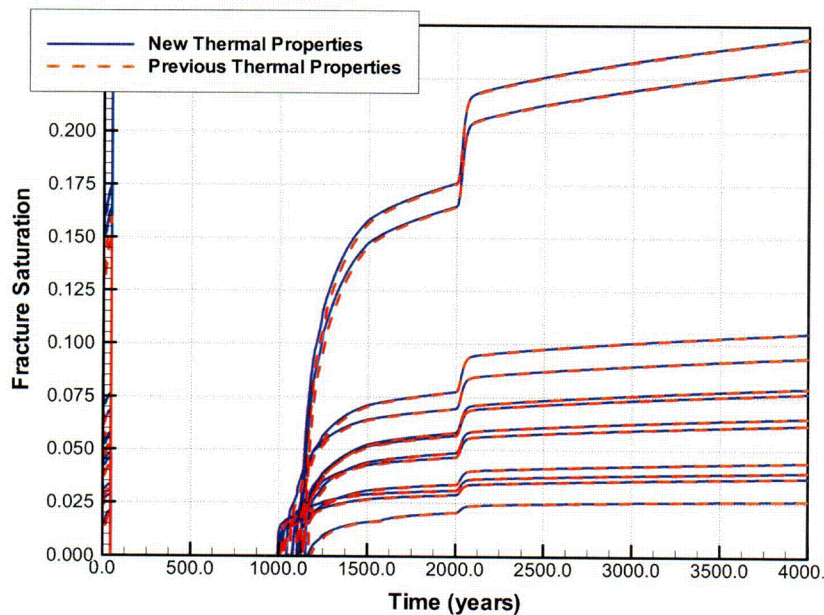




Output DTN: LB0404DSCPTHSM.001.

NOTE: Figure shows all rock discretization elements along the drift periphery from the crown to the springline.

Figure C-5. Evolution of Rock Temperature for Tptpmn Submodel with Flux Multiplication Factor 1 (Realization 1), Comparing New vs. Previous Thermal Properties (Simulation Cases MN-HET-NEW-01 vs. MN-HET-01)

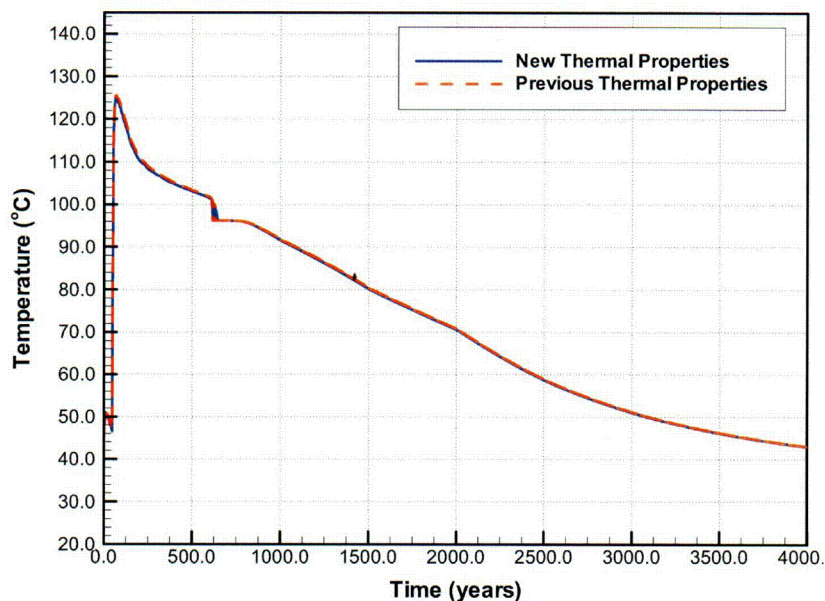


Output DTN: LB0404DSCPTHSM.001.

NOTE: Figure shows all rock discretization elements along the drift periphery from the crown to the springline.

Figure C-6. Evolution of Fracture Saturation for Tptpmn Submodel with Flux Multiplication Factor 1 (Realization 1), Comparing New vs. Previous Thermal Properties (Simulation Cases MN-HET-NEW-01 vs. MN-HET-01)

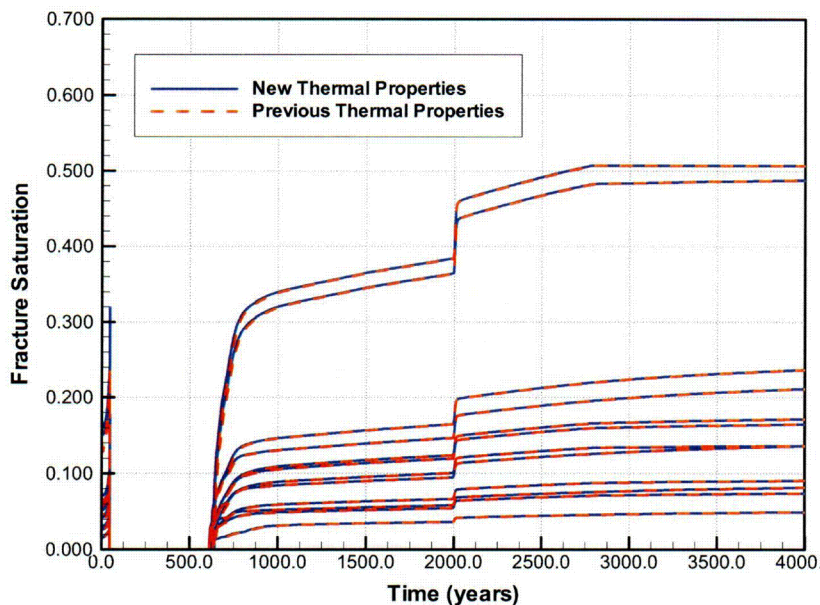




Output DTN: LB0404DSCPTHSM.001.

NOTE: Figure shows all rock discretization elements along the drift periphery from the crown to the springline.

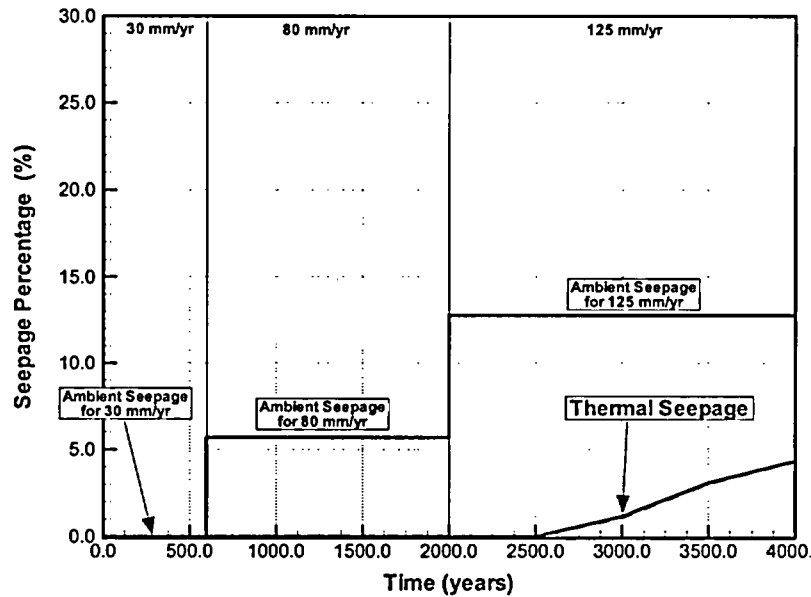
Figure C-7. Evolution of Rock Temperature for Tptpmn Submodel with Flux Multiplication Factor 5 (Realization 1), Comparing New vs. Previous Thermal Properties (Simulation Cases MN-HET-NEW-02 vs. MN-HET-02)



Output DTN: LB0404DSCPTHSM.001.

NOTE: Figure shows all rock discretization elements along the drift periphery from the crown to the springline.

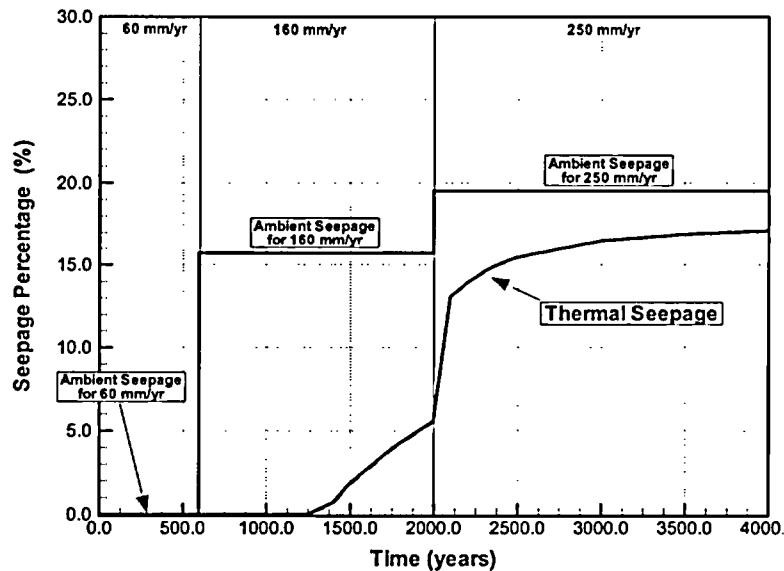
Figure C-8. Evolution of Fracture Saturation for Tptpmn Submodel with Flux Multiplication Factor 5 (Realization 1), Comparing New vs. Previous Thermal Properties (Simulation Cases MN-HET-NEW-02 vs. MN-HET-02)



Output DTN: LB0404DSCPTHSM.001.

NOTE: The solid blue line represents new thermal properties; the dashed red line represents previous thermal properties.

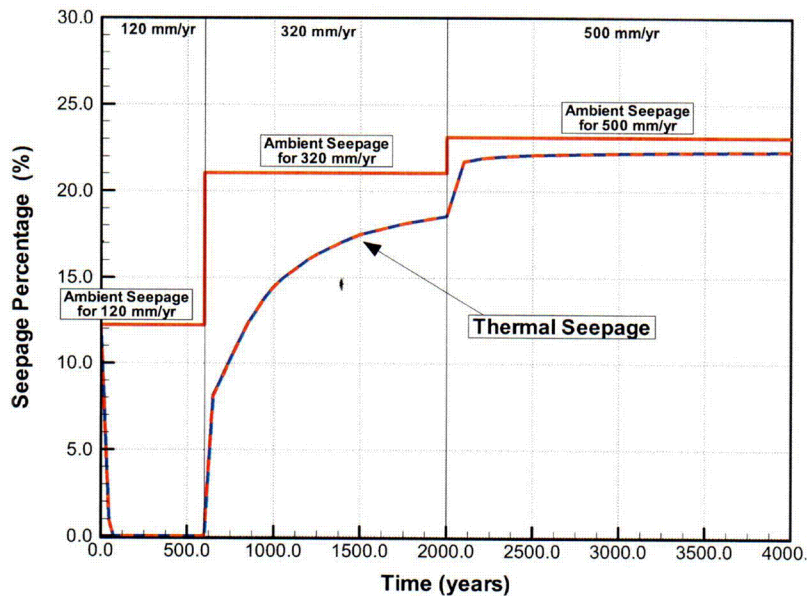
Figure C-8. Evolution of Thermal Seepage for Tptpmn Submodel with Flux Multiplication Factor 5 (Realization 1), Comparing New vs. Previous Thermal Properties (Simulation Cases MN-HET-NEW-02 vs. MN-HET-02).



Output DTN: LB0404DSCPTHSM.001.

NOTE: The solid blue line represents new thermal properties; the dashed red line represents previous thermal properties.

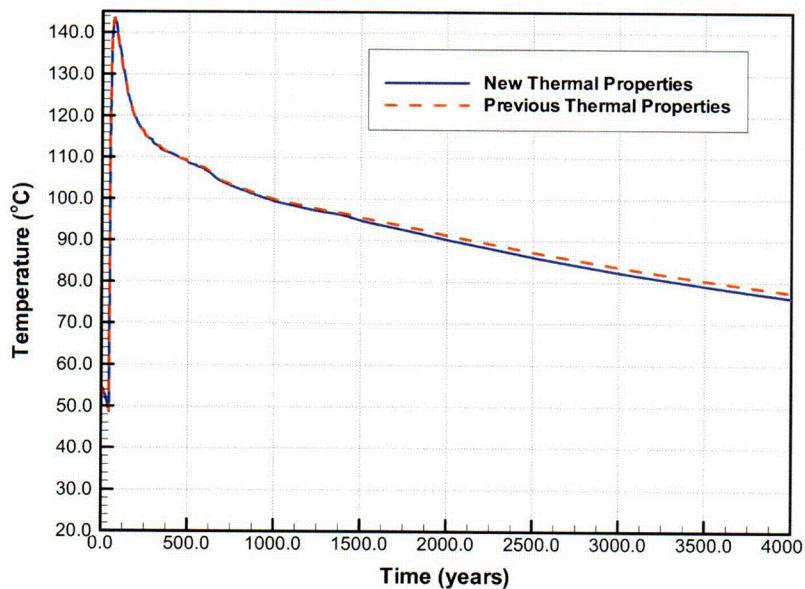
Figure C-9. Evolution of Thermal Seepage for Tptpmn Submodel with Flux Multiplication Factor 10 (Realization 1), Comparing New vs. Previous Thermal Properties (Simulation Cases MN-HET-NEW-03 vs. MN-HET-03)



Output DTN: LB0404DSCPTHSM.001.

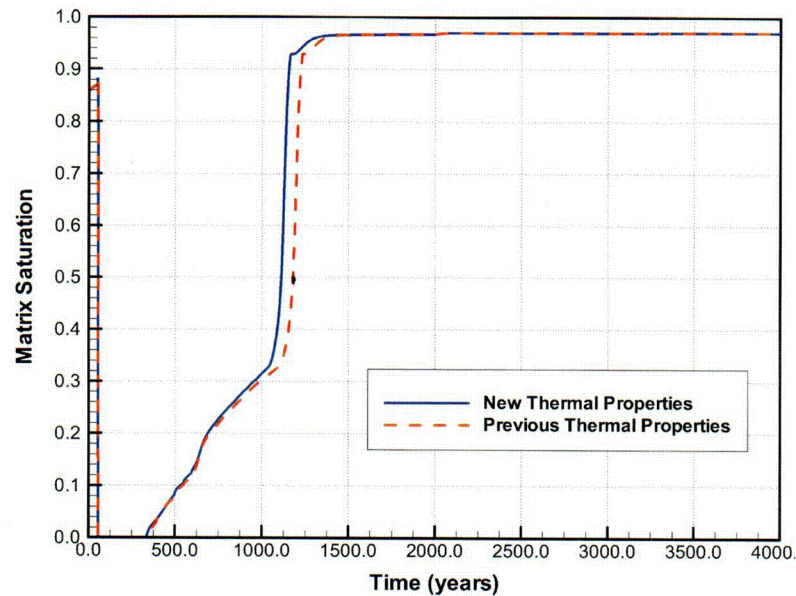
NOTE: The solid blue line represents new thermal properties; the dashed red line represents previous thermal properties.

Figure C-10. Evolution of Thermal Seepage for Tptpmn Submodel with Flux Multiplication Factor 10 (Realization 1), Comparing New vs. Previous Thermal Properties (Simulation Cases MN-HET-NEW-03 vs. MN-HET-03)



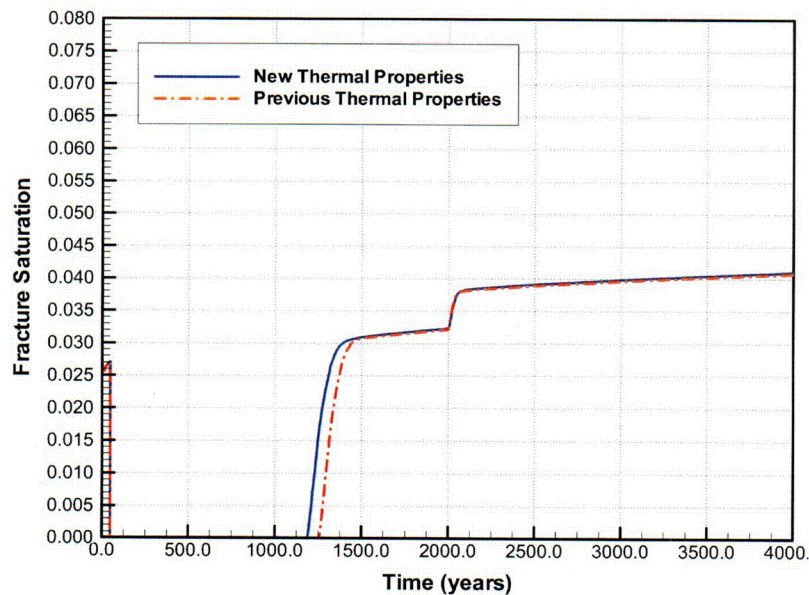
Output DTN: NA (See Section 8.5).

Figure C-11. Evolution of Rock Temperature at the Drift Crown for Tptpll Submodel, Comparing New vs. Previous Thermal Properties (Simulation Cases LL-HOM-NEW-01 vs. LL-HOM-01)



Output DTN: NA (See Section 8.5).

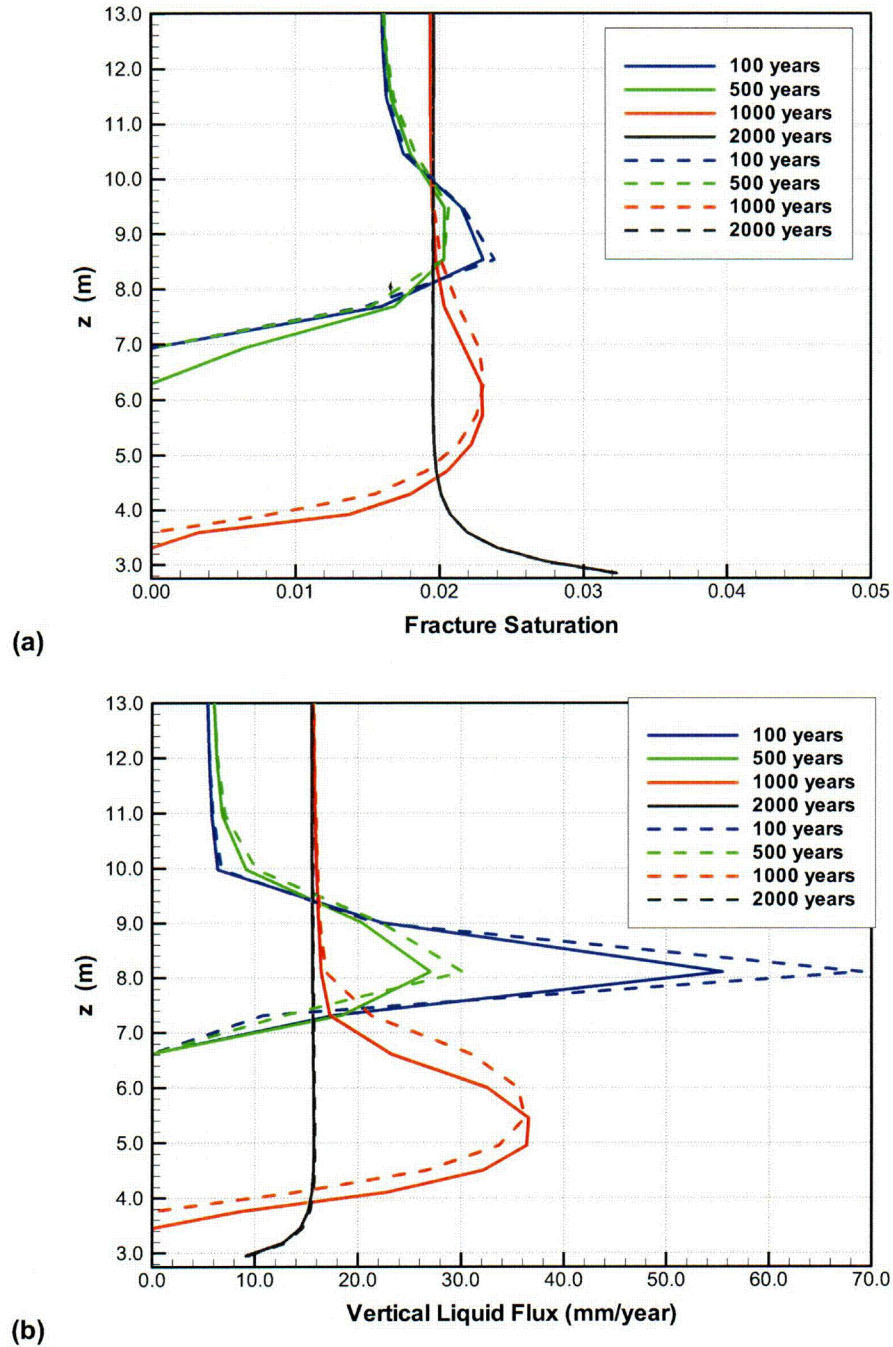
Figure C-12. Evolution of Matrix Saturation at the Drift Crown for Tptpl Submodel, Comparing New vs. Previous Thermal Properties (Simulation Cases LL-HOM-NEW-01 vs. LL-HOM-01)



Output DTN: NA (See Section 8.5).

Figure C-13. Evolution of Fracture Saturation at the Drift Crown for Tptpl Submodel, Comparing New vs. Previous Thermal Properties (Simulation Cases LL-HOM-NEW-01 vs. LL-HOM-01)





Output DTN: NA (See Section 8.5).

NOTE: The solid blue line represents new thermal properties; the dashed red line represents previous thermal properties.

Figure C-14. (a) Fracture Saturation and (b) Vertical Liquid Flux in a Vertical Cross Section above Drift Crown for Tptpl Submodel, Comparing New vs. Previous Thermal Properties (Simulation)

## **APPENDIX D**

### **TOP AND BOTTOM MODEL BOUNDARY CONDITIONS**





1. Extracting Top and Bottom Boundary Conditions from DTN: LB0303THERMSIM.001 [DIRS 165167]

- a. Download the contents of the DTN from the TDMS.
- b. Locate the folder “LB0303THERMSIM.001.zip.” On a PC, open the DTN with the help of WinZip (double click on the folder).
- c. Locate the file SAVE\_2\_20\_03\_as\_final\_calibrated and open it (double click to open).
- d. Using the ‘Find’ facility under ‘Edit’, first find ‘Tp Tph74’. The first number in the line immediately following ‘Tp Tph74’ is the pressure (in Pa), the second number is gas saturation plus ten (gas saturation is dimensionless), and the third number is temperature (in degrees centigrade). Since ‘Tp Tph74’ is at the top of Column ‘h74’, the top boundary condition at the top of Column ‘h74’ is
  - i. Pressure: 86304 Pa (rounded off)
  - ii. Gas Saturation:  $10.9899999 - 10 = 0.99$  (rounded off)
  - iii. Temperature: 17.33°C (rounded off)

These numbers are given in the 4th row and 3rd column of Table 4.1-6 as the top boundary conditions.

- e. Repeat step (d) for “Bt Bth74” for bottom boundary conditions in column ‘h74’
- f. Repeat step (d) for ‘Tp Tph28’ for top boundary conditions in Column ‘h28’, which represents the top boundary condition for the Tptpmn submodel.
- g. Repeat step (d) for ‘Bt Bth28’ for bottom boundary condition at Column ‘h28’ (or bottom boundary condition in the Tptpmn submodel).

2. Extracting Top and Bottom Boundary Conditions from DTN: LB991131233129.004 [DIRS 162183]

- a. Download the contents of the DTN from the TDMS.
- b. Locate the folder “LB991131233129.004.zip.” On a PC, open the DTN with the help of WinZip (double click on the file name).
- c. Locate the file “pa99cal\_ecm.out” and open it by double clicking on it.
- d. Using the ‘Find’ facility under ‘Edit’, first find ‘Tpj34’. The second number in the same line with ‘Tpj34’ is the pressure (in Pa), the third number is temperature (in degrees centigrade), and the fourth number is gas saturation (gas saturation is dimensionless). Since ‘Tpj34’ is at the top of Column ‘j34’, the top boundary condition at the top of Column ‘j344’ is
  - i. Pressure: 84765 Pa
  - ii. Gas Saturation: 0.99 (rounded off)
  - iii. Temperature: 16.08°C (rounded off)

These numbers are given in the 4th row and 2nd column of Table 4.1-6 as the top boundary conditions.

- e. Repeat step (d) for “Btj34” for bottom boundary conditions in column ‘j34’
- f. Repeat step (d) for ‘Tpi64’ for top boundary conditions in Column ‘i64’, which represents the top boundary condition for the Tptpmn submodel.
- g. Repeat step (d) for ‘Bti64’ for bottom boundary condition at Column ‘i64’ (or bottom boundary condition in the Tptpmn submodel).

INTENTIONALLY LEFT BLANK

## **APPENDIX E**

### **EXTRACTION OF CONTACT ELEVATION FROM THREE-DIMENSIONAL UZ NUMERICAL GRIDS**



The procedures for extraction of contact elevation between various stratigraphic layers in selected vertical columns from three-dimensional UZ numerical grids are provided below. Procedures are also provided for calculating the thicknesses of the various stratigraphic layers in those selected columns. The procedures below are explained for the vertical columns (adopted and revised) utilized for the Tptpl submodel. Contact elevations and thicknesses of the stratigraphic layers in selected columns (adopted and revised) of the Tptpmn submodel can also be obtained following similar procedures.

1. Extraction of Column Data From DTN: LB03023DKMGRID.001 [DIRS 162354]

- a. Download DTN: LB03023DKMGRID.001 from the TDMS. Unzip the contents of LB03023DKMGRID.001 using WinZip on a PC.
- b. Transfer the file 'mesh\_3dn.dkm' to a Unix platform.
- c. Execute the following commands on a Unix machine (for Column 'h74'):  
    >> grep 'h74' mesh\_3dn.dkm > mesh\_h74  
    >> grep -v 'F' mesh\_h74 >> mesh\_mat\_h74
- d. Use an editor to open file "mesh\_mat\_h74" and use the editor to remove all element connections for which the cosine vector is not  $-1.000E+01$ . This will ensure that one has only vertical connections between elements. Save this file.
- e. The last column in 'mesh\_mat\_h74' gives the elevation of the center of the various elements in Column 'h74' (element names are given in the first column of 'mesh\_mat\_h74', the second and third column provide the rock type and the volume of the elements. The fifth and sixth columns give the x- and y-coordinates of the center of the elements.
- f. Now use the interface distances in the connection section of the elements in conjunction with the elevations of the center of the elements to calculate the elevations at the top of each element. Repeat this for the first element of each rock type; the result is the elevation of the top of each geological layer. These results are given in the second column of Table 4.1-9
- g. **Example:** Locate element M0003h74 in file 'mesh\_mat\_h74.' This is the only element in rock type tcw13 (noted as 'tcwM3' to indicate that it is a matrix element not a fracture). Its grid center elevation is 1321.4 m. This element is connected to element M002Dh74, which is the last element in tcw12, and its center is located at 1333.7 m. To find the elevation of the interface between elements M002Dh74 and M0003h74, do the following:  
    Check the vertical connection between these elements. Their vertical connection is the sixth connection in the list of connections. The distance of the interface between those two elements is 2.662 from the center of M0003h74 or 9.670 m from the center of M002Dh74. Either way, the elevation of their interface is 1324.1 m ( $\sim 1321.4 + 2.662$  or  $1333.7 - 9.670$ ). Since M002Dh74 is the last element in tcw12 and M0003h74 is the first element in tcw13, this is the elevation at the top of tcw13. This is noted in the second column of Table 4.1-9.
- h. The thickness of each layer is calculated by taking a difference of the successive layers. These results are given in the third column of Table 4.1-9.  
    **Example:** The thickness (= 34.5 m) of the 'tsw34' stratigraphic layer is calculated by subtracting the elevation of the top of 'tsw35' (= 1129.7 m) from the elevation of the top of the 'tsw34' layer (= 1164.2 m).



## 2. Extraction of Column Data From DTN: LB990501233129.004 [DIRS 111475]

- a. Download DTN: LB990501233129.004 from the TDMS. Unzip the contents of LB990501233129.004 using WinZip on a PC.
- b. Transfer the files to a Unix platform. Then go into the directory 3-D\_Grid\_Calib. Find the file 3d2kcalib\_pcl.mesh.
- c. Execute the following commands on a Unix machine (for Column 'j34'):  
    >> grep 'j34' 3d2kcalib\_pcl.mesh > mesh\_j34  
    >> grep -v 'F' mesh\_j34 >> mesh\_mat\_j34
- d. Use an editor to open file "mesh\_mat\_j34" and use the editor to remove all element connections for which the cosine vector is not  $-1.000E+01$ . This will ensure that one has only vertical connections between elements. Save this file.
- i. The last column in 'mesh\_mat\_j34' gives the elevation of the center of the various elements in Column 'j34' (element names are given in the first column of 'mesh\_mat\_j34', the second and third column provide the rock type and the volume of the elements. The fifth and sixth columns give the x- and y-coordinates of the center of the elements.
- j. Now take an average of the elevations of the center of the elements to calculate the elevations at the top of each element. Repeat this for the first element of each rock type, the result is the elevation of the top of each geological layer. These elevations (in meters) are given in the second column of Table 4.1-9.
- k. **Example:** Locate element Mdj34 in file 'mesh\_mat\_j34.' This is the only element in rock type tcw13 (noted as 'tcwM3' to indicate that it is a matrix element not a fracture). Its grid center elevation is 1328.7494 m. This element is connected to element Mcj34, which is the last element in tcw12, and its center is located at 1355.3887 m. To find the elevation of the interface between elements Mcj34 and Mdj34, calculate the arithmetic average of 1355.3887 m and 1328.7494 m. The result is an elevation of 1342.1 m (rounded off) at the top of 'tcw13.' This is noted in the second column in Table 4.1-8 (check for 'tcw13').
- l. The thickness of each layer is calculated by subtracting the elevations of successive layers. The resultant thicknesses are provided in the third column of Table 4.1-9. **Example:** For the 'tsw34' stratigraphic layer, its top elevation is at 1164.2 m. The top elevation of the 'tsw35' layer is at 1129.7 m. Thus, the thickness of the 'tsw34' layer is  $1169.2 - 1132.0 = 37.2$  m. This result is provided in the third column of Table 4.1-9 (check value for 'tsw34').

**APPENDIX F**

**DERIVATION OF THERMAL PROPERTIES FOR UZ MODEL LAYERS IN  
DTN: LB0402THRMLPRP.001**



Thermal properties include rock grain density, dry and wet rock thermal conductivities, rock grain specific heat capacity, matrix porosity, lithophysae porosity, and fracture porosity. These properties are basic inputs into model studies involving heat flow.

Thermal properties for the UZ model layers in DTN: LB0210THRMLPRP.001 [DIRS 160799] were developed from the thermal-property data for the various lithostratigraphic layers (DTNs: SN0206T0503102.005 [DIRS 160258] and SN0208T0503102.007 [DIRS 160257]). The first of these two DTNs supplies thermal properties for most of the lithostratigraphic layers except the geological layers at the repository horizon. The second DTN deals with thermal properties of the geological layers in the repository horizon, namely the upper lithophysal, the middle nonlithophysal, the lower lithophysal, and the lower nonlithophysal stratigraphic units of Topopah Spring welded tuff.

Wet and dry thermal conductivity, matrix porosity, and bulk density data for the nonrepository lithostratigraphic layers have been updated. The most recent qualified data for these parameters can be found in DTN: SN0303T0503102.008 [DIRS 162401]. The heat capacity values of the lithostratigraphic layers are taken from DTN: SN0402T0503102.010 [DIRS 170993]. The thermal properties of the UZ model layers have thus been updated based on data available in three DTNs: SN0208T0503102.007 [DIRS 160257], SN0402T0503102.010 [DIRS 170993], and SN0303T0503102.008 [DIRS 162401].

In most cases, a UZ model layer directly corresponds to a unique lithostratigraphic unit. In such instances, the thermal properties are adopted directly from their corresponding stratigraphic unit without alteration. On the other hand, when a UZ model layer is composed of two or more adjacent lithostratigraphic units, the averaging technique of Francis (1997 [DIRS 127326], pp. 5 to 7) is used for estimating the properties while assuming an equal thickness for all the relevant units. The conceptual model underlying this technique is that heat flow is one-dimensional and in a direction normal to interfaces between the units under consideration. This is appropriate considering that heat flow in the ambient system and in the disturbed system (during repository heating) at Yucca Mountain is predominantly vertical. (This is because the horizontal dimensions of the repository horizon are much larger than the vertical dimension.) The corresponding equivalent thermal conductivity ( $\lambda_{k,eq}$  or  $\lambda_{k,eq}$ ), grain density ( $\rho_{g,eq}$ ), and heat capacity ( $C_{p,eq}$ ) are calculated using the following equations which were derived from those of Francis (1997 [DIRS 127326], pp. 5 to 7) assigning a uniform thickness for different geologic units within each model layer containing more than one geologic units:

$$\lambda_{k,eq} = \frac{n \prod_{i=1}^n \lambda_{k,i}}{\sum_{j=1}^n \left( \prod_{i=1, i \neq j}^n \lambda_{k,i} \right)} \quad (k = \text{wet or dry}) \quad (\text{Eq. F-1})$$

$$\rho_{g,eq} = \frac{\sum_{i=1}^n \rho_{g,i}}{n} \quad (\text{Eq. F-2})$$

$$C_{p,eq} = \frac{\sum_{i=1}^n C_{p,i} \rho_{g,i}}{n \rho_{g,eq}} \quad (\text{Eq. F-3})$$

where  $n$  is the total number of the involved lithostratigraphic units, and  $\lambda_{g,i}$ ,  $\rho_{g,i}$  and  $C_{p,i}$  are heat conductivity, grain density, and heat capacity, respectively, for a lithostratigraphic unit  $i$ . Note that the use of an equal thickness for all the relevant units within a model layer is adequate here because differences between thermal properties for these units (within a model layer) are not significant. Additionally, resultant matrix porosities are the simple arithmetic mean of the porosities for the constituent stratigraphic units. The calculated thermal properties for the UZ model layers are given in Table F-1. The determination of the properties is described in scientific notebooks (Wang 2003 [DIRS 161123], pp. 69 to 79; Wang 2004 [DIRS 170510], pp. 30 to 33).

The thermal conductivities listed in Table F-1 are matrix thermal conductivities. For lithophysal stratigraphic units and corresponding UZ model layers, it is often necessary to use the bulk thermal conductivities instead of the matrix thermal conductivities. For stratigraphic units Tptpul, Tptpmn, Tptpll and Tptpln (or UZ model layers tsw33, tsw34, tsw35 and tsw36), lithophysal porosities are listed in Table F-1 (from DTN: SN0208T0503102.007 [DIRS 160257]). For these stratigraphic units, the bulk thermal conductivities are also listed in DTN: SN0208T0503102.007 [DIRS 160257]. The bulk thermal conductivities of the corresponding UZ model layers are listed in Table F-2. For further details, refer to the Scientific Notebooks (Wang 2004 [DIRS 161123], pp. 69 to 79; Wang 2004 [DIRS 170510], pp. 30 to 33).

The thermal properties of the faults are developed using the averaging techniques discussed above (Francis 1997 [DIRS 127326]). The UZ model represents faults as having four layers that are defined by the major hydrogeologic units (HGU), TCw, PTn, TSw, and CHn/Cfu. For each of these units, averages are taken across all the stratigraphic subunits. For example, to obtain the matrix thermal properties of tcwf, averages were taken over Tpcr, Tpcp, Tpcpv3, and Tpcpv2. The details of the calculations can again be found in scientific notebooks (Wang 2003 [DIRS 161123], pp. 76 to 79; Wang 2004 [DIRS 170510], pp. 30 to 33). The calculated fault thermal properties are listed in Table F-3.

The data reported in Tables F-1, F-2, and F-3 have been compiled and submitted to the TDMS under output DTN: LB0402THRMLPRP.001.

Table F-1. Matrix Thermal Properties for the UZ Model Layers

Model Layer	Grain Density (kg/m <sup>3</sup> )	Grain Specific Heat Capacity (J/kg-K)	Dry Thermal Conductivity (W/m-K)	Wet Thermal Conductivity (W/m-K)	Matrix Porosity (-)	Lithophysae Porosity (-)
tcw11	2486	985.0	1.3000	1.8100	0.1190	N/A
tcw12	2486	985.0	1.3000	1.8100	0.1190	N/A
tcw13	2385	1040.1	0.5724	0.9092	0.2105	N/A
ptn21	2374	1040.1	0.4900	1.0600	0.3850	N/A
ptn22	2374	1040.1	0.4900	1.0600	0.3850	N/A
ptn23	2374	1040.1	0.4900	1.0600	0.3850	N/A
ptn24	2374	1040.1	0.4900	1.0600	0.3850	N/A
ptn25	2374	1040.1	0.4900	1.0600	0.3850	N/A
ptn26	2374	1040.1	0.4900	1.0600	0.3850	N/A
tsw31	2441	1012.0	0.8998	1.1057	0.0775	N/A
tsw32	2486	985.0	1.3000	1.8100	0.1190	N/A
tsw33	2344	985.0	1.3223	1.9093	0.1429	0.123
tsw34	2466	985.0	1.4553	2.1276	0.1287	0.025
tsw35	2325	985.0	1.3998	2.0707	0.1486	0.088
tsw36	2473	985.0	1.5356	2.1958	0.1058	0.03
tsw37	2473	985.0	1.5356	2.1958	0.1058	0.03
tsw38	2396	1040.1	0.6880	0.7960	0.0360	N/A
tsw39	2374	1040.1	0.4900	1.0600	0.3850	N/A
ch1[v,z]	2374	1040.1	0.4900	1.0600	0.3850	N/A
ch2[v,z]	2504	1037.5	0.5950	1.2600	0.3330	N/A
ch3[v,z]	2504	1037.5	0.5950	1.2600	0.3330	N/A
ch4[v,z]	2504	1037.5	0.5950	1.2600	0.3330	N/A
ch5[v,z]	2504	1037.5	0.5950	1.2600	0.3330	N/A
ch6[v,z]	2504	1037.5	0.5950	1.2600	0.3330	N/A
pp4	2557	1040.1	0.5690	1.1300	0.3000	N/A
pp3	2557	1040.1	0.5690	1.1300	0.3000	N/A
pp2	2587	1012.2	0.7405	1.3347	0.2545	N/A
pp1	2519	1040.1	0.5959	1.1493	0.2767	N/A
bf3	2485	1021.1	0.7877	1.3434	0.1937	N/A
bf2	2506	1040.1	0.6112	1.1584	0.2640	N/A
tr3	2658	1021.4	0.6408	1.2337	0.2910	N/A
tr2	2635	1040.1	0.5350	1.1000	0.3320	N/A

Output DTN: LB0402THRMLPRP.001.



Table F-2. Bulk Thermal Conductivities of Repository Model Layers

Model Layer	Dry Thermal Conductivity (W/m-K)	Wet Thermal Conductivity (W/m-K)
tsw33	1.1636	1.6785
tsw34	1.4191	2.0743
tsw35	1.2788	1.8905
tsw36	1.4901	2.1304
tsw37	1.4901	2.1304

Output DTN: LB0402THRMLPRP.001.

Table F-3. Fault Thermal Properties

Major Unit	Fault Layer	Grain Density (kg/m <sup>3</sup> )	Grain Specific Heat Capacity (J/kg-K)	Dry Thermal Conductivity (W/m-K)	Wet Thermal Conductivity (W/m-K)	Matrix Porosity (-)
TCw	tcwf	2435	1012.0	0.7948	1.2104	0.1648
PTn	ptnf	2374	1040.1	0.4900	1.0600	0.3850
TSw	tswf	2400	1003.3	0.9696	1.3923	0.1383
CHn	chnf	2509	1034.4	0.5884	1.1761	0.3068
CFu	cfuf	2565	1029.8	0.6419	1.2124	0.2645

Output DTN: LB0402THRMLPRP.001.

## **APPENDIX G**

### **QUALIFICATION OF DATA FROM DTN: SN9908T0872799.004 FOR INTENDED USE IN THIS REPORT**



## G.1 PURPOSE OF DATA QUALIFICATION

Although DTN: SN9908T0872799.004 [DIRS 108437] is the technical output of the calculation presented in *Tabulated In-Drift Geometric and Thermal Properties Used in Drift-Scale Models for TSPA-SR* (CRWMS M&O 2000 [DIRS 171790], Table 2), unqualified inputs were used in the development of those results, which were thus identified by that report as requiring further verification. The purpose of this data qualification effort is to qualify the values derived from DTN: SN9908T0872799.004 [DIRS 108437], for the parameters shown in Table G-1, as adequate for their intended use in the drift-scale modeling of TH seepage in this report. Some of the data from SN9908T0872799.004 [DIRS 108437], which have been used to develop the predictions in this report, have since been superseded. Even though these data have been superseded, the data are shown below to be qualified as adequate for their intended use in this report. This qualification is done following AP-SIII.2Q, *Qualification of Unqualified Data*, and in accordance with the Data Qualification Plan included in Section G.8.

Table G-1. Parameters and Values from DTN: SN9908T0872799.004 [DIRS 108437] to be Qualified

Parameter	Value
<b>Waste Package and Drip Shield Dimensions and Attributes</b>	
Location of waste package center above bottom of drift	1.945 m
Location of waste package center below the drift springline	0.805 m
Air gap between waste package surface and the inside of drip shield (only used for collapsed drift scenarios in Section 6.2.5)	0.396 m
Inside radius of drip shield	1.231 m
Waste package shell density	8189.2 kg/m <sup>3</sup>
Waste package specific heat	488.86 J/kg/K
<b>Invert Properties</b>	
Invert intrinsic permeability	$6.152 \times 10^{-10} \text{ m}^2$
Invert porosity	0.545
Invert grain density	2530 kg/m <sup>3</sup>
Invert specific heat	948 J/kg/K

## G.2 PURPOSE OF DATA BEING QUALIFIED

The data being qualified in this appendix relates to dimensions, configuration, and properties of the in-drift materials for a typical emplacement drift. These data were needed to enable the development of the TH seepage model (based on the TOUGH2 simulator). The primary purpose (see Section 1) of the TH seepage model is to estimate the quantity of seepage that could enter a repository drift; hence, the configuration and properties that are assigned to the in-drift components (such as the waste packages and the invert) have little impact on the predictions of seepage by the model. Consequently, the data evaluation criteria presented below are based on reasonableness of the input data, both in terms of design changes, as well as in the scientific sense, rather than actual input requirements of the model.

### G.3 QUALIFICATION METHODS

Consistent with AP-SIII.2Q, the method selected to qualify the data in Table G-2 is adopted from Method 2 in Attachment 3 of the qualification procedure:

- Corroborating Data - The data to be qualified are compared with either more recent project data, or with similar data developed by duplicate or independent calculations since DTN: SN9908T0872799.004 [DIRS 108437] was developed. A comparison is made with current controlled YMP documentation or data in the TDMS for corroboration.

### G.4 QUALIFICATION PROCESS ATTRIBUTES

Consistent with AP-SIII.2Q from Attachment 4, the attributes associated with this data qualification include:

3. *The extent to which the data demonstrate the properties of interest (e.g., physical, chemical, geologic, mechanical).*

This attribute is justified for application here because the data being qualified were developed specifically for the repository waste emplacement drifts.

10. Extent and quality of corroborating data or confirmatory testing results.

This attribute is appropriate because of the availability of the newer project data that supersedes the data directly used in this report and can corroborate the values in DTN: SN9908T0872799.004 [DIRS 108437].

### G.5 DATA EVALUATION CRITERIA

Consistent with AP-SIII.2Q, criteria have been established to evaluate the adequacy of the data being qualified. In general terms, the data selected to represent the in-drift environment must be reasonably consistent with either (1) the dimensions, geometry, and configuration with the current repository layout, or (2) the results of comparable calculations.

- (1) The dimensions and properties associated with the waste package and drip shield should be within a factor of 25 percent of the most recent values (if a single value is available), or within the range from the most recent source;
- (2) Because the properties of the invert have little impact on the model, the values that were used should be scientifically reasonable, and thus values of porosity, specific heat, and density should be within 25 percent of the most recent values, if a single value is available for them or they should be located within the range of values obtained from the most recent source. The value of permeability should be within one order of magnitude of the most recent value.

## G.6 EVALUATION OF DATA TO BE QUALIFIED

Table G-2 contains the input model data that is to be qualified. The model input value can be compared to the values given in the corroborative information.

Table G-2. In-Drift Geometry and Property Choices for TH Seepage Model

Parameter	Model Input		Corroborative Information	
	Source	Value	Value	Source
<b>Waste Package and Drip Shield Dimensions and Attributes</b>				
Location of waste package center above bottom of drift	DTN: SN9908T0872799.004 [DIRS 108437]	1.945 m	1.750 – 2.150 m	BSC 2004 [DIRS 168489] (center line of waste package height above invert from Figure 1) and BSC 2004 [DIRS 169776] (invert thickness)
Location of waste package center below the drift springline	DTN: SN9908T0872799.004 [DIRS 108437]	0.805 m	0.6 – 1.0 m	BSC 2004 [DIRS 168489] (drift diameter and center line of waste package height above invert from Figure 1) and BSC 2004 [DIRS 169776] (invert thickness)
Air gap between waste package surface and the inside of drip shield (only used for collapsed drift scenarios in Section 6.2.5)	DTN: SN9908T0872799.004 [DIRS 108437]	0.396 m	0.367 – 1.132 m	BSC 2004 [DIRS 168489]), Figure 1
Inside radius of drip shield	DTN: SN9908T0872799.004 [DIRS 108437]	1.231 m	1.285 m	BSC 2004 [DIRS 168283]
Waste package shell density (see also Section 4.1.1.6)	DTN: SN9908T0872799.004 [DIRS 108437]	8189.2 kg/m <sup>3</sup>	8690 kg/m <sup>3</sup>	DTN: MO0003RIB00071.000 [DIRS 148850]  Mass density of Alloy 22 (N06022), which is the outer barrier of the following WPs: 21-PWR AP, 44-BWR, 5 DHLW/DOE SNF-SHORT, 5 DHLW/DOE SNF-LONG. The density of the waste package internal cylinder is 2,175-3,495 kg/m <sup>3</sup> (BSC 2004 [DIRS 167758]).
Waste package specific heat	DTN: SN9908T0872799.004 [DIRS 108437]	488.86 J/kg/K	378- 731 J/kg/K	BSC 2004 [DIRS 167758], Table 20.



Table G-2. In-Drift Geometry and Property Choices for TH Seepage Model (Continued)

Parameter	Model Input		Corroborative Information	
	Source	Value	Value	Source
<b>Invert Properties (Continued)</b>				
Invert intrinsic permeability	DTN: SN9908T0872799.004 [DIRS 108437]	$6.152 \times 10^{-10} \text{ m}^2$ (2 to 4.75 mm particles)	$6.0 \times 10^{-10} \text{ m}^2$ (3 mm particle) <sup>(a)</sup>	BSC 2003 [DIRS 170881], Section 6.4 and Attachment XI; CRWMS M&O 2001 [152016], Attachment XV
Invert porosity	DTN: SN9908T0872799.004 [DIRS 108437]	0.545	0.55 <sup>(b)</sup>	BSC 2003 [DIRS 170881], Attachment XI; CRWMS M&O 2001 [DIRS 152016], Attachment XIV
Invert grain density	DTN: SN9908T0872799.004 [DIRS 108437]	2530 kg/m <sup>3</sup>	2530 kg/m <sup>3</sup> <sup>(c)</sup>	BSC 2003 [DIRS 170881], Attachment XI; CRWMS M&O 2001 [DIRS 152016], Attachment XIV
Invert specific heat	DTN: SN9908T0872799.004 [DIRS 108437]	948 J/kg/K	930 J/kg/K <sup>(d)</sup>	BSC 2003 [DIRS 170881], Attachment XI

<sup>a</sup> The permeability of the invert is estimated from the curve fitting analysis presented in CRWMS M&O 2001 [DIRS 152016].

<sup>b</sup> The porosity of the invert is calculated using measured data (from the sources cited) for grain density (2530 kg/m<sup>3</sup>) and bulk density (1150 kg/m<sup>3</sup>) of crushed tuff sieved between 2.00 to 4.75 mm.

<sup>c</sup> The grain density of invert material is the measured (from the source cited) grain density of crushed tuff sieved between 2.00 and 4.75 mm.

<sup>d</sup> The specific heat of invert material is the average of the 11 (4-10 crushed tuff) samples listed in DTN: GS000483351030.003 [DIRS 152932].

## G.7 FINDINGS OF DATA QUALIFICATION EFFORT

The parameters grouped under “Waste Package and Drip Shield Dimensions and Attributes” in Table G.2 are repository design information that has evolved since the current TH seepage models were developed. The comparison of these model input data with the more recent values shows that all of the model input values are within 25 percent of the current values or that they reside within the range of current values, and thus meet the criteria of acceptability for use in this model report. The model input data are therefore demonstrated to be qualified for their application.

The input values for the parameters grouped under “Invert Properties” in Table G-2 can be corroborated by either the duplication of the calculations used in *Tabulated In-Drift Geometric and Thermal Properties Used in Drift-Scale Models for TSPA-SR* (CRWMS M&O 2000 [DIRS 171790]) to generate the values used in the TH seepage modeling, or by comparable derivations of values. For the parameters of intrinsic permeability, porosity, grain density, and heat capacity of the invert, *Advection Versus Diffusion in the Invert* (BSC 2003 [DIRS 170881]), as well as *Water Distribution and Removal Model* (CRWMS M&O 2001 [DIRS 152016]), reproduced the same or similar calculations as those that were used as input to DTN: SN9908T0872799.004 [DIRS 108437]. Both of these reports were developed, checked and approved under the current post-PVAR YMP QA procedures (BSC 2003 [DIRS 170881] was developed under AP-SIII.9Q and CRWMS M&O 2001 [DIRS 152016] was developed under AP-3.10Q). The comparison of

the model input data for invert properties with the more recent values shows that all of the model input values meet the criteria of acceptability for use in the TH seepage model.

Based on the above assessment, the data shown on Table G-1 have been demonstrated to be qualified for their application as input to the TH seepage models.

## G.8 DATA QUALIFICATION PLAN

A Data Qualification Plan was developed for the above qualification effort, in accordance with Attachment 2 of AP-SIII.2Q. A facsimile of this plan is provided below.

<b>BSC</b>	<b>DATA QUALIFICATION PLAN</b>	QA: QA
		Page 1 of 1

<b>Section I. Organizational Information</b> <b>Qualification Title</b> Qualification of In-drift Configuration, Dimensions, and Component Properties for MDL-NBS-HS-000015. <b>Requesting Organization</b> Near Field Environment and Transport						
<b>Section II. Process Planning Requirements</b> <b>1. List of Unqualified Data to be Evaluated</b> See Table G-1 (of MDL-NBS-HS-000015 REV01), Parameters and Values from DTN: SN9908T0872799.004 [DIRS 108437] to be Qualified.  This is data relating to dimensions, configuration, and properties of in-drift materials for a typical emplacement drift. These data were needed to develop the Thermal-Hydrology (TH) Seepage Model (based on the TOUGH2 simulator). The primary purpose of this model is to estimate the quantity of seepage that could enter a repository drift and not to model the flow behavior of seepage water inside the emplacement drift. Hence the configuration and properties that are assigned to the in-drift components have little or no impact on these seepage predictions. <b>2. Type of Data Qualification Method(s)</b> [Including rationale for selection of method(s) (Attachment 3) and qualification attributes (Attachment 4)] Qualification Methods from Attachment 3 of AP-SIII.2Q: (2) Corroborating Data - The unqualified data will be compared with current, controlled YMP documentation or with qualified data in the TDMS.  Attributes used from Attachment 4 of AP-SIII.2Q: Item 3) The extent to which data demonstrate properties of interest; and Item 10) Extent and quality of corroborating data.  <b>3. Data Qualification Team and Additional Support Staff Required</b> Chairperson: Jens Birkholzer, Lawrence Berkeley National Laboratory Technically competent individual: Sumit Mukhopadhyay, Lawrence Berkeley National Laboratory						
<b>4. Data Evaluation Criteria</b> The TH Seepage Model (based on TOUGH2 simulator) model is created such that all of the heat generated inside an emplacement drift is transmitted to the host rock. Thus the criteria for having acceptable data is: 1. In total, the data selected to represent the in-drift environment must be reasonably consistent with either the dimensions, geometry, and configuration with the repository layout; or with the results of comparable calculations. 2. The selection of the in-drift component dimensions should be within a factor of 25 percent of the most recent values or, if a single value is not appropriate, should reside within the suggested range from the most recent source. The same criteria should apply for values of porosity, specific heat and density. The value of permeability should be within one order of magnitude of the most recent value. <b>5. Identification of Procedures Used</b> AP-SIII.10Q, Models AP-SIII.2Q, Qualification of Unqualified Data						
<b>Section III. Approval</b> <table border="1"> <tr> <td>Qualification Chairperson Printed Name Jens Birkholzer</td> <td>Qualification Chairperson Signature <i>Jens Birkholzer</i></td> <td>Date 8-16-04</td> </tr> <tr> <td>Responsible Manager Printed Name Near Field Environment and Transport</td> <td>Responsible Manager Signature <i>W. H. H. H.</i></td> <td>Date 8/16/04</td> </tr> </table>	Qualification Chairperson Printed Name Jens Birkholzer	Qualification Chairperson Signature <i>Jens Birkholzer</i>	Date 8-16-04	Responsible Manager Printed Name Near Field Environment and Transport	Responsible Manager Signature <i>W. H. H. H.</i>	Date 8/16/04
Qualification Chairperson Printed Name Jens Birkholzer	Qualification Chairperson Signature <i>Jens Birkholzer</i>	Date 8-16-04				
Responsible Manager Printed Name Near Field Environment and Transport	Responsible Manager Signature <i>W. H. H. H.</i>	Date 8/16/04				

INTENTIONALLY LEFT BLANK

## **APPENDIX H**



### **DATA QUALIFICATION PLAN FOR QUALIFICATION OF VENTILATION EFFICIENCY VALUE**



The ventilation efficiency value used as direct input to the TH seepage model was calculated using unqualified software. The value has been qualified for use in this report in Section 4.1.1.3, in accordance with the data qualification plan presented below. The original of this plan is included in the records package for this model report.

<b>BSC</b>	<b>DATA QUALIFICATION PLAN</b>		QA: QA
			Page 1 of 1

<b>Section I. Organizational Information</b>		
Qualification Title		
Qualification of Ventilation Efficiency Value from Table 6-6 of BSC 2002 [160975]		
Requesting Organization		
Near Field Environment and Transport		
<b>Section II. Process Planning Requirements</b>		
1. List of Unqualified Data to be Evaluated		
The ventilation efficiency value of 86.3 percent, as reported in Table 6-6 of BSC 2002 [160975]. The value was calculated using unqualified software.		
2. Type of Data Qualification Method(s) [Including rationale for selection of method(s) (Attachment 3) and qualification attributes (Attachment 4)]		
Qualification Method, from Attachment 3 of AP-SIII.2Q, Rev 1, ICN 1: Corroborating Data. The unqualified data will be compared with more recent, qualified, project ventilation efficiency values calculated with qualified software and reported in the current project reports and available in the TDMS.		
Attributes used from Attachment 4: (3) The extent to which the data demonstrate the properties of interest, and (10) extent and quality of corroborating data.		
3. Data Qualification Team and Additional Support Staff Required		
Chairperson: Jens Birkholzer, Lawrence Berkeley National Laboratories Technically competent individuals: Sumit Mukhopadhyay and Jonny Rudquist		
4. Data Evaluation Criteria		
The value of 86.3% for the ventilation efficiency will be considered qualified if it falls within the range of standard deviation of the ventilation efficiency values reported in the current YMP model reports and qualified DTNs in the TDMS.		
5. Identification of Procedures Used		
AP-SIII.2Q, Qualification of Unqualified Data AP-SIII.10Q, Models NB 9/23/04		
<b>Section III. Approval</b>		
Qualification Chairperson Printed Name	Qualification Chairperson Signature	Date
Jens Birkholzer		9/24/04
Responsible Manager Printed Name	Responsible Manager Signature	Date
Ernest Hardin		9/24/04



INTENTIONALLY LEFT BLANK